Cannabidiol modulation of ion channels and neuronal excitability

HARVARD UNIVERSITY
Graduate School of Arts and Sciences

DISSERTATION ACCEPTANCE CERTIFICATE

The undersigned, appointed by the

Division of Medical Sciences

in the subject of Biological and Biomedical Sciences

have examined a dissertation entitled

Cannabidiol modulation of ion channels and neuronal excitability

presented by Hanxiong Bear Zhang

candidate for the degree of Doctor of Philosophy and hereby certify that it is worthy of acceptance.

Signature: Gary Yellen
Gary Yellen (Apr 20, 2023 17:34 EDT)

Typed Name: Dr. Gary Yellen

Signature: chinfei chen
Chinfei Chen (Apr 20, 2023 17:29 EDT)

Typed Name: Dr. Chinfei Chen

Signature: jonathan b. cohen
jonathan b. cohen (Apr 20, 2023 17:37 EDT)

Typed Name: Dr. Jonathan Cohen

Signature:
Diane Lipscombe (Apr 21, 2023 15:08 EDT)

Typed Name: Dr. Diane Lipscombe

Date: April 20, 2023

Cannabidiol modulation of ion channels and neuronal excitability

A dissertation presented

by

Hanxiong Bear Zhang

to

The Division of Medical Sciences

In partial fulfillment of the requirements

for the degree of

Doctor of Philosophy

In the subject of

Biological and Biomedical Sciences

Harvard University

Cambridge, Massachusetts

April 2023

Dissertation Advisor: Bruce P. Bean Hanxiong Bear Zhang

Cannabidiol modulation of ion channels and neuronal excitability

Abstract

Cannabidiol (CBD) is a non-intoxicating phytocannabinoid from *Cannabis sativa*. In human clinical trials and animal models, CBD shows anti-epileptic and analgesic efficacy. The goal of my thesis work was to explore how CBD modulates various ion channels to affect neuronal excitability.

In Chapter 1, I describe CBD inhibition of primary nociceptive neuron (nociceptor) excitability at sub-micromolar concentrations. CBD is more potent than the local anesthetic bupivacaine in reducing nociceptor firing. The reduction in firing can be explained by inhibition of both tetrodotoxin (TTX)-sensitive sodium currents (mostly Nav1.7) and TTX-resistant sodium currents (Nav1.8). CBD binds particularly tightly to the slow inactivated states of Nav1.8 with a K_d (dissociation constant) of 150 nM. The data suggest a molecular explanation for CBD's analgesic effect and a strategy for analgesic drug development by targeting slow inactivated states of Nav1.8.

In Chapter 2, I describe CBD inhibition of human Nav1.7 (hNav1.7) channels, with results suggesting that CBD binds tightly to inactivated states of the channel, with a K_d (dissociation constant) of 65 nM. CBD-bound hNav1.7 channels show decreased availability and slowed recovery rate. The electrophysiological data suggesting that CBD stabilizes the inactivated states of Nav1.7 channels is consistent with structures of CBD bound to hNav1.7 obtained by

our collaborators, showing two distinct binding sites, including a novel binding site adjacent to the receptor site for the inactivating “wedge” of the channel. These data provide a plausible structural correlate of state-dependent inhibition of hNav1.7 by CBD and a structural blueprint for future design of CBD-based analgesic drugs with improved properties.

In Chapter 3, I describe enhancement of Kv7 currents by CBD at concentrations as low as 30 nM. CBD enhances Kv7.2/7.3 current by shifting the voltage dependence of channel activation in the hyperpolarizing direction. Enhancement is observed for Kv7 channels mediating M-current in native neurons as well as for cloned human Kv7.2/7.3 channels.

Together, these results show that CBD acts at sub-micromolar levels to inhibit multiple types of voltage-dependent sodium channels and to activate Kv7.2/7.3 channels and suggest that a combination of these effects may contribute to the efficacy of CBD in treating epilepsy and pain.

Acknowledgements

I am extremely grateful for the scientific advisors I have over the years: Bruce Bean, Gary Yellen, Wade Regher, Michael Do, Jeffry Isaacson and Yudong Zhou whose mentorship deeply shapes my thesis work.

I am also thankful for the love from my family and friends: F Liu, XY Zhang, MJ Yuan, friends in Bean lab and the Harvard BBS program. They support me during the ups and downs.

Table of Contents

Introduction

Cannabidiol as a phytocannabinoid with anti-epileptic and analgesic effects

Cannabidiol is a non-intoxicating phytocannabinoid present in *Cannabis sativa* (Mechoulam et al., 1970). Recently, it has been shown to be efficacious as an anti-epileptic medicine for Lennox-Gastaut syndrome (Thiele et al., 2019) and Dravet syndrome (Devinsky et al., 2014, 2017). In 2018, cannabidiol was launched as a clinical drug in the US under the name of Epidiolex after its approval by FDA for Lennox-Gastaut syndrome and Dravet syndrome. In addition to functioning as an anti-epileptic agent, CBD has shown potential as a treatment for postoperative pain (Alaia et al., 2022) and neuropathic pain (Xu et al., 2020) in clinical trials. Studies using animal models suggest CBD also relieves arthritic pain (Malfait et al., 2000; Hammell et al., 2015), mechanical and thermal allodynia (Abraham et al., 2019). Understanding the molecular action of mechanism of CBD in treating epilepsy and pain can provide guidance for developing future anti-epileptic (Pozo and Barker-haliski, 2023) and analgesic medications.

Molecular targets of CBD

CBD has been demonstrated to interact with a large number of proteins including many membrane proteins. The key molecular action of mechanism of CBD has remained inconclusive and heavily dependent on the concentration level being used. Unlike another prevalent phytocannabinoid Δ(9)-tetrahydrocannabinol (Δ9-THC), CBD does not act as an agonist on CB1 or CB2 receptors (Pertwee, 2008). Instead, CBD acts as a negative allosteric modulator of CB1 receptors (Laprairie et al., 2015; Straiker et al., 2018). At submicromolar concentrations, CBD prevents depolarization-induced suppression of excitation by negatively modulating the

endogenous endocannabinoid signaling (Kreitzer and Regehr, 2001; Wilson and Nicoll, 2001; Straiker et al., 2018).

CBD was found to antagonize an orphan receptor GPR55, as shown by biochemical assaysbased on GTPγS (at submicromolar level)(Ryberg et al., 2007) and by electrophysiological recording in hippocampal slices (Kaplan et al., 2017; Rosenberg et al., 2023) (16 μM CBD and 1 μM respectively).

Like many other anti-epileptic and analgesic drugs, CBD inhibits voltage-gated sodium channels (Köhling, 2002; Brodie, 2017; Alsaloum et al., 2020). Voltage-gated sodium channels underlie the upstroke of the action potential and repetitive firing of neurons (Bennett et al., 2019). A previous study using automated patch clamp showed that CBD inhibits hNav1.1-hNav1.7 channels expressed in human embryonic kidney (HEK) cells (Ghovanloo et al., 2018). The potency of CBD inhibition on voltage gated sodium channels in this study falls into low micromolar range, with the half maximal inhibitory concentration (IC_{50}) ranging from 1.9 μM on hNav1.4 to 3.8 μM on hNav1.5. In this study , inhibition of sodium channels by CBD was measured after long depolarizations which suggests the measured IC_{50} represents potency for binding to channels in inactivated states rather than resting states (Hodgkin and Huxley, 1952; Bean et al., 1983). The inhibitory effect of CBD on voltage-gated sodium channel was also observed independently in hNav1.6 (Patel et al., 2016) (at 1 μM), hNav1.2 (Mason and Cummins, 2020) (at 1 μM) and sodium channels in SH-SY5Y cells (Hill et al., 2014) (at 10 μM).

Voltage-gated calcium channels are important for synaptic releases, neuronal excitability, gene transcription and peptide release (Simms and Zamponi, 2014). Different research groups have tested 1 μM CBD on Cav1, Cav2 and Cav3 and found CBD inhibits Cav1 in ventricular

myocytes (Ali et al., 2015) and heterologously-expressed Cav3 (Ross et al., 2008; Harding et al., 2023) but not heterologously-expressed Cav2.

The action of CBD on voltage-gated potassium channels remains unclear in the context of epilepsy and pain. CBD was discovered to inhibit potassium channels in cardiac cells and heterologous hERG channels at low micromolar concentrations (Orvos et al., 2020; Topal et al., 2021; Isaev et al., 2022). Enhancement of Kv7 might provide an explanation for CBD anti-epileptic effect because Kv7 activation dampens neuronal firing (Brown and Passmore, 2009).

Lastly, CBD activates TRP channels such as TRPV1 at 10 μM (Anand et al., 2020), TRPV2 at low micromolar concentrations (Qin et al., 2008), and TRPV3 at low micromolar concentrations (de Petrocellis et al., 2012).

The action of CBD on a variety of ion channels leads to the hypothesis that CBD can alter neuronal excitability. Indeed at > 10 μM concentration, CBD reduces action potential firing of hippocampal pyramidal neurons (Kaplan et al., 2017; Khan et al., 2018). For interneurons in the central nervous system, CBD shows mixed effect on their excitability: it can either enhance or reduce the firing depending on interneuron subpopulation (Khan et al., 2018).

It remains unclear how CBD affects nociceptor excitability and ion channels with specific expression in nociceptors.

Molecular determinants of excitability of primary nociceptive neurons

Mammalian neurons generally express more than a dozen of voltage-gated ion channels which together determine the firing pattern and action potential shape (Bean, 2007). Primary nociceptive neurons in dorsal root ganglion (DRG) express at least 3 types of voltage-gated sodium channels (Nav1.7, Nav1.8 and Nav1.9) (Bennett et al., 2019; Zheng et al., 2019), 4 types

of voltage-gated potassium channels (Kv1, Kv2, Kv3 and Kv4) (Zheng et al., 2019) and 2 types of voltage-gated calcium channels (Blair and Bean, 2002; Lee, 2013) (high-voltage activated and low-voltage activated calcium channels). Among all the voltage-gated ion channels, Nav1.7, Nav1.8 and Nav1.9 are of particular interest due to their significant contribution to action potential firing and restrictive expression in the peripheral nervous system (Bennett et al., 2019).

Nav1.7 has been considered a promising molecular target for developing pain treatment due to its human genetic link to pain and its importance in deciding the action potential threshold of the first action potential in nociceptors. Gain of function Nav1.7 gene is associated with primary erythermalgia in patients (Yang et al., 2004). Loss of function of Nav1.7 is linked to inherited insensitivity to pain (Cox et al., 2006). Nav1.7 has a low threshold for activation and fast kinetics of activation which contributes to deciding the voltage threshold and the rising phase of first action potential (Blair and Bean, 2002; Bennett et al., 2019). Despite huge interest in developing analgesic medicines targeting Nav1.7, Nav1.7 inhibitors have shown limited efficacy in preclinical and clinical trials (Eagles et al., 2022). There are several hypotheses to explain the lack of efficacy of Nav1.7 inhibitors (Eagles et al., 2022): 1. Other voltage-gated sodium channels contribute to action potential firing of nociceptors.(Blair and Bean, 2003) 2. Pharmacokinetic issue of current Nav1.7 inhibitors. 3. Genetic link of Nav1.7 to pain is weakened because insensitivity to pain from loss of function of Nav1.7 might be due to concurrent upregulation of endogenous opioid signaling (Minett et al., 2012).

Gain of function of Nav1.9 was found in patients with a familial painful channelopathy (Han et al., 2017). Although Nav1.9 channels can produce substantial persistent sodium currents

(Cummins et al., 1999), Nav1.9 availability requires long hyperpolarization steps (minutes at -120 mV) to remove its inactivation (Bosmans et al., 2011) which limits its contribution to nociceptor firing from physiological resting membrane potential of -76 mV on average (Blair and Bean, 2002).

A selective Nav1.8 inhibitor VX-548 demonstrated efficacy in patients with acute pain after surgeries (ClinicalTrials.gov Identifier: NCT05034952 and NCT04977336). Nav1.8 is shown to play a crucial role in maintaining repetitive firing of nociceptors (Blair and Bean, 2003). This is due to unique biophysical properties of Nav1.8: Nav1.8 is available at moderate depolarization range from -60 mV to -40 mV in contrast to Nav1.7 which inactivates completely at the above voltage range (Rush et al., 1998; Blair and Bean, 2003). During stimuli of capsaicin, the membrane potential of nociceptors reaches steady-state level of approximate -40 mV where only Nav1.8 currents flow but Nav1.7 currents do not (Blair and Bean, 2003). Therefore, targeting Nav1.8 presents a novel opportunity for developing analgesic drugs.

State-dependent inhibition of sodium channels by anti-epileptic and analgesic medicine

Many anti-epileptic and analgesic drugs inhibit sodium channels by binding more tightly to the inactivated states of channels induced after depolarizations than resting state of channels at resting membrane potential. The state-dependent inhibition is observed in lidocaine (Bean et al., 1983), phenytoin (Kuo and Bean, 1994), lamotrigine (Kuo and Lu, 1997), carbamazepine (Kuo et al., 1997) and lacosamide (Peng et al., 2020). The state-dependent inhibition property is favorable for treating diseases associated with neuronal hyperactivity including pain and epilepsy because drugs with this property bind more tightly to the inactivated states of channels which are more pronounced in neurons that fire at pathologically high firing frequency

and stay at depolarized resting membrane potential. Drugs with state-dependent inhibition have less effect on neurons that fire at lower physiological frequency by binding less tightly to resting states of channels which are the dominating states at hyperpolarized resting membrane potential. Consistent with existing anti-epileptic and analgesic drugs, CBD shares the state-dependent inhibition, with tighter binding to inactivated states of hNav1.1-hNav1.7 (Ghovanloo et al., 2018).

Sodium channels often have at least two types of inactivated states, distinguished by the rate of entering and recovering from the inactivated state: a fast inactivated state, which has a time constant on the magnitude of millisecond for development and recovery of inactivation, and a distinct slow inactivated state, with a time constant of hundreds of millisecond or longer (Vilin and Ruben, 2001; Jo and Bean, 2017). Compared to other Nav-family channels, Nav1.8 channels have an unusual biophysical characteristic in that entry into slow inactivated states occurs at more hyperpolarized voltages than entry into fast inactivated states (Blair and Bean, 2003). For example at -40 mV, the slow inactivated state of Nav1.8 in nociceptors is the dominant type of inactivated state rather than fast inactivated state, which is the opposite of other voltage-gated sodium channels (Blair and Bean, 2003; Jo and Bean, 2017). Occupancy of slow inactivated states at subthreshold levels makes targeting the slow inactivated state a promising strategy for developing state-dependent Nav1.8 inhibitors for pain treatment.

Structures of CBD binding to ion channels

The first structure of CBD binding to ion channels was obtained with TRPV2 (Pumroy et al., 2019). In TRPV2, CBD binding was seen in a hydrophobic pocket between the S5 and S6 helices. The authors suggested that CBD-bound TRPV2 can enter three hypothetical states based on the

heterogeneity in the structures that were seen: pre-open, desensitized and partial open states. Subsequently, a structure of CBD bound to bacterial sodium channels was solved, showing CBD present at a site between fenestrations and central hydrophobic cavity of the channel. However, bacterial sodium channels have significantly different stuctures that mammalain sodium channels, and the mechanism of inactivation is different. A structure of CBD bound to a mammalian sodium channels might help interpret the state-dependent inhibition by binding of CBD to the inactivated states, which is likely important for its effects on pain and epilsepsy.

Concluding remarks

In my thesis I report the effect of CBD on firing mouse nociceptors and its action on three types of voltage-gated ion channels. In Chapter 1, I describe how CBD inhibits action potential firing of nociceptors and CBD inhibition of Nav1.8 by binding tightly to the slow inactivated states using experiments and simulations. In Chapter 2, I discuss inhibition of CBD on human Nav1.7 channels by binding to the inactivated states, together with the structure of CBD bound to human Nav1.7 channels solved by our collaborators, revealing that CBD has two binding sites in Nav1.7 channels, including a site close to the receptor site of allosteric inactivation. Finally, in Chapter 3 I show CBD enhancement cloned of Kv7.2/7.3 channels expressed in a cell line, as well as of native M-current in superior cervical ganglion neurons and hippocampal neurons. Together, my thesis provides new information about the action of CBD on firing of pain-sensing neurons and on three types of voltage gated ion channels. Together with work by others, this work may help facilitate future discovery of novel ion channel-targeted drugs to treat pain and epilepsy.

Chapter 1 Cannabidiol inhibition of murine primary nociceptors: Tight binding to slow inactivated states of Nav1. 8 channels

Journal of Neuroscience, volume 41, issue 30, pages 6371-6387, 2021

Han-Xiong Bear Zhang, Bruce P Bean

Contributions to the work

I did all of the experiments in this chapter, and worked with Bruce Bean in designing the experiments, making the figures, doing the modeling, and writing and revising the paper.

Abstract

The non-psychoactive phytocannabinoid cannabidiol (CBD) has been shown to have analgesic effects in animal studies but little is known about its mechanism of action. We examined effects of CBD on intrinsic excitability of primary pain-sensing neurons. Studying acutely-dissociated capsaicin-sensitive mouse DRG neurons at 37°C, we found that CBD effectively inhibited repetitive action potential firing, from 15-20 action potentials evoked by 1-s current injections in control to 1-3 action potentials with 2 μM CBD. Reduction of repetitive firing was accompanied by reduction of action potential height, widening of action potentials, reduction of the afterhyperpolarization, and increased propensity to enter depolarization block. Voltage clamp experiments showed that CBD inhibited both TTX-sensitive (TTX-S) and TTX-resistant (TTX-R) sodium currents in a use-dependent manner. CBD showed strong state-dependent inhibition of TTX-R channels, with fast binding to inactivated channels during depolarizations and slow unbinding on repolarization. CBD alteration of channel availability at various voltages suggested that CBD binds especially tightly (K_d of ~150 nM) to the slow inactivated state of TTX-R channels, which can be substantially occupied at voltages as negative as -40 mV. Remarkably, CBD was more potent in inhibiting TTX-R channels and inhibiting action potential firing than the local anesthetic bupivacaine. We conclude that CBD might produce some of its analgesic effects by direct effects on neuronal excitability, with tight binding to the slow inactivated state of Nav1.8 channels contributing to effective inhibition of repetitive firing by modest depolarizations.

Introduction

Cannabidiol (CBD), a non-psychoactive phytocannabinoid present in marijuana (Mechoulam et al., 1970), has been developed as an anti-epileptic agent (Epidiolex) and shown to be effective in treating Dravet Syndrome (Devinsky et al., 2017, 2018b,2019; Miller et al., 2020) and Lennox-Gastaut syndrome (Devinsky et al., 2018a; Thiele et al., 2018) epilepsies. The molecular mechanism of action of CBD in epilepsy is still unclear (Jones et al., 2010; Rosenberg et al., 2015,2017; Franco and Perucca, 2019; Gray and Whalley, 2020). Unlike Δ(9)-tetrahydrocannabinol (THC), the other major phytocannabinoid in marijuana, CBD does not act as a direct primary ligand at CB1 or CB2 receptors, the G-protein coupled receptors activated by endocannabinoids (Pertwee, 2005). However, CBD can inhibit the effects of endocannabinoids naturally released by neurons to modulate synaptic transmission (Straiker et al., 2018), by a negative allosteric effect mediated by cannabidiol binding to CB1 receptors at a site distinct from the primary binding site (Laprairie et al., 2015; Straiker et al., 2018). CBD actions in the CNS may also reflect its activity as an antagonist of the lipid-activated G protein-coupled receptor GPR55 (Kaplan et al., 2017; Ryberg et al., 2007). In addition, CBD can act at micromolar concentrations to directly inhibit a wide range of ion channels, including voltage-dependent sodium channels (Hill et al., 2014; Patel et al, 2016; Ghovanloo et al. 2018; Mason and Cummins, 2020) and modifies the intrinsic excitability of central neurons (Kaplan et al., 2017; Khan et al., 2018).

Although efficacy of oral CBD in humans has been demonstrated in rigorous large-scale clinical trials only for specific epilepsies, there are anecdotal reports that oral CBD is effective in inhibiting pain (Argueta et al., 2020; Tran and Kavuluru, 2020). Small clinical trials have shown

reduction in myofascial pain by CBD applied in a transdermal cream (Nitecka-Buchta et al., 2019) and relief of peripheral neuropathic pain by topical cannabidiol oil (Xu et al., 2020). In animal experiments, CBD has been shown to relieve pain in rodent models of inflammatory and arthritic pain by oral administration (Malfait et al., 2000; Costa et al., 2004, 2007; Rock et al., 2018), intraperitoneal injection (Malfait et al., 2000; Gallily et al., 2018) and transdermal application (Hammell et al., 2015). Oral CBD relieved allodynia in a mouse sciatic nerve injury model (Abraham et al., 2019) and reduced a pain index and enhanced locomotion in dogs with osteoarthritis (Verrico et al., 2020).

CBD effects on pain could involve a mixture of effects on the CNS (Maione et al., 2011; De Gregorio et al., 2019) and the periphery. Here, we examined effects of CBD on the excitability of primary sensory neurons, using a preparation of acutely dissociated neurons in which well-defined concentrations of CBD can be applied. We find that sub-micromolar concentrations of CBD inhibit excitability of nociceptors by state-dependent binding to voltage-dependent sodium channels, in a manner suggesting especially tight binding to slow inactivated states of Nav1.8 channels.

Materials and methods

Cell preparation. Acutely dissociated dorsal root ganglion (DRG) neurons were prepared as previously described (Liu et al., 2017; Zheng et al., 2019). Briefly, DRGs were removed from Swiss Webster mice of either sex (P9-P14). Ganglia were removed in ice-cold Ca^{2+}-free, Mg^{2+}-free (CMF) Hank's balanced salt solution (ThermoFisher) under a dissection microscope. Ganglia were treated for 20 minutes at 37°C with 20 U/ml papain (Worthington Biochemical, Lakewood, NJ) in CMF Hank's solution and then treated for 20 minutes at 37°C with 3 mg/ml collagenase

(Type I; Roche Diagnostics, Indianapolis, IN) and 4 mg/ml dispase II (Roche Diagnostics) in CMF Hank's solution. Cells were dispersed by gentle trituration with a fire-polished glass Pasteur pipette in a solution composed of two media combined in a 1:1 ratio: Leibovitz's L-15 medium (Invitrogen, Grand Island, NY) supplemented with 5 mM HEPES, and DMEM/F12 medium (ThermoFisher) supplemented with 10% Heat-Inactivated Fetal Bovine Serum (ThermoFisher) ; this solution also had added 130 ng/ml nerve growth factor (NGF) (Sigma-Aldrich). Cells were then plated on glass coverslips and incubated at 37°C (95% O2, 5% CO2) for 1.5-2 hours, after which they were stored at 4°C in Neurobasal medium (ThermoFisher) supplemented with 200 ng/ml NGF (Invitrogen), 1% penicillin and streptomycin (Sigma), 2% B-27 supplement (Gibco, ThermoFisher), and 30 mM NaCl. Cells were used within 48 hours. Storage at 4°C prevented neurite growth, enabling faster decay of capacity transients, more accurate voltage clamp, and the ability to lift cells in front of flow pipes to facilitate temperature control and to enable rapid solution exchange.

Electrophysiology. Recordings were performed at 37°C using a Molecular Devices Multiclamp 700B Amplifier. Voltage or current commands were delivered and signals were recorded using a Digidata 1322A data acquisition system (Molecular Devices) controlled by pCLAMP 10.3 software (Molecular Devices). Electrodes were pulled on a Sutter P-97 puller (Sutter Instruments) and shanks were wrapped with Parafilm (American National Can Company) to allow optimal series resistance compensation without oscillation. The resistances of the pipettes were 3-9 MΩ. Seals were formed in Tyrode's solution consisting of 155 mM NaCl, 3.5 mM KCl, 1.5 mM $CaCl_2$, 1 mM $MgCl_2$, 10 mM HEPES, 10 mM glucose, pH 7.4 adjusted with NaOH. After establishing whole-cell recording, cell capacitance was nulled and series resistance

was partially (70-80%) compensated. Cells were lifted off the bottom of the recording chamber and placed in front of an array of quartz flow pipes (250 µm internal diameter, 350 µm external, Polymicro Technologies) attached with styrene butadiene glue (Amazing Goop, Eclectic Products) to an aluminum rod (1x1 cm) whose temperature was controlled to 38°C by resistive heating elements and a feedback-controlled temperature controller (TC-344B; Warner Instruments). With the end of the rod and the flow pipes (extending 1 mm from the end of the rod) lowered just below the surface of the bulk chamber solution, the solution exiting from the flow pipes is maintained at 37°C (Carter and Bean, 2009).

Current and voltage records were filtered at 5 or 10 kHz and digitized at 100 or 200 kHz. Analysis was performed with Igor Pro 6.12 (Wavemetrics) using DataAccess (Bruxton Software) to import pClamp data. Voltage-clamp current records were corrected for linear capacitive and leak current by subtracting scaled responses to 5 mV hyperpolarizations delivered from the holding potential. Action-potential-clamp current records were corrected by subtracting current elicited by a scaled (0.1) inverted action potential waveform. In analyzing current clamp experiments, action potentials were defined using criteria of action potential peak >0 mV and height >40 mV.

Current clamp experiments were done using cells that had resting potentials negative to -50 mV, which showed robust and reproducible firing. The range of resting potentials for cells used in current clamp experiments in Figures 1.1, 1.2 and 1.14 was -50.7 to -86.6 mV (mean -65.4 ± 1.48 mV, n = 35). Action potentials in control were elicited from the cell's natural resting potential. CBD and bupivacaine often produced a depolarization of the resting potential, and a

steady negative current was injected to bring the membrane potential back to the control resting value in order to allow better comparison of action potentials.

Solutions. Current clamp recordings (and voltage clamp recordings of overall ionic currents) used external Tyrode's solution and an internal solution consisting of 140 mM K aspartate, 13.5 mM NaCl, 1.8 mM $MgCl_2$, 0.09 mM EGTA, 9 mM HEPES, 14 mM creatine phosphate (Tris salt), 4 mM MgATP, 0.3 mM Tris-GTP, pH 7.2 adjusted with KOH. Reported membrane potentials are corrected for a liquid junction potential of -10 mV between the internal solution and the Tyrode's solution in which current was zeroed before sealing onto the cell, measured using a flowing 3 M KCl reference electrode as described by Neher (1992). Voltage clamp recordings of sodium current used an internal Cs-based solution (140 mM CsCl, 13.5 mM NaCl, 1.8 mM $MgCl_2$, 0.09 mM EGTA, 9 mM HEPES, 14 mM creatine phosphate (Tris salt), 4 mM MgATP, 0.3 mM Tris-GTP, pH adjusted to 7.2 with CsOH and an external solution of Tyrode's solution with added 10 mM TEACl to inhibit potassium currents and 30 µM CdCl2 to inhibit voltage-dependent calcium currents. Currents through TTX-resistant sodium channels were isolated by including 300 nM TTX in the solution.

CBD was obtained as a 1 mg/mL solution in methanol (Sigma-Aldrich). The methanol was evaporated using a gentle stream of nitrogen and CBD was dissolved in dimethylsulfoxide (DMSO) to make a stock solution of 10 mM, which was aliquoted and stored at 4°C. In all experiments, control solutions were prepared to contain the same concentration of DMSO as the CBD-containing solutions to be tested. Some early experiments used the 1 mg/mL methanol solution as a stock solution, with equivalent methanol added to the control solutions. There was no obvious difference in the effects of CBD seen using methanol and DMSO stock solutions

but the higher-concentration DMSO stocks were preferred because previous control experiments have shown that DMSO at >1:1000 dilutions has no obvious effect on electrophysiological behavior of neurons. CBD was applied acutely in all experiments except in those of Figure 1.13B,C, where cells were pre-incubated in 300 nM CBD for 1-2 hours before recording.

Experimental Design and Statistical Analyses. Numbers of cells and animals used for each experiment are given in figure legends. Data are represented as mean ± SEM. P-values were calculated (in Microsoft Excel Version 140.7266.5000) using paired or non-paired Student's t-tests as appropriate. Data are available from the authors upon request.

Model. The model for state-dependent binding of CBD was implemented in IgorPro (Wavemetrics, Lake Oswego, OR) using fourth-order Runge-Kutta integration with a 200-µs step size. The parameters of the model were chosen in two steps. In the first, voltage-dependent rate constants were assigned for transitions between resting (R), fast inactivated (F), and slow inactivated (S) states in order to approximate the experimental measurements summarized in Figure 1.11, as well as roughly matching the kinetics of entry into slow and fast inactivated states described in Figures 1.7, 1.8, and 1.10, along with the more comprehensive measurements of kinetics in a previous study (Blair and Bean, 2003). To match experimental data, it was necessary to allow entry of channels into the slow inactivated state both directly from the resting state (the primary pathway for small depolarizations in the range from -60 to -40 mV, where fast inactivation is minimal) and also from the fast inactivated state, to describe entry into slow inactivation during prolonged steps to voltages where channels first enter into fast inactivated states (as for steps to 0 mV, Figure 1.8). The model was constructed to satisfy

microscopic reversibility; first choosing the forward and backward rate constants for movement between R to F, those for movement between R and S, and the forward rate constant from F to S, and then setting the rate constant for movement from S to F determined by the other rate constants to preserve microscopic reversibility. After setting the parameters for movement between the resting, fast inactivated and slow inactivated states, rate constants for binding and unbinding of CBD to each state were chosen by trial and error to match the experimental results for the shift in midpoint of availability curves determined with 50-ms conditioning pulse (mostly but not exclusively fast inactivation) and with 5-sec conditioning pulses followed by 10-ms at -100 mV, which in control conditions measures the voltage-dependence of slow inactivation.

Results

CBD reduces the excitability of nociceptors

We first tested the effect of CBD on action potential firing of acutely dissociated small-diameter DRG neurons in current clamp. The identity of neurons as nociceptors was confirmed by inward currents at -70 mV induced by 1 µM capsaicin applied at the end of each recording and only capsaicin-sensitive neurons were included in the analysis. CBD dramatically reduced the number of action potentials during step current injections (Figure 1.1). At 2 µM, CBD reduced the number of action potentials evoked by an 80-pA current injection from 17.1 ± 2.9 in vehicle to 2.0 ± 1.0 in 2 µM CBD (n = 14 pairs, p= 0.0002). Remarkably, the effects of CBD were more dramatic than those of bupivacaine, one of the most potent local anesthetics, which reduced firing evoked by an 80-pA curent injection from 20.1 ± 6.2 action potentials in vehicle to 10.6 ± 4.0 in 2 µM bupivacaine (n = 7 pairs, p= 0.02) (Figure 1.1 C)

Figure 1.1 Inhibition of action potential firing in mouse nociceptors by CBD compared to bupivacaine. A, Effect of 2 μM CBD on action potential firing elicited by 1-s current injections ranging from 15 pA to 80 pA in a capsaicin-sensitive mouse nociceptor. B, Collected results for number of action potentials during 1-s current injections in control and 2 μM CBD. Mean± SEM, n=14 pairs. C, Number of action potentials during 1-s current injections in control and 2 μM bupivacaine. Mean± SEM, n=7 pairs.

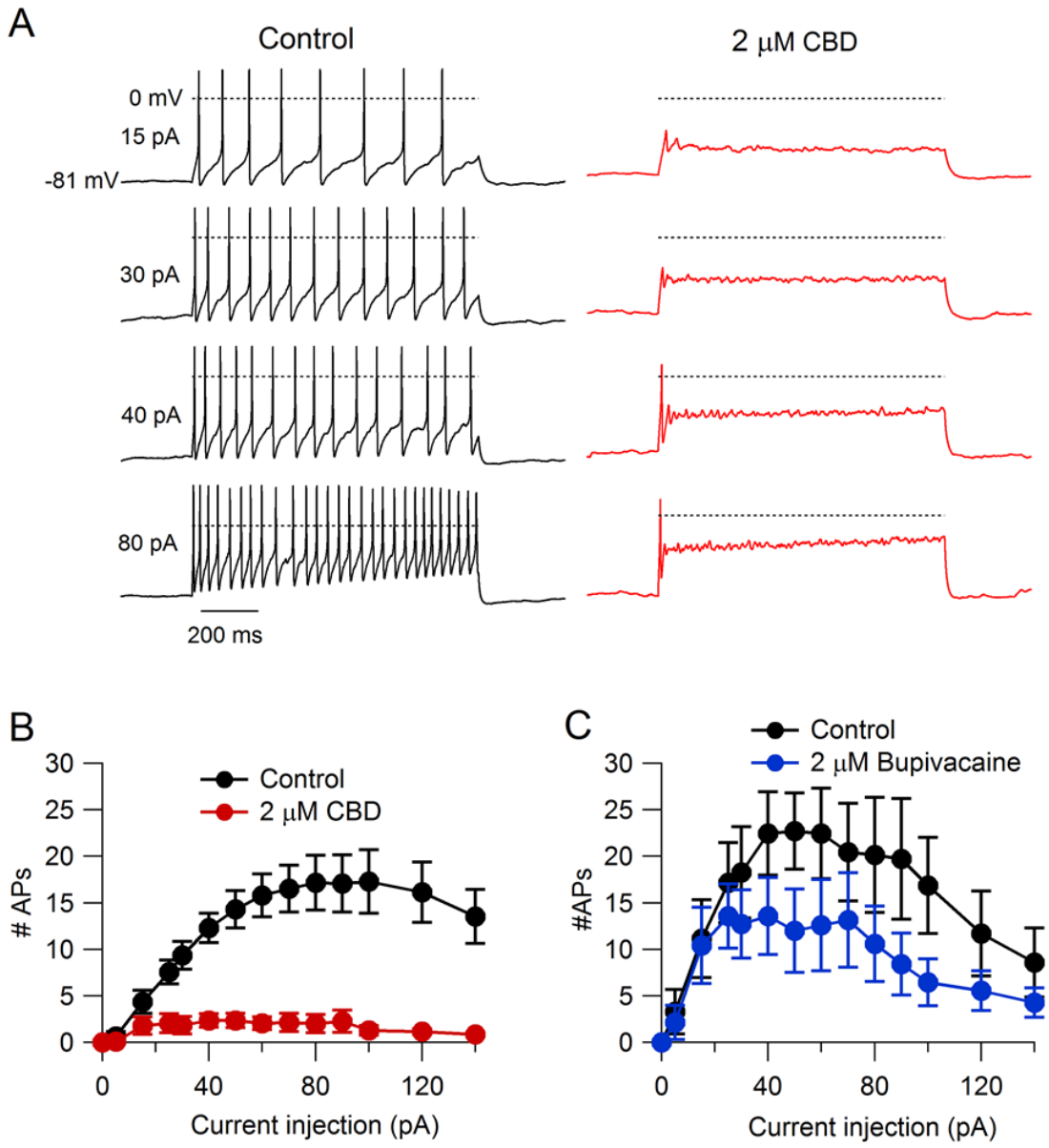

Figure 1.1 (Continued)

Figure 1.2 shows the effect of CBD on action potential shape. CBD decreased the height of the action potential (from 104 ± 3 mV in vehicle to 71 ± 6 mV in 2 µM CBD; n = 10 pairs, $p<0.0001$) , increased the width of the action potential (from 2.4 ± 0.1 ms in vehicle to 4.0 ± 0.3 ms in 2 µM CBD n = 10 pairs, $p= 0.0002$), and produced a depolarizing shift in the trough of the first action potential during a current injection (from -75.3 ± 2.3 mV in vehicle to -65.8 ± 2.8 mV in 2 µM CBD for a 40-pA current injection , n= 10 pairs, $p<0.0001$). Bupivacaine had smaller effects on all of these parameters (Figure 1.2C-E).

Figure 1.2 Effect of CBD on action potential shape compared to bupivacaine. A, The first action potential evoked by a 1-s 80-pA current injection in control and 2 μM CBD (same cell as Figure 1.1). **B,** The first action potential evoked by a 1-s 40-pA current injection in control and 2 μM bupivacaine. **C,** Collected results for the effect of 2 μM CBD (n=10) or 2 μM bupivacaine (n=6) on the peak of the first action potential elicited by 40-pA current injections. Control to 2 μM CBD, $p<0.0001$. Control to 2 μM bupivacaine, $p=0.07$. **D,** Collected results for the effect of 2 μM CBD (n=10) or 2 μM bupivacaine (n=6) on the width of the first action potential (measured at half action potential height). Control to 2 μM CBD, $p=0.0002$. Control to 2 μM bupivacaine, $p=0.27$. **E,** Collected results for the effect of 2 μM CBD (n=10) or 2 μM bupivacaine (n=6) on the membrane potential of the trough after the first action potential. Control to 2 μM CBD, $p<0.0001$. Control to 2 μM bupivacaine, $p=0.009$.

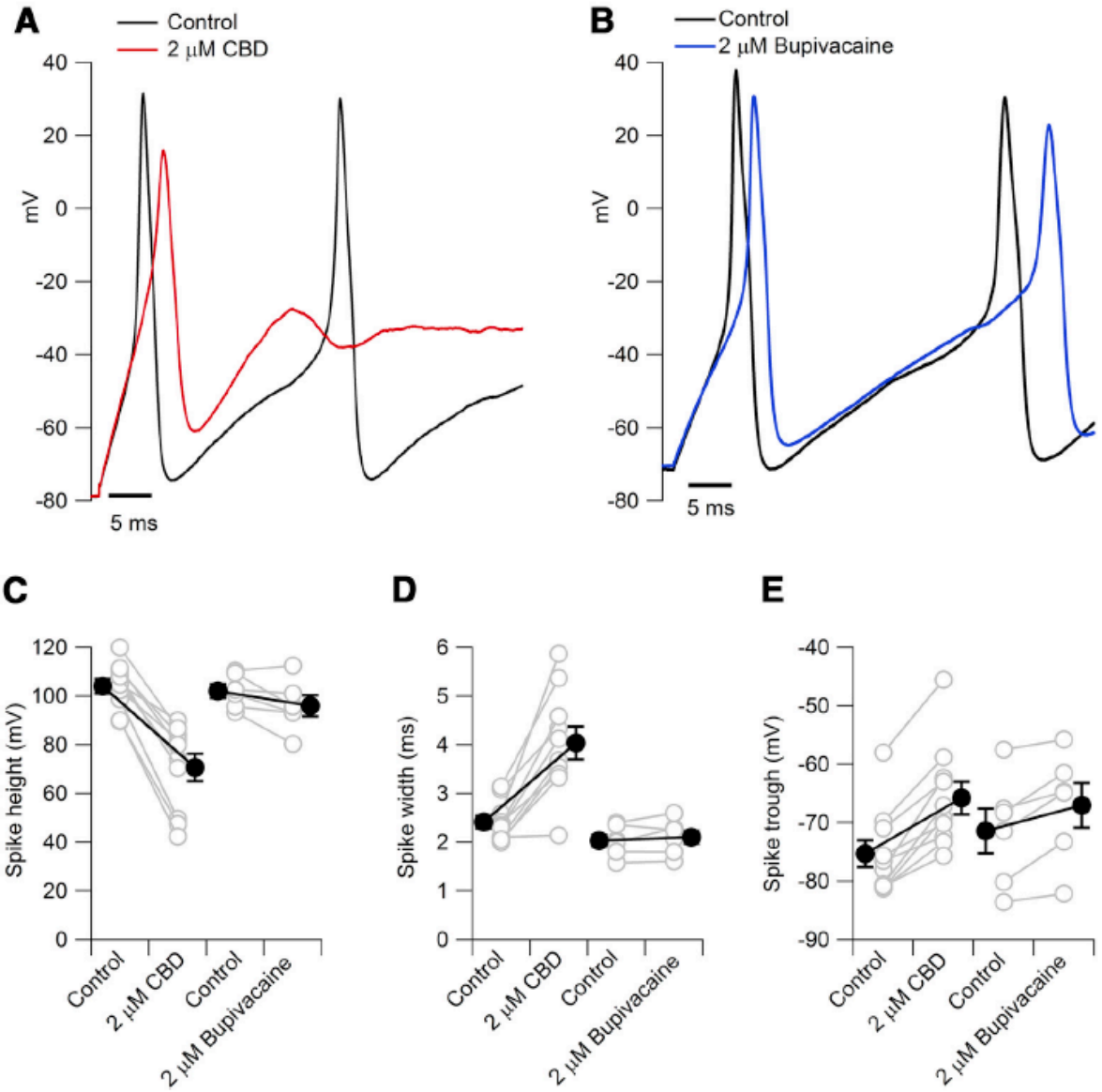

Figure 1.2 (Continued)

CBD inhibits voltage-activated inward and outward currents

To explore the action of CBD on particular ion channels in nociceptors, we next did a series of voltage clamp experiments. Examining overall currents evoked by voltage steps from -80 mV, CBD produced a dose-dependent reduction of both inward and outward components of current (Figure 1.3). Inhibition of inward currents was more dramatic than inhibition of outward currents. In collected results, the peak inward current at -10 mV was reduced by 2 µM CBD to 60 ± 4% of control (n = 13 pairs, p<.0001) and by 5 µM CBD to 21 ± 2% of control (n = 7 pairs, p<0.0001). Peak outward current measured at +20 mV was reduced to 83 ± 3% by 2 µM CBD (n = 13 pairs, p<.0001) and to 60 ± 4% by 5 µM CBD (n = 7 pairs, p<.0001).

Figure 1.3 Effect of CBD on overall voltage-activated currents in nociceptors. A, Currents evoked by depolarization before and after 2 µM CBD. 200-ms voltage steps were applied at 0.2 Hz from a holding voltage of -80 mV. B, Effect of 2 µM CBD on peak inward and peak outward currents as a function of test pulse voltage. Same cell as in A. C, Collected results for inhibition of peak currents evoked by voltage steps from -80 mV to -10 mV (inward current) and +20 mV (outward current). Mean± SEM, n=8 for 2 µM CBD and n=7 for 5 µM CBD.

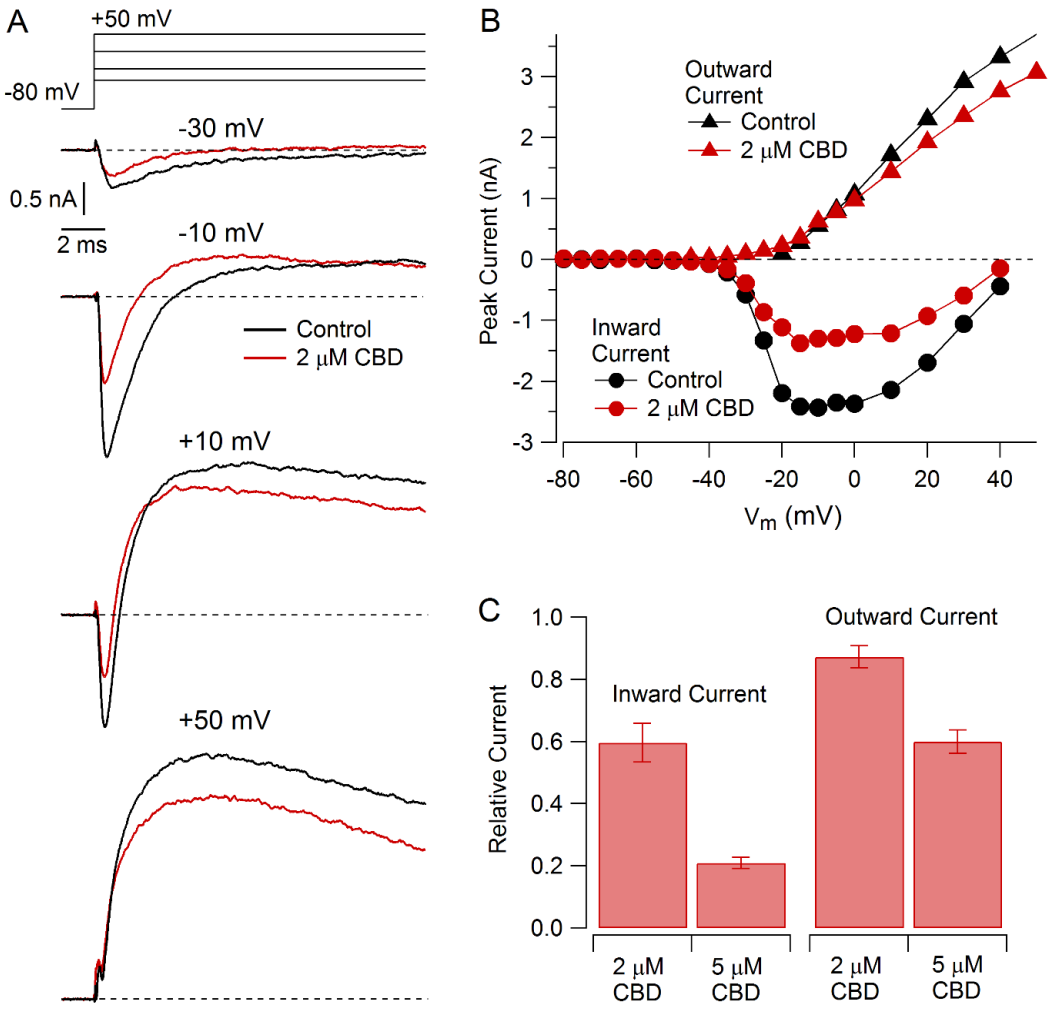

Figure 1.3 (Continued)

Previous work has shown the ability of CBD to inhibit a number of different types of heterologously-expressed sodium channels (Hill et al., 2014; Ghovanloo et al., 2018; Patel et al., 2016; Mason and Cummins, 2020) as well as native sodium currents in cultured cortical neurons (Hill et al., 2014). Quantifying the concentration-dependent effects of CBD is less straightforward than for many agents because the approach to steady-state can be very slow. For example, Hill et al. found that 10 µM CBD inhibited sodium current in cultured cortical neurons slowly at room temperature, requiring about 20 minutes to approach an average steady-state inhibition by ~70%. Interestingly, Ghovanloo et al. (2018) found that CBD inhibited heterologously-expressed Nav1.2 channels in HEK-293 cells more slowly and less potently at 33°C than 20°C, suggesting the importance of testing on native neurons at physiological temperature. Figure 1.4 shows the time-course of inhibition of sodium current in mouse nociceptors at 37°C. The time-course of inhibition by 5 µM CBD could be fit by an exponential function with an average time constant of 76 ± 8.7 ms (n=8), so that steady-state was approached in 4-5 minutes. On washout of CBD, there was progressive reversal of its effects (Figure 1.4), but this was so slow that it was incomplete even after more than 10 minutes of washing and we did not attempt to quantify the recovery kinetics.

Figure 1.4 Time-course of CBD inhibition of voltage-activated sodium current. A, Inhibition by 5 µM CBD of sodium current evoked by a 15-ms step from -70 mV to 0 mV applied every 5 seconds. Red line: Fit of a single exponential curve (τ = 65.2 seconds). Inset: Current in control and in 5 µM CBD. **B**, Collected results for effect of 5 µM CBD on total sodium current after inhibition reached steady-state. N=8, red symbol mean± SEM. **C**, Collected results for time-constant of inhibition. N=8, red symbol mean± SEM.

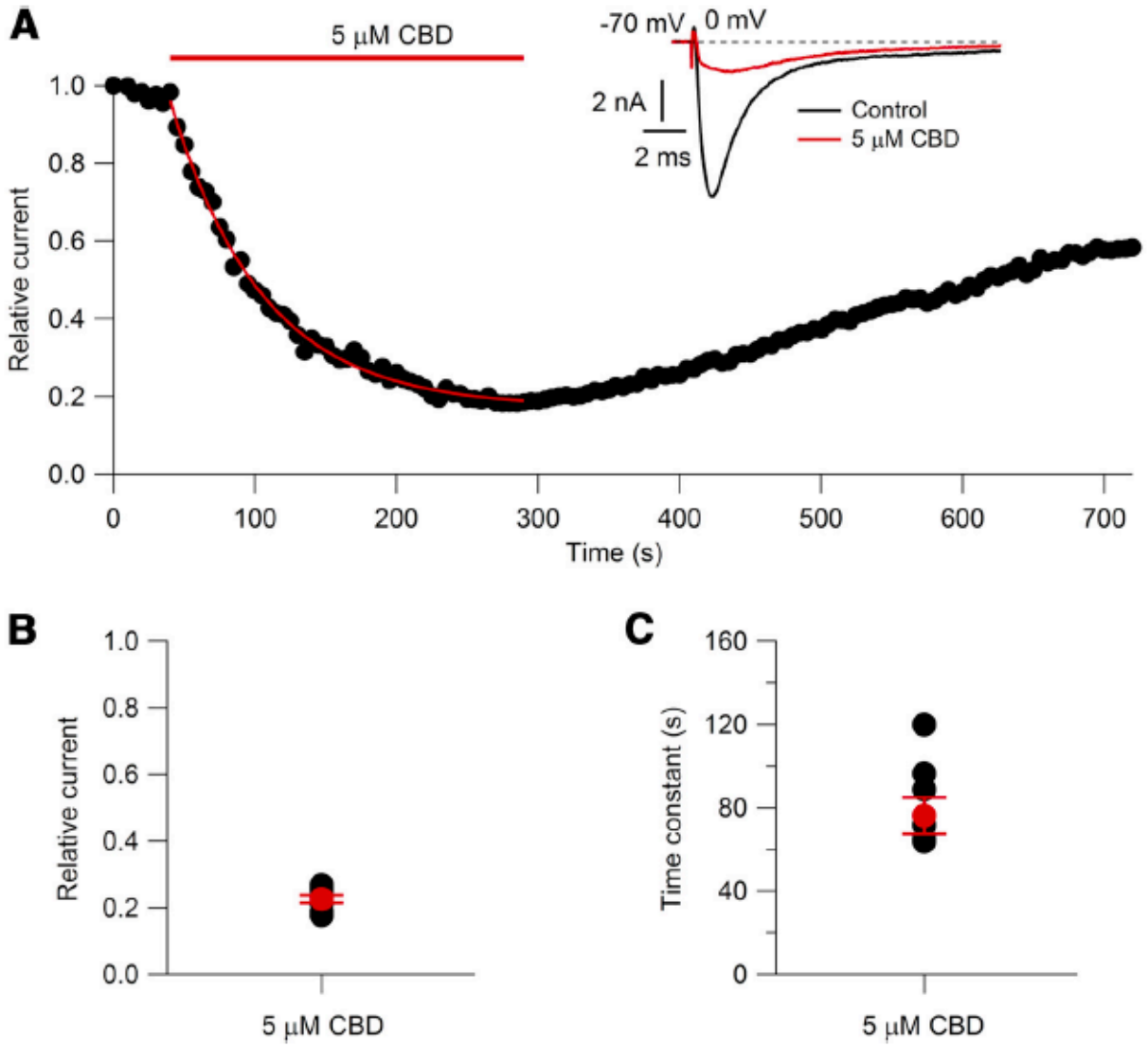

Figure 1.4 (Continued)

We were particularly interested in characterizing the effects of CBD on native TTX-resistant sodium channels, because Nav1.8-mediated TTX-resistant sodium current is prominent in small-diameter DRG neurons (Roy and Narahashi, 1992; Rush et al., 1998), carries the majority of the sodium current during action potentials in rat primary nociceptors (Renganathan et al., 2001; Blair and Bean, 2002), and is critical for supporting repetitive firing of small-diameter DRG neurons (Renganathan et al., 2001; Blair and Bean, 2002; Rush et al., 2007). The effects of CBD on this current have not been previously described. Figure 1.5 shows the results of experiments characterizing the effect of CBD on the TTX-sensitive and TTX-resistant components of sodium current in a mouse nociceptor, taking advantage of the rapid onset and reversibility of TTX inhibition to isolate TTX-S and TTX-R components of current before and after CBD inhibition. Studied with test pulses delivered from a holding potential of -70 mV, CBD inhibited both components of current with similar potency, with 5 μM CBD inhibiting TTX-S current to an average of 9 ± 2% of control and TTX-R current to 15 ± 2% of control ($n=7$, $p<0.001$ for TTX-S and TTX-R current).

Figure 1.5 CBD inhibition of TTX-S and TTX-R components of sodium current. A, Voltage protocol for currents shown in C and D. Depolarizing steps (100-ms) were applied from a holding voltage of -70 mV at 0.2 Hz. B, Solution sequence for isolating TTX-S and TTX-R components before and after CBD. C, TTX-S currents evoked before and after 5 μM CBD. D, TTX-R currents evoked before and after 5 μM CBD.

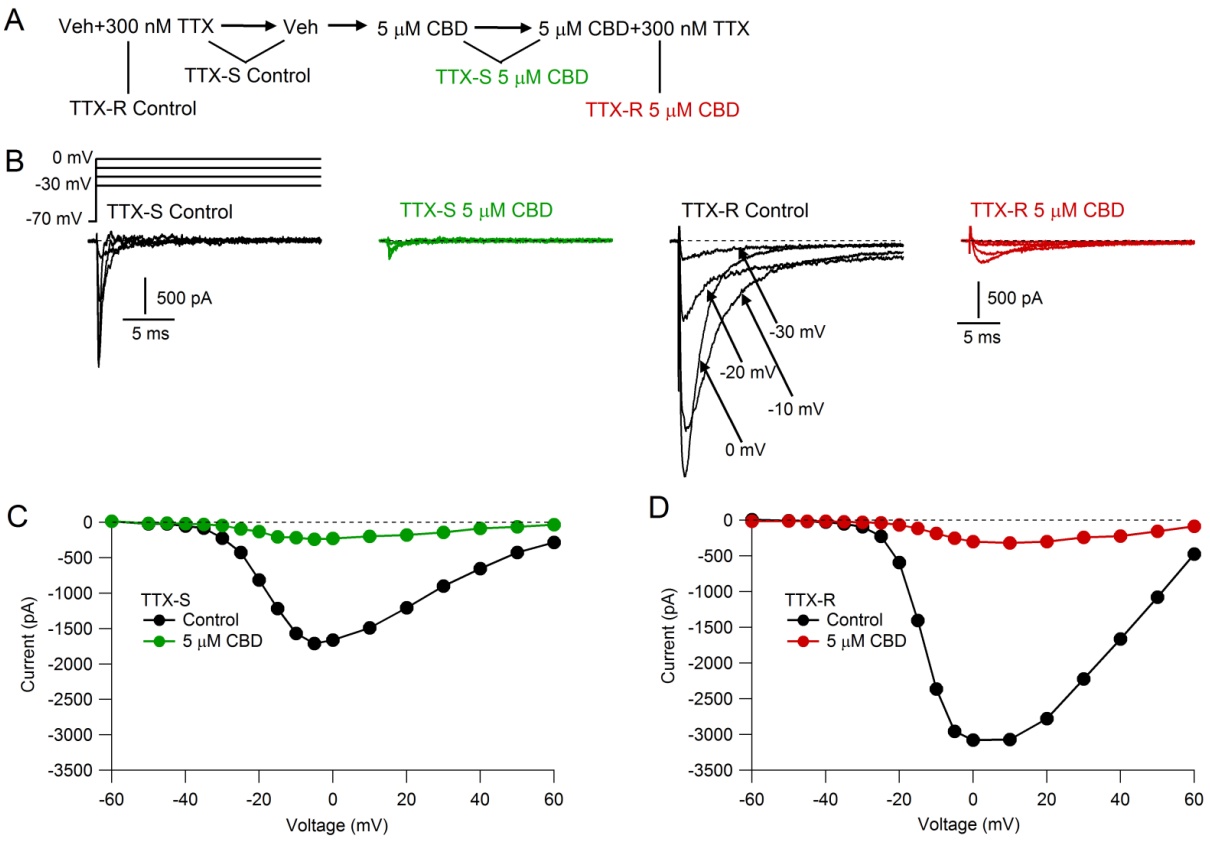

Figure 1.5 (Continued)

Use-dependent inhibition of action potential-evoked sodium currents

We next examined the effects of CBD on TTX-S and TTX-R currents flowing during physiological action potential waveforms, performing action potential clamp experiments with a previously recorded action potential waveform recorded at 37 °C. As expected from the ability of TTX-S channels to be activated by smaller depolarizations and with more rapid kinetics, the TTX-S component of overall sodium current flowed earlier in the action potential than TTX-R current (Figure 1.6A, B). To explore possible use-dependent effects on CBD inhibition, the action potential waveform was delivered at frequencies of either 5 Hz or 20 Hz. Both TTX-S and TTX-R current showed substantial frequency-dependent reduction in control solutions, with TTX-S current during the 60th action potential reduced to 72 ± 5% of that evoked by the first action potential during 5 Hz stimulation and to 52 ± 5% during 20 Hz stimulation (n=8). TTX-R current showed slightly less frequency-dependent reduction, with TTX-R current during the 60th action potential reduced to 80 ± 5% of that evoked by the first action potential during 5 Hz stimulation and to 56 ± 7% during 20 Hz stimulation (n=8). CBD inhibited both TTX-S and TTX-R components of current in a use-dependent manner. Application of 2 μM CBD reduced the TTX-S current evoked by the first action potential to 45 ± 5% of control (n=8) and TTX-R current to 67 ± 8% of control (n=8). After stimulation at 20 Hz, 2 μM CBD reduced TTX-S current during the 60th action potential to 37 ± 6% compared to the current evoked by the 60th action potential in control (and to 18 ± 2% compared to the current evoked by the first action potential in control) and CBD reduced TTX-R current during the 60th action potential to 40 ± 7% compared to the current evoked by the 60th action potential in control (and to 25 ± 7% compared to the current evoked by the first action potential in control). Use-dependent

reduction of both TTX-R and TTX-S current was also seen to a lesser extent with 5 Hz stimulation (Figure 1.6C). Thus, 2 μM CBD produces both tonic and use-dependent reduction of both TTX-S and TTX-R currents during stimulation by physiological waveforms at physiological frequencies at physiological temperature.

Figure 1.6 Use-dependent inhibition by CBD of TTX-S and TTX-R currents evoked by action potential waveforms. A, left: TTX-S and TTX-R sodium currents evoked by action potential waveforms delivered at 5 Hz in a nociceptor in control. A previously-recorded AP waveform evoked by a 0.2 ms current injection was used as command voltage, with membrane potential held at -80 mV for 10 s before delivery of action potential waveforms repeated at 5 Hz. Solid lines: currents elicited by the 1st action potential waveform; dashed lines: currents elicited by the 60th action potential waveform. Right: Same cell in 2 μM CBD. B, Collected results showing the change in action potential-evoked TTX-R and TTX-S sodium currents produced by 5 Hz stimulation in the absence and presence of 2 μM CBD. Mean± SEM, N=8, for TTX-S current, $p=0.0014$ for 1st AP control, $p<0.0001$ between 1st AP 2 μM CBD and 60th AP 2 μM CBD; for TTX-R current, $p=0.01$ for 1st AP control, $p<0.0001$ between 1st AP 2 μM CBD and 60th AP 2 μM CBD. C, collected results with 20 Hz stimulation. Mean± SEM, N=8, for TTX-S current, p= p <.0001 for 1st AP control, $p = 0.00013$ between 1st AP 2 μM CBD and 60th AP 2 μM CBD; for TTX-R current, p= 0.0006 for 1st AP control, $p <0.0001$ between 1st AP 2 μM CBD and 60th AP 2 μM CBD.

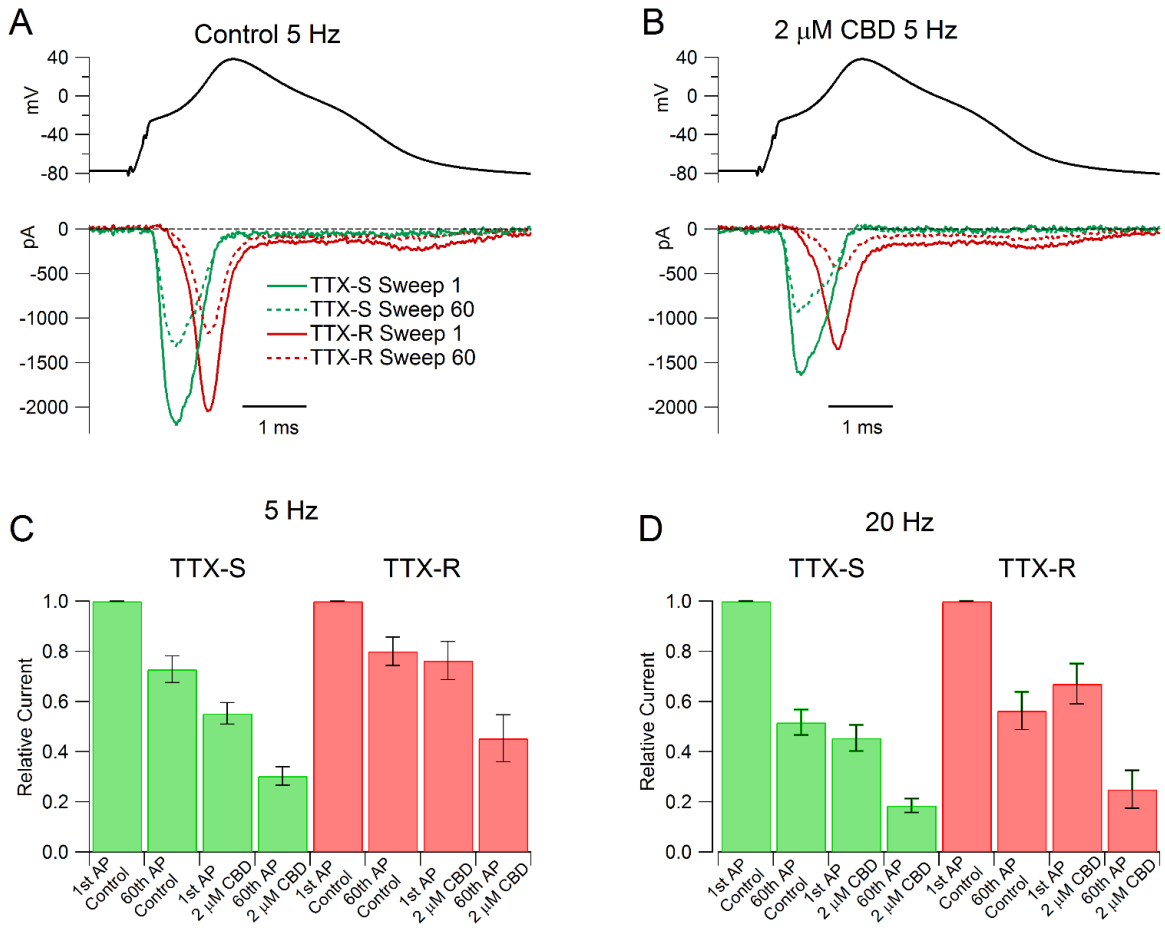

Figure 1.6 (Continued)

CBD slowing of recovery of availability of TTX-R channels

The use-dependent inhibition of TTX-R current by CBD suggests that channel inhibition is increased during repeated depolarizations and that the extra inhibition does not recover completely in between depolarizations. To explore how CBD alters recovery of channel availability of TTX-R channels, we used a two-pulse experiment (Figure 1.7). A 20-ms conditioning pulse to 0 mV induced inactivation, and after a variable time at -70 mV a test pulse assayed the recovery of channel availability. In control, about 85% of the channels recovered quickly from inactivation, with a time constant (fit to collected data) of 1.03 ms. Interestingly, however about 10% of the channels did not fully recover even in 300 ms, the longest time tested in this protocol. CBD reduced the sodium current evoked by the first pulse to 0 mV and also dramatically slowed the recovery of channel availability of the remaining channels after they experienced the 20-ms depolarization to 0. In the presence of CBD, recovery of availability occurred with two phases, a fast component similar to recovery of channels in control (making up 28% of the total extent of recovery in 300 ms) and a larger much slower component that could be fit reasonably well by a time constant of 66 ms.

Figure 1.7 Effect of CBD on the time course of the recovery of availability of TTX-R sodium channels following a 20-ms prepulse to 0 mV. A, Following the 20-ms prepulse to 0 mV, a 3-ms test pulse to 0 mV assayed the fraction of available channels following various times at -70 mV. B,C Recovery of availability in 10 msec at -70 mV in control and (in the same cell) in the presence of 5 µM CBD. D,E, Collected results for recovery of availability in control (black) and 5 µM CBD (red) for this protocol (mean ± SEM, n=6 pairs). Recovery in control was fit by a single exponential of 1.03 ms to an asymptote of 0.85; recovery in 5 µM CBD was fit by a double exponential to an asymptote of 0.80, with a fast time constant (a fraction of 28%) set to match the recovery of unmodified channels together with a dominant slower time constant (66 ms).

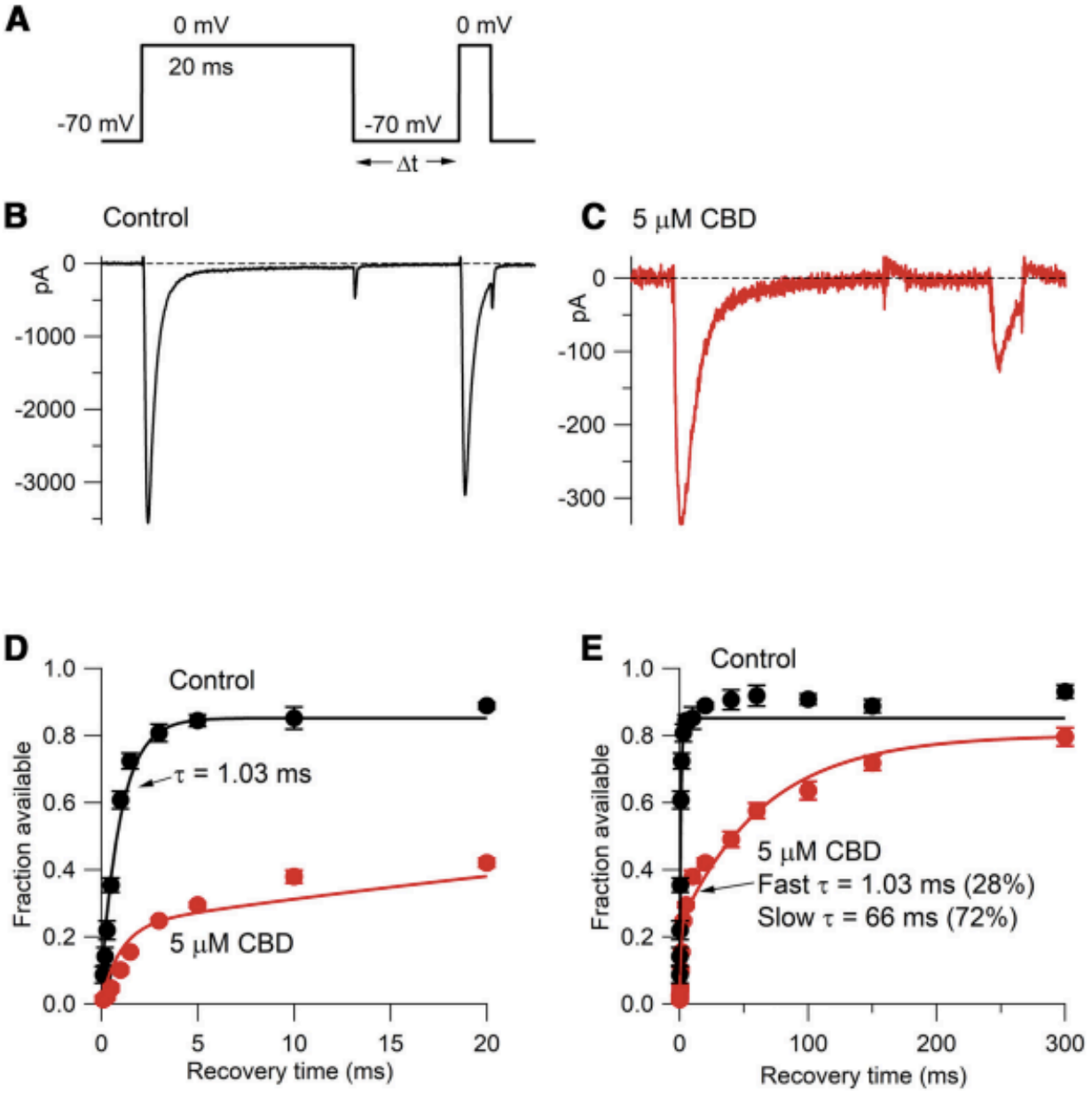

Figure 1.7 (Continued)

A reasonable interpretation of this result is that during the 20-ms conditioning step to 0 mV, CBD binds to a fraction of channels that were initially unbound at the holding voltage of -70 mV, presumably reflecting tighter binding to inactivated channels than resting channels, and that the recovery of availability in CBD occurs by the CBD-bound inactivated channels converting to CBD-bound resting channels followed by unbinding of CBD from the channels now in the lower-affinity resting state. With this sequence, the recovery of availability in CBD is slower than in control because it requires an extra unbinding step. It is also possible that the recovery of CBD-bound inactivated channels occurs by CBD first unbinding from the inactivated state followed by recovery from the unbound inactivated state to the unbound resting state. With either route, CBD must unbind for channels to become available, and the rate of recovery is slowed because of this additional step. (In the model of Figure 1.12, CBD-bound inactivated channels recover to the unbound resting state mainly by the first route, with additional slowing of recovery because the movement of CBD-bound inactivated states to CBD-bound resting states is slower than movement of CBD-free inactivated channels to resting channels).

We then explored how quickly inactivated channels bind CBD to enter slowly recovering states (Figure 1.8) by varying the duration of a prepulse to 0 mV followed by 6 ms at -70 mV, a duration that allows nearly complete recovery of unmodified inactivated channels but little recovery of CBD-bound channels. In the presence of CBD, the slowly-recovering fraction of channels began to develop within a few ms during depolarization, and the development of slowly-recovering channels could be fit by a time constant of 8.5 ms. We interpret this as reflecting the time course with which CBD binds to inactivated states of the channels to produce “extra” inhibition over that present at the holding voltage of -70 mV.

Figure 1.8 Time-course of CBD-induced entry into slowly recovering states of TTX-R channels. A, Voltage protocol (top) and currents in control (middle) and after application of 5 μM CBD (bottom), with a prepulse duration of 20 ms. B, Collected results (mean ± SEM, n=6 pairs) for fraction of available channels after pre-pulse conditioning in control (black) and in 5 μM CBD (red). Solid red curve: single exponential of time constant 8.5 ms.

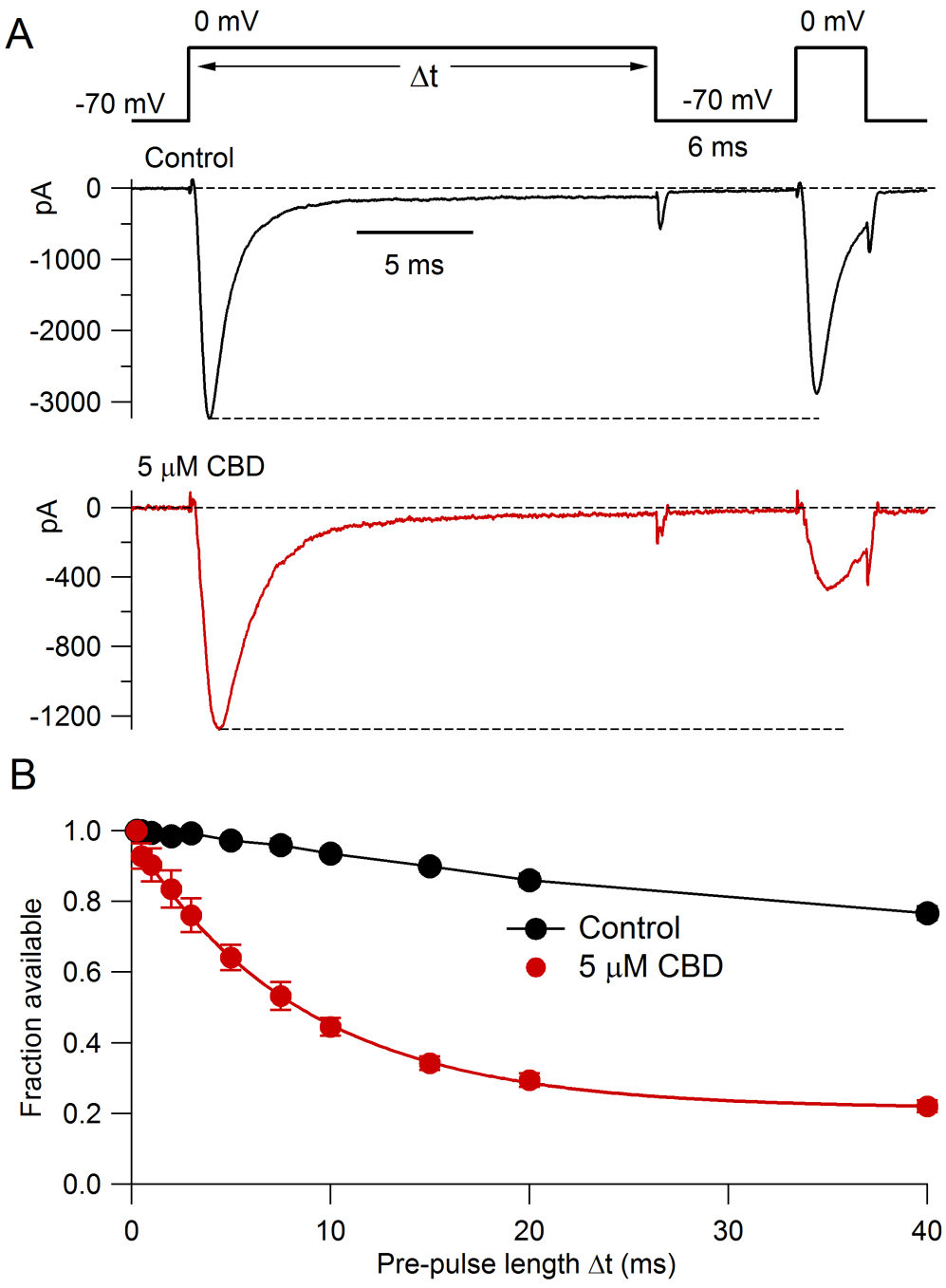

Figure 1.8 (Continued)

Interestingly, even in control conditions a small but significant fraction of channels entered slowly-recovering states during prepulse durations greater than about 5 ms. In control, the fraction of slowly-recovering channels reached an average of 24% ± 1% with a 40-ms prepulse. This can be interpreted as reflecting entry of unmodified TTX-R channels into a slow inactivated state from which recovery is slow (Roy and Narahashi, 1992; Rush et al., 1998; Blair and Bean, 2002; Tripathi et al., 2006; Choi et al., 2006, 2007; Binshtok et al., 2008). Even with a prepulse of 20 ms, about 10% of channels enter the slow inactivated state.

The main purpose of the experiments shown in Figures 1.7 and 1.8 was to illustrate the action of CBD to place TTX-R channels into a state from which channel availability recovers far more slowly than in control. A secondary observation in these experiments was that the currents in the presence of CBD had slower decay kinetics than in control. For example, the currents evoked by the 20-msec conditioning pulse in Figure 1.7 decay with a time constant of 0.87 ms in control and with a time constant of 1.40 ms in the presence of 5 μM CBD. The slower decay of currents in CBD was seen systematically (e.g. Figure 1.8A) and the difference did not result from the different sizes of the currents (such as might be produced by a series resistance error) because the decay kinetics of currents in control showed little or no change as the size of the test pulse current evoked by a pulse to 0 mV changed over a ten-fold range with different degrees of recovery from inactivation. Whether the slower decay of TTX-R currents reflects differential inhibition by CBD of multiple populations of TTX-R channels with different kinetics or an effect of CBD on kinetics of a homogeneous population of channels remains to be determined and might be best approached using cloned channels.

Altered availability of TTX-R sodium channels with CBD

To determine quantitatively how tightly CBD binds to inactivated channels, we characterized the effect of CBD using conditioning pulses to alter the distribution of channels between resting and inactivated states. With such protocols, tighter binding of drug to inactivated states compared to resting states is manifested by a change in the voltage-dependence of channel availability and the shift in the midpoint of channel availability can be used to estimate the K_d for drug binding to the inactivated state (Bean et al., 1983). Figure 1.9A shows results from experiments using 50-ms conditioning pulses, long enough to reach steady-state for conventional fast inactivation (Blair and Bean, 2002). With this protocol, 5 μM CBD produced a shift in mid-point of channel availability of -7.6 ± 0.4 mV (n=6). Because of the evidence for an important physiological role of slow inactivated states of Nav1.8 channels for controlling nociceptor excitability (Rush et al., 1998; Tripathi et al., 2006; Blair and Bean, 2003; Choi et al., 2007) we also examined longer conditioning pulses. We found that the shift of channel availability became progressively larger with longer conditioning prepulses, with a shift of mid-point of -10.6 ± 0.5 mV (n=5) for 200-ms conditioning pulses (Figure 1.9B) and -15.7 ± 0.6 mV (n=4) for 5-s conditioning pulses (Figure 1.9C). Bupivacaine produced similar but smaller effects on channel availability, with 5 μM bupivacaine producing a -10.9 ± 0.8 mV (n=6) shift in the midpoint of availability with 5-s conditioning pulses. Thus, the stronger effects of CBD on nociceptor firing compared to bupivacaine are paralleled by stronger effects on channel availability, suggesting tighter binding of CBD to inactivated states of TTX-R channels compared to bupivacaine.

Figure 1.9 Alteration of availability of TTX-R sodium channels by CBD. A, Voltage-dependent availability of TTX-R sodium channels measured by a 3-ms test pulse to 0 mV following 50-ms conditioning pulses in the absence (black) and presence (red) of 5 μM CBD. Availability is normalized to the maximal test pulse current measured in each condition. Symbols: mean ± SEM. Solid line: Boltzmann equation, $1/(1 + \exp((V - V_h)/k))$, where V is holding voltage, V_h is voltage of half-maximal availability, and k is the slope factor. Control: V_h = -22.2±1.4 mV, k = 4.6±0.1 mV; 5 μM CBD: V_h = -29.8±1.7mV, k = 6.1±0.4 mV. Values of V_h and k are mean values of fits to data from individual cells (n=6) and V_h is mean ± SEM for measurements in individual cells. B, Availability measured using 200-ms conditioning pulses. Symbols and statistics as in A. Control: V_h = -32.3 ± 0.4 mV, k = 4.7±0.4 mV; 5 μM CBD: V_h = -43.0±0.4 mV, k = 7.6±0.4 mV (n=5). C, Availability measured using 5-s conditioning pulses. Symbols and statistics as in A. Control: V_h = -36.7 ± 2.2 mV, k = 4.4±0.2 mV; 5 μM CBD: V_h = -52.5±2.1 mV, k = 5.0±0.0 mV (n=4).

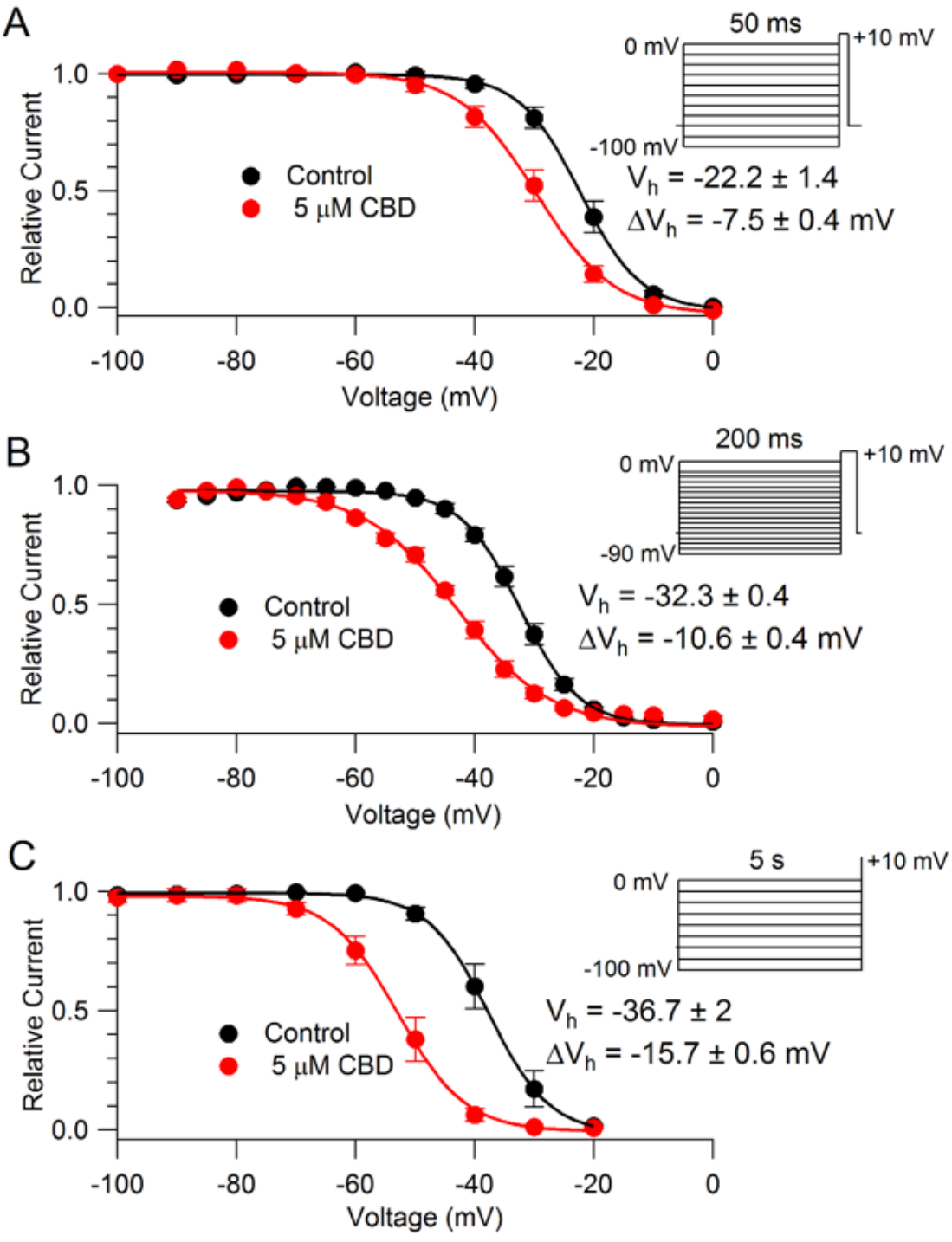

Figure 1.9 (Continued)

Time-course of recovery from slow inactivated states

The larger shifts in midpoint of channel availability with longer conditioning prepulses raises the possibility that CBD binds tightly to slow inactivated channels, which would be increasingly populated during longer conditioning pulses. We next designed protocols to test this idea. First, we tested the effect of CBD on recovery of availability using conditioning pulses designed to put channels into slow inactivated states. Figure 1.10 shows the effect of CBD on recovery of availability following long (300 ms or 10 s) depolarizations to 0 mV. To decrease the time required to assay the time course of recovery following long conditioning pulses, we used a pulse protocol in which the time course of recovery was determined in a single sweep, assaying availability by multiple short test pulses presented at a range of times after the long conditioning pulse. After a conditioning pulse of 300 ms under control conditions, channels recovered availability with a dominant time constant of 730 ms, far more slowly than the dominant time constant of 1 ms for recovery after a conditioning pulse of 20 ms (Figure 1.7). Following the 300 ms conditioning pulse, the time constant of 730 ms accounted for ~ 93% of the recovery of availability, with about 7% of the channels recovering within 2-3 ms. Thus it appears that ~93% of channels end up in a slow inactivated state after a 300 ms pulse to 0 mV. In the presence of 5 µM CBD, recovery of availability after a 300 ms conditioning pulse was slower, with a dominant time constant of about 2 seconds. This suggests that CBD binds to slow inactivated channels and that recovery of availability of CBD-bound slow inactivated states is even slower than recovery from normal CBD-free slow inactivated states

Figure 1.10 Time-course of recovery from fast inactivated and slow inactivated states in control. A, Voltage protocols. **B,** Time-course of recovery from inactivation at -70 mV following 20-ms (red symbols, mean ± SEM, n=6) or 300-ms (blue symbols, mean ± SEM, n=6) conditioning depolarizations. Black line: Single exponential function fit to first 10 ms of recovery following the 20-ms conditioning pulse. **C,** Recovery from inactivation shown on a longer time scale. Black line: Single exponential function fit to recovery after 300-ms conditioning pulse (fit to times from 200 ms to 6 seconds).

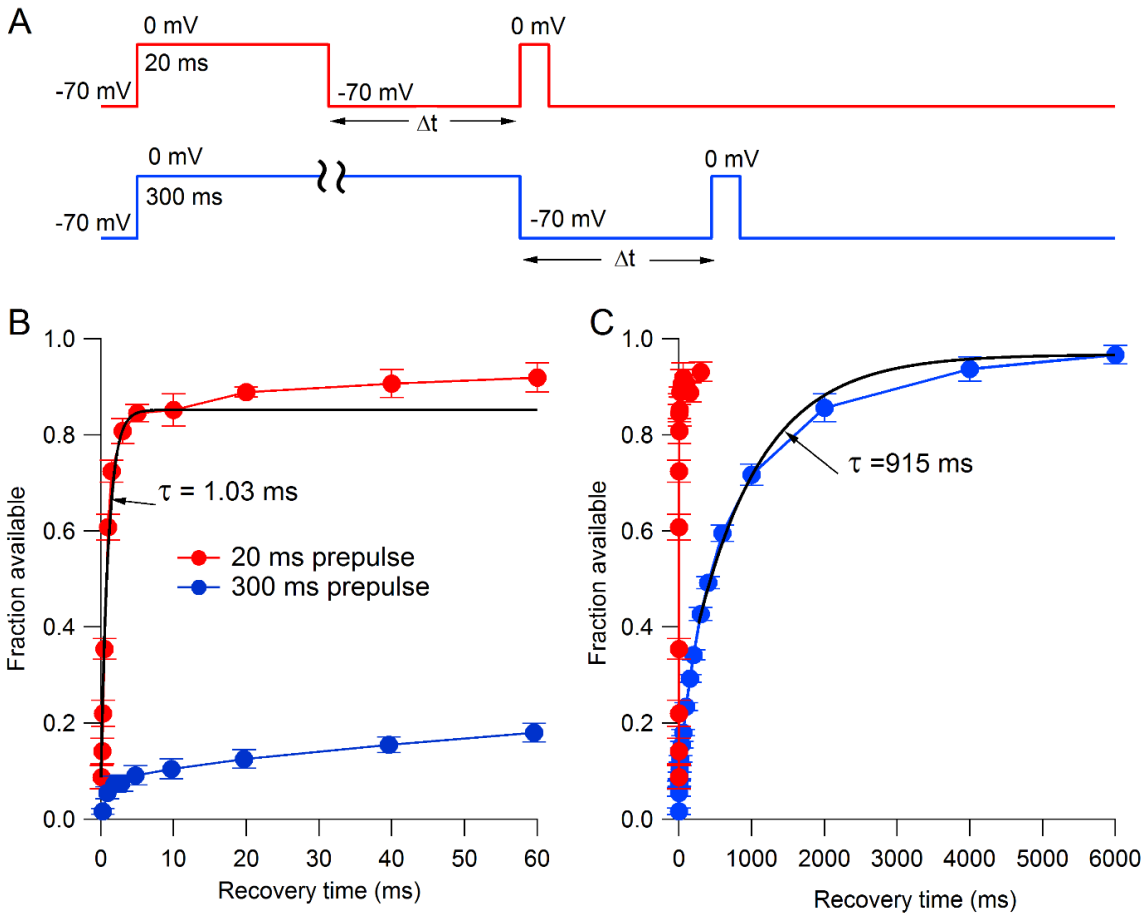

Figure 1.10 (Continued)

CBD binding to slow versus fast inactivated states

We next attempted to estimate quantitatively the binding affinity of CBD to fast and slow inactivated states. Figure 1.11 shows the results of an experiment designed to compare the voltage dependence of fast inactivation and slow inactivation in the same cell. The voltage-dependence of fast inactivation was assayed using 50-ms prepulses to various voltages followed by a test pulse to +10 mV. The voltage-dependence of channel availability could be fit well by a Boltzmann function with a midpoint of -21 and a slope factor of 5.0 mV (Figure 1.11A). Figure 1.11B shows the results in the same cell of a protocol designed to measure the voltage dependence of slow inactivation, using 5-s conditioning pulses to various voltages followed by 10-ms at -100 mV (long enough for complete recovery from fast inactivation but little recovery from slow inactivation) and then a test pulse. The voltage dependence of slow inactivation could be fit well by a Boltzmann function (going to zero) with a midpoint of –36.9 and a slope factor of 5.5 mV. Thus, slow inactivation has a midpoint about 16 mV hyperpolarized to that of fast inactivation (in collected results, -17 ± 1.4 mV more negative, n=6). It should be noted that the measurement of fast inactivation is not perfect because there is almost certainly some entry of channels into slow inactivation during the 50-ms conditioning pulse, because with 40-ms steps to 0 mV ~20% of channels enter slow inactivation (Figure 1.6). Thus if pure fast inactivation could be measured it would likely have a slightly depolarized midpoint compared to that measured with 50-ms conditioning pulses.

Figure 1.11 CBD alteration of availability of TTX-R sodium channels measured with protocols to emphasize fast or slow inactivation. A, Voltage-dependent availability of TTX-R sodium channels measured by a 3-ms test pulse to 0 mV following 50-ms conditioning pulses in the absence (black) and presence (red) of 5 µM CBD. Solid lines: Boltzmann equation, $I_{Max}/(1 + \exp((V - V_h)/k))$, where I_{Max} is maximal test pulse current ,V is holding voltage, V_h is voltage of half-maximal availability, and k is the slope factor. For the example cell, control: I_{Max} = -3866 pA, V_h = -21.0 mV, k = 5.0 mV; 5 µM CBD: I_{Max} = -1781 pA , V_h = -29.4 mV, k = 7.1 mV, Δ V_h = -8.4 mV. For collected results with 50-ms conditioning pulses: V_h = -22.2±1.4 mV, k = 4.6±0.1 mV; 5 µM CBD: V_h = -29.8±1.7mV, k = 6.1±0.4 mV. Δ V_h = -7.5±0.4 mV. B, Availability using a protocol to measure voltage-dependence of slow inactivation, with 5-s conditioning pulses followed by a 10-ms return to -100 mV to allow recovery from fast inactivation followed by the test pulse. Symbols as in A. For the example cell, control: I_{Max} = -3336 pA, V_h = -36.9 mV, k = 5.5 mV; 5 µM CBD: I_{Max} = -2190 pA ,V_h = -52.1 mV, k = 6.0 mV, ΔV_h = -15.2 mV. For collected results with 5-s conditioning pulses: control: Vh = -39.2±2.7 mV, k = 5.2±0.4 mV; 5 µM CBD: V_h = -53.0±3.3mV, k = 5.6±0.3 mV. ΔV_h= -13.7±1.4 mV

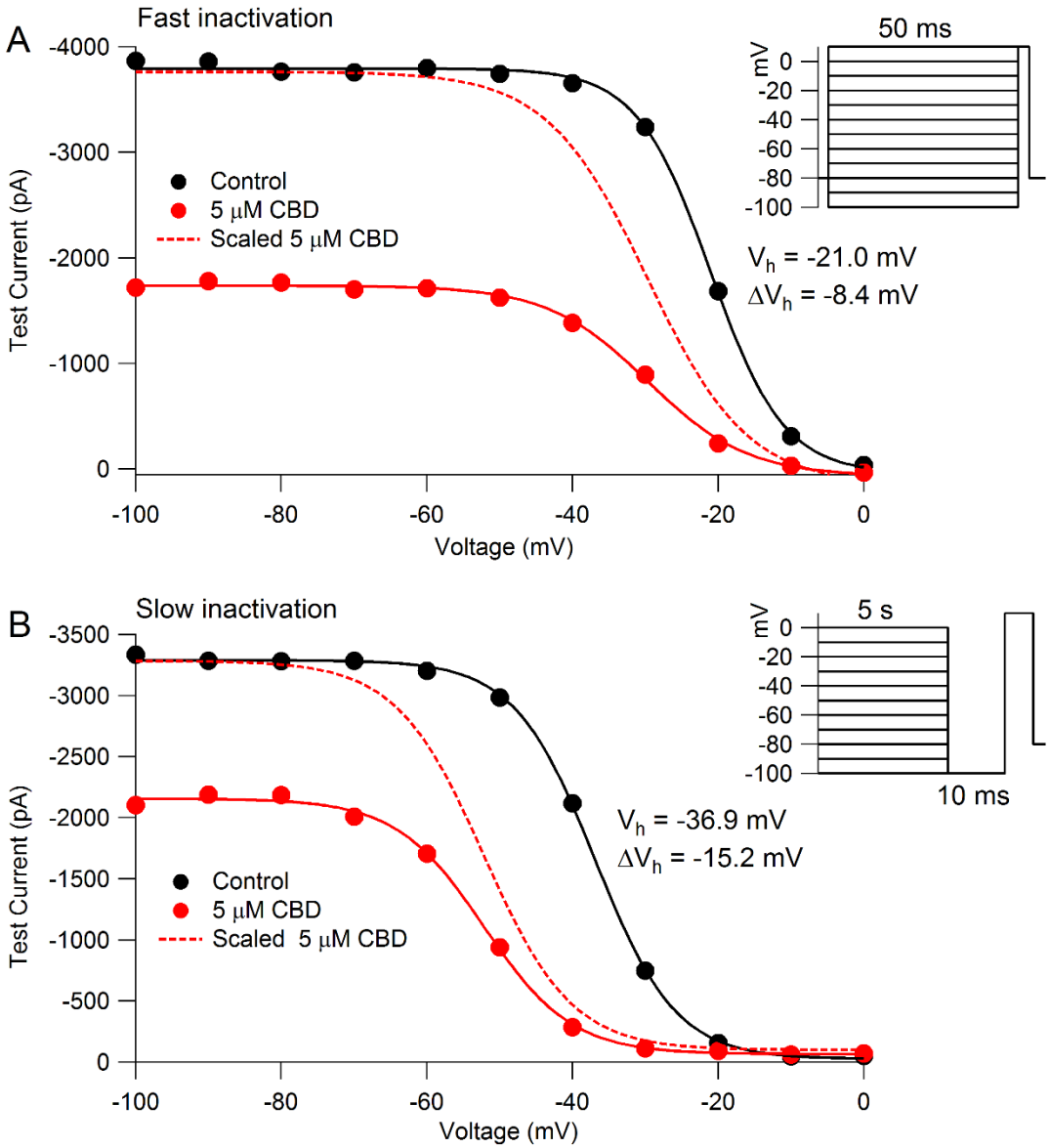

Figure 1.11 (Continued)

In these experiments, we also measured the effect of CBD on the voltage-dependence of channel availability measured with the two protocols. Consistent with the results in the protocols in Figure 1.9, CBD altered the midpoint of channel availability much more (-13.8 ± 1.5 mV) with the slow inactivation protocol than with the fast inactivation protocol (-7.6 ± 0.42 mV, measured in the same 6 cells).

Model for state-dependent CBD binding to Nav1.8 channels

These results suggest substantially tighter binding of CBD to slow inactivated states of the channel than to fast inactivated states. However, the pulse protocols do not cleanly separate fast inactivated from slow inactivated states. And although the shift in midpoint of availability is smaller in the protocol using 50-ms conditioning pulses, this could in principle be because 50-ms is too little time for CBD to reach steady-state binding (Karoly et al., 2010). To better quantify the affinity of CBD to the different states, we developed a model incorporating state-dependent CBD binding that gave a reasonable approximation of the experimental results (Figure 1.12) in terms of both voltage-dependence and time-dependence of the state-dependent effects, which can better distinguish binding to fast vs slow inactivated states (Karoly et al., 2010). Voltage-dependent rate constants for movement of channels between resting, fast inactivated, and slow inactivated channels were chosen to approximate experimental data for the voltage-dependent occupancy of the various states with conditioning pulses of various durations. Then, rate constants for CBD binding and unbinding to each state were developed that could roughly predict the shifts in midpoint of availability seen experimentally with short or long prepulses. The best match to experimental data was obtained by relatively weak binding to the resting state R (K_R=5 μM), much tighter binding to the fast

inactivated state F (K_F=0.60 μM), and even tighter binding to the slow inactivated state S (Ks=0.15 μM). The model is clearly oversimplified, because detailed kinetic models of fast inactivation would require multiple fast inactivated states corresponding to channels with different positions of the S4 voltage-sensing regions of the channel (distinguishing, for example, inactivation from various closed states and the open state). The assumption of a single slow inactivated state is also clearly over-simplified, because experiments like those in Figure 1.10 examining the rate of recovery from slow inactivated states show different rates depending on the conditioning pulse duration; this is similar to previous observations in Nav1.1 and Nav1.2 channels (Toib et al., 1998) and suggests the existence of multiple slow inactivated states (Vilin and Ruben, 2001). Nevertheless, the general result from the model that CBD binding to slow inactivated states must occur with higher affinity than binding to fast inactivated states seems unlikely to be changed by more detailed models incorporating multiple fast and slow inactivated states.

Figure 1.12 Model for CBD interaction with TTX-R Na channels. A, CBD is assumed to bind weakly to the resting state R (KR=5 μM), tightly to the fast inactivated state F (KF=0.60 μM), and more tightly to the slow inactivated state S (Ks=0.15 μM). Channels move between R, F, and S states with voltage-dependent rate constants chosen to approximate voltage-dependent occupancy in the different states with conditioning pulses of various durations (B-D). Channels move from R to F with a forward rate constant of 3/(1+exp(-(V+8.7)/6.5) and a backward rate constant of 0.12+ 0.9/(1+exp(V+23.7/6.5). Channels move from R to S with a forward constant of 0.004/(1+exp(-(V+14.3)/9.3)) and a backward constant of 0.004/(1+exp((V+64.3)/9.3)). Channels move from F to S with a forward rate constant of 0.005 and a backward rate constant determined by other rate constants to preserve microscopic reversibility. CBD binds to R with an on-rate (KonR) of 0.02 ms-1 μM-1 and unbinds with off-rate (koffR) of 0.1 ms-1. CBD binds to F with an on-rate (KonF) of 0.02 ms-1 μM-1 and unbinds with off-rate (koffF) of 0.012 ms-1. CBD binds to S with an on-rate (KonS) of 0.02 ms-1 μM-1 and unbinds with off-rate (koffS) of 0.003 ms-1. The rate constants for movements from R-CBD to F-CBD and F-CBD to S-CBD are the same as for movements from R to F and from F to S. To preserve microscopic reversibility, the rate constant for movement from F-CBD to R-CBD is multiplied by a factor of (koffF/koffR)*(konR/konF) relative to that for F to R and the rate constant for movement from S-CBD to F-CBD is multiplied by a factor of (koffS/koffF)*(konF/konS) relative to that for S to F. For preserving microscopic reversibility in the cycle of unbound and bound R and S states, the rate constant from R-CBD to S-CBD is the rate constant from R to S divided by the square root of (koffS/koffR)*(konR/konS) and the rate constant S-CBD to R-CBD is the rate constant from S to R multiplied by the square root of

(Continued) (koffS/koffR)*(konR/konS). B, Prediction of voltage-dependence of fast inactivation (red) and slow inactivation (blue) at equilibrium if each occurred in the absence of the other. C, Left, prediction of channel fraction in R state (i.e. available channels) after 50-ms conditioning pulses in control (solid black line) and with 5 µM CBD (solid red line). Dashed red line shows channel availability in CBD normalized to 1 at -100 mV. Right, Occupancy of channels in fast and slow inactivated states in control (solid lines) and occupancy of channels in the corresponding CBD-states with 5 µM CBD (dashed lines). D, Left, prediction of channel fraction in R state with the indicated protocol for measuring slow inactivation, with 5-s conditioning pulses followed by 10 ms at -100 mV to allow recovery of channels in the fast inactivated state. Right, Occupancy of channels in fast and slow inactivated states in control (solid lines) and occupancy of channels in the corresponding CBD-bound states with 5 µM CBD (dashed lines).

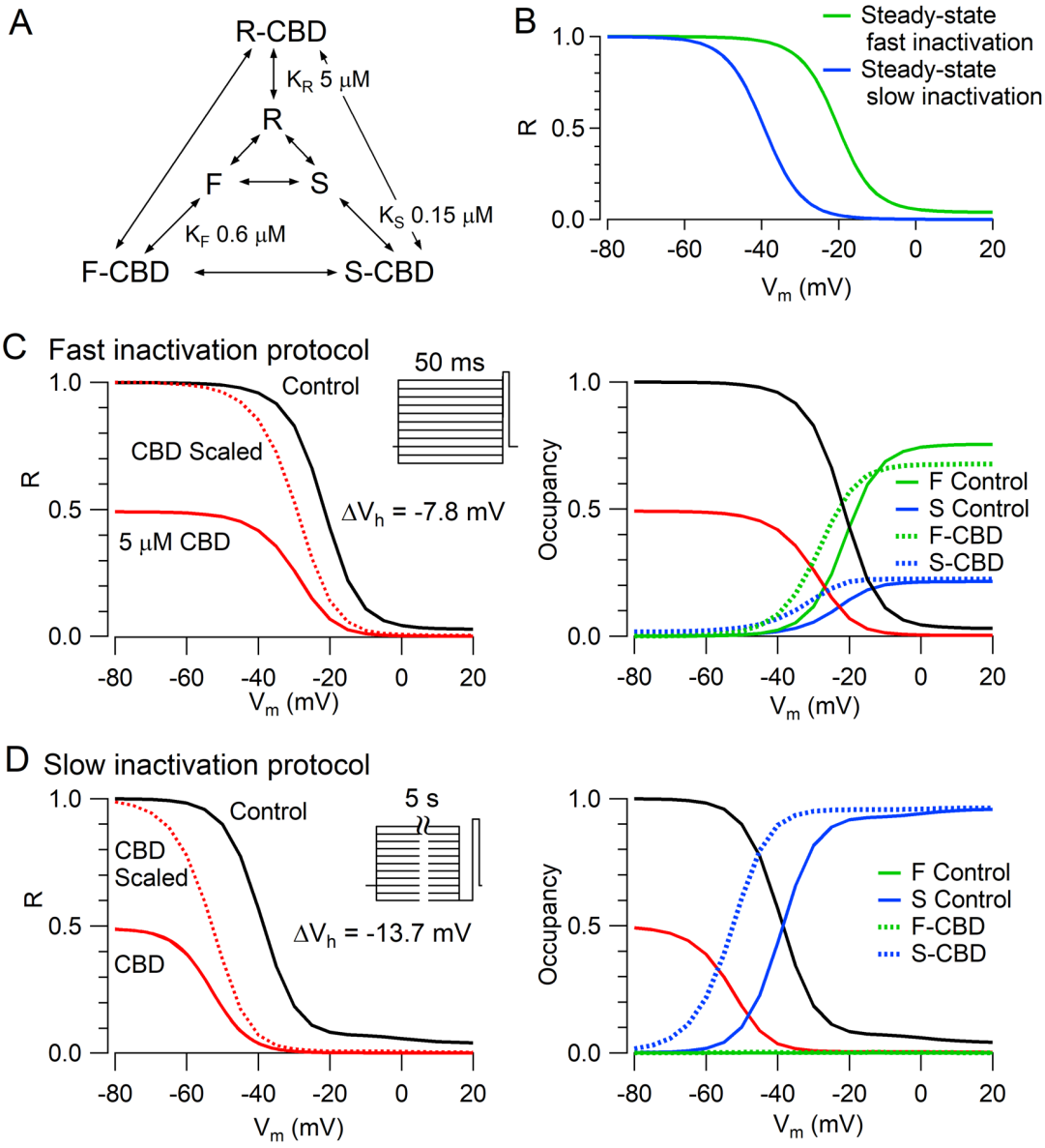

Figure 1.12 (Continued)

Although the model is designed mainly to interpret quasi-steady-state occupancy of the various states of the channel and not detailed kinetics, the chosen rate constants provide generally reasonable simulations of kinetics of development and recovery of availability in different conditions (for example, slowing of recovery of availability from CBD-bound states). In the model, rate constants for binding and unbinding of CBD from various states are much faster than the kinetics of development of CBD inhibition and recovery from CBD inhibition when CBD is washed on and washed off cells (e.g. Figure 1.4). We believe the slow kinetics of wash-on and wash-off likely reflect slow equilibration of CBD between the aqueous solution and the membrane. Because of the highly lipophilic nature of CBD, the membrane concentration of CBD is expected to be far higher than the aqueous concentration once equilibrium is reached, which takes 4- 5 minutes (Figure 1.5). The kinetics in experiments using voltage changes to alter CBD binding to the various states of the channel, which are much faster, likely reflect state-dependent binding and unbinding of CBD to the channel after a steady-state CBD concentration has been achieved in the membrane. The model uses the CBD concentrations in the external aqueous solution, since these are known exactly. A more detailed model might use the CBD concentration in the membrane, but this is unknown. In the simplest case, the membrane concentration might scale linearly with the concentration in the external aqueous solution, but it seems possible that the relationship might be more complicated.

Altered availability of TTX-R sodium channels and reduced firing with sub-micromolar CBD

Although the model in Figure 1.12 suggests CBD binding to slow inactivated states with a K_d of ~150 nM, it is based on experiments using much higher (5 μM) concentrations of CBD. To test the model more rigorously, we did a series of voltage clamp experiments with lower

concentrations of CBD. First, we examined inhibition of TTX-R sodium current using a voltage protocol designed to put a substantial fraction of channels into slow inactivated states, with a 2-s conditioning pulse at -40 mV (expected from the results in Figure 1.11B to put ~ 1/3 of the channels into the slow inactivated state) followed by a test pulse to +10 mV. We saw effective inhibition of current by both 300 nM CBD and 1 μM CBD using this protocol. (Figure 1.13A). Because the action of these concentrations of CBD was slow, we interspersed recordings examining CBD inhibition with "sham-application" cells in which control (DMSO-containing) solution was applied for the same amount of time. With 5-minute applications of CBD, currents were reduced to 0.69 ± 0.09 (n=6) of pre-drug current by 300 nM CBD and to 0.58 ± 0.06 (n=6) by 1 μM CBD, with minimal effects of equivalent sham application of control solution (0.96 ± 0.03 of the initial value after 5 minutes; n=6; p=0.02 for comparison between 300 nM CBD and sham application, p=0.003 for comparison between 1 μM CBD and sham application).

Figure 1.13 Effects of 300 nM and 1 µM CBD on TTX-R sodium channels. A, Inhibition of TTX-R sodium current by 300 nM CBD (red, n=6 cells from 3 animals) and by 1 µM CBD (blue, n=6 cells from 2 animals). Currents were evoked by a 15-ms step to +10 mV after a 2-s depolarization at -40 mV, applied once every 30 seconds. Black symbols: data for cells with the same protocol with extended recording in control solution (n=6 cells from 4 animals.) $P < 0.05$ after 60 s between 300 nM CBD and control; $p<0.05$ after 0 s between 1 µM CBD and control. B, Effect of 300 nM CBD on the time course of the recovery of availability of TTX-R sodium channels following a 2-s prepulse to -40 mV. Cells were pre-incubated with 300 nM CBD or control (DMSO-containing) solution for 1-2 hours. Representative recovery time course in control (black) and 300 nM CBD (red). Right, Collected results for fraction available after 4-ms recovery at -70 mV, normalized to test pulse before conditioning pulse. Relative current = 0.68±0.04, n=12 cells from 3 animals for control; 0.48±0.05, n=11 cells from 3 animals for 300 nM CBD, p=0.009. C, Availability using the protocol of Figure 1.11B to measure voltage-dependence of slow inactivation, with 5-s conditioning pulses followed by a 10-ms return to -100 mV to allow recovery from fast inactivation followed by the test pulse. V_h = -38.3±1.2 mV, n=12 from 3 animals for control; V_h = -43.6±1.9 mV, n=11 cells from 3 animals for 300 nM CBD, p=0.026. D, Prediction of the model in Figure 1.12 for channel fraction in R state (i.e. available channels) with the protocol in C in control (solid black line) and with 300 nM CBD (solid red line). Dashed red line shows channel availability in CBD normalized to 1 at -100 mV. Blue line shows occupancy of the slow inactivated state in control; in the presence of 300 nM CBD, blue dashed line shows occupancy of CBD-bound slow inactivated state and green dashed line shows occupancy of CBD-free slow inactivated state.

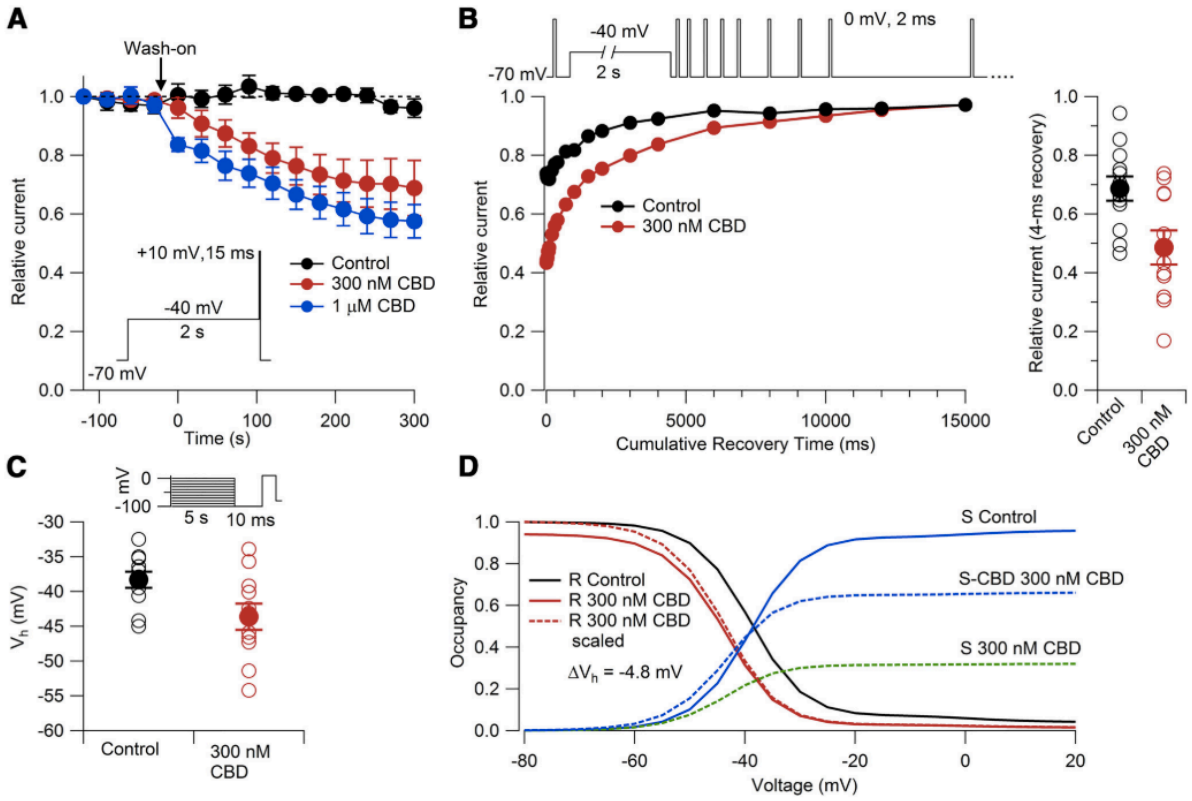

Figure 1.13 (Continued)

A somewhat surprising feature of these experiments was that the rate of inhibition by 1 μM CBD was not much different than that by 300 nM CBD. Although the reasons for this are not clear, it suggests that the rate-limiting step is not CBD binding to the channel but some other process, perhaps partitioning of CBD into the membrane or into the cell. Because of the possibility that a 5-minute application was not enough to reach steady-state, especially with low concentrations of CBD, we also did a series of experiments in which we pre-incubated cells with 300 nM CBD for 1-2 hours. In these population-study experiments, the substantial cell-to-cell variation in the size of the TTX-R sodium current precluded making a simple comparison of current sizes. Therefore, we used protocols similar to those in Figure 1.10 and Figure 1.11B designed to assay the fraction of channels that enter slowly-recovering states during long depolarizations to -40 mV (slow inactivated states in control, and with CBD present, a combination of CBD-free slow inactivated states and CBD-bound inactivated states). Figure 1.13B shows results with a protocol in which a 2-s step to -40 mV was followed by a series of 2-ms steps to 0 mV delivered at various times after the return to -70 mV to assay the time-course of recovery. As expected, in control a substantial fraction of channels (on average, 32 ± 4 %, n=12) recovered slowly. The fraction of slowly-recovering channels was significantly larger in cells incubated in 300 nM CBD (52 ± 5 %, n=11), consistent with substantial binding of 300 nM CBD to slow inactivated states. We also measured the effect of 300 nM CBD incubation on the voltage-dependence of channel availability using a protocol to assay slow inactivation as in Figure 1.11B, with a 5-s conditioning pulses to various voltages followed by 10-ms at -100 mV and then a test pulse. As illustrated in Figure 1.13C, in these experiments there was a ~-5 mV shift in the mid-point of curves in cells incubated with 300 nM CBD (V_h = -43.6 ± 1.9 mV, n=11)

compared to control (V_h = -38.3 ± 1.2 mV, n=12; p = 0.02). We found that this shift is remarkably close to the predictions of the model in Figure 1.12, which predicts V_h = -39.1 for control and V_h = -43.9 with 300 nM CBD (Figure 1.13D).

We next examined whether sub-micromolar concentrations of CBD can modify the firing of nociceptors. Figure 1.14 shows the effects of 500 nM CBD on nociceptor firing. These experiments showed that 500 nM CBD had little effect on firing evoked by small current injections but significantly reduced the ability of cells to fire repetitively throughout 1-s current injections with current injections of 90 pA and above. In collected results (Figure 1.14B), 500 nM CBD applied for 4 minutes reduced the number of action potentials evoked by 1-s 100-pA current injections from 23.1±5.6 in control to 7.6±2.5 in 500 nM CBD (n=7, p=0.01). This effect was much greater than small changes seen during sham applications of control solution for the same period of time (Figure 1.14C), where the number of action potentials changed from 22.4±5.8 to 19.7±5.9 during the 4-minute sham application (p=0.3). The effect of 500 nM CBD to reduce maintained firing during moderately strong current injections seems consistent with high-affinity binding to slow inactivated states reached during depolarizations to near -40 mV and above, although there may well be additional effects of 500 nM CBD on TTX-S channels or other channels influencing firing.

Figure 1.14 Inhibition of action potential firing in mouse nociceptors by 500 nM CBD. A, Action potential firing elicited by 1-s current injections at 40 pA and 90 pA before and after 4-min wash-on of 500 nM CBD. B, Collected results for number of action potentials during 1-s current injections before and after 4-min in 500 nM CBD. N=7 cells from 3 animals, p=0.047 for 90 pA, p=0.01 for 100 pA. C, Same for sham application in cells in which current was recorded for > 4 minutes in control solution. N=7 cells from 3 animals. Data are shown as mean± SEM.

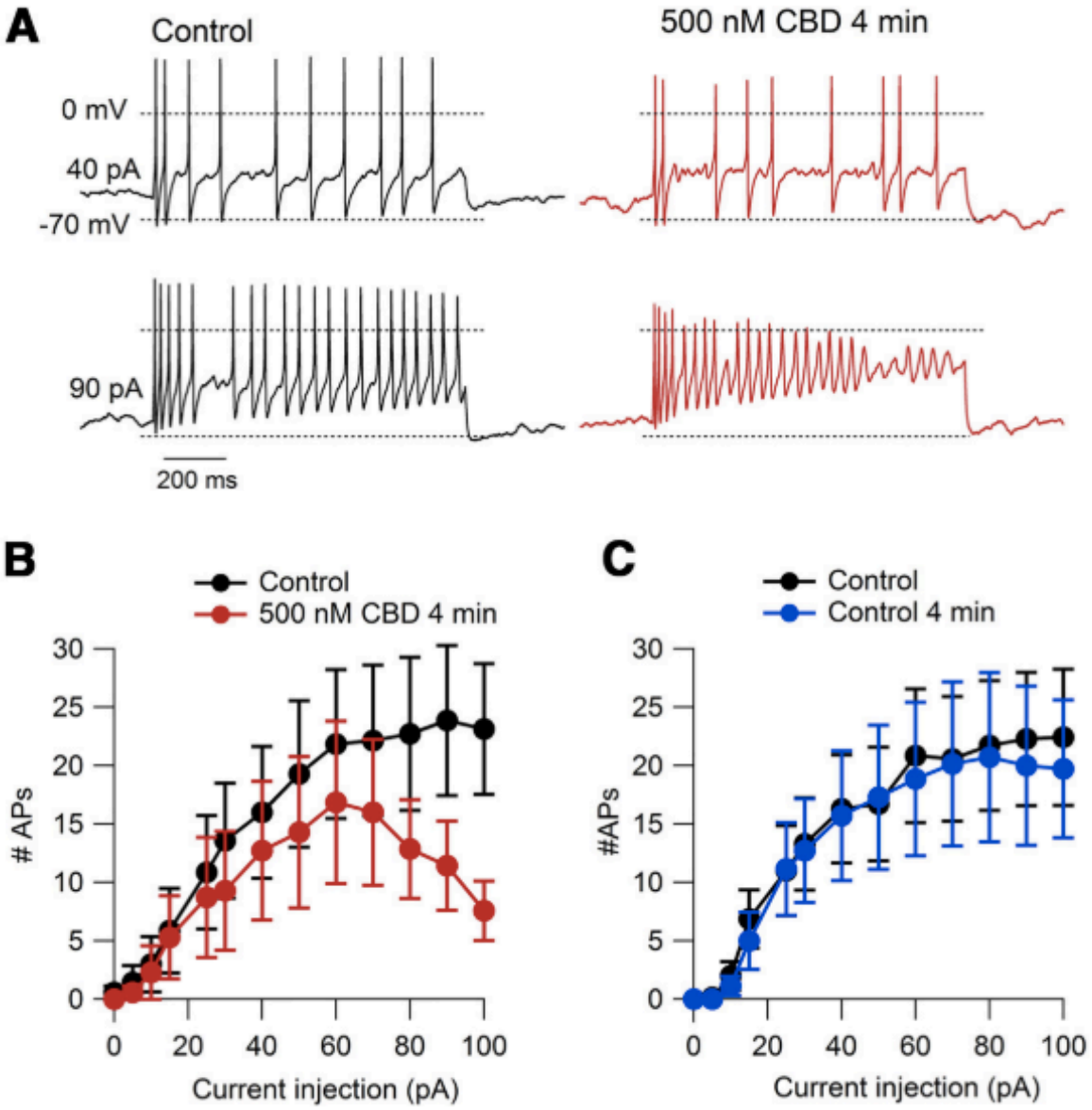

Figure 1.14 (Continued)

Discussion

These results show that CBD at concentrations as low as 500 nM significantly reduces excitability of mouse nociceptors, with a concentration of 2 μM inhibiting firing very effectively, producing more effective inhibition than the same concentration of bupivacaine, one of the most potent local anesthetics. CBD inhibits both TTX-sensitive and TTX-resistant sodium channels, which play complementary roles in controlling nociceptor excitability (Cummins et al., 2007; Bennett et al., 2019).

We find that CBD binds tightly to slow inactivated states of TTX-R channels. TTX-R channels are unusual in that the voltage-dependence of slow inactivation is hyperpolarized compared to fast inactivation (Blair and Bean, 2003; Figure 1.11), the opposite of most other sodium channels (Vilin and Ruben, 2001; Ulbricht, 2005; Ghovanloo et al., 2016). In the neurons we studied, about 30% of channels enter slow inactivated states at -40 mV (Figure 1.11); in some other subtypes of small DRG neurons, 20-60% of channels can be in the slow inactivated state even at -60 mV (Cardenas et al., 2006) and up to 90% at -50 mV (Tripathi et al., 2006). Also, entry into slow inactivated states of TTX-R channels is rapid compared to slow inactivation in other types of sodium channels, so that with repeated 5-ms depolarizations or action potentials, cumulative inactivation can reduce currents substantially at frequencies of 1-10 Hz (Fazan et al., 2001; Tripathi et al., 2006; Figure 1.6). As a result, slow inactivation of TTX-R current can limit repetitive firing induced by depolarizing stimuli like capsaicin (Blair and Bean, 2003) and can slow axonal conduction mediated by TTX-R sodium channels (De Col et al., 2008) . Conversely, some excitation-enhancing agents like interleukin-1 beta and tumor necrosis factor activate second messenger pathways that disrupt slow inactivation of TTX-R

channels (Binshtok et al, 2008; Gudes et al., 2015). The significance of slow inactivation of TTX-R channels under physiological conditions suggests that pharmacological agents targeting these states may be especially effective in reducing repetitive firing of nociceptors. In fact, carbamazepine, effective for treating neuropathic pain in a subset of patients, also interacts with higher affinity with slow-inactivated than fast-inactivated states of TTX-R channels (Rush and Elliott, 1997; Cardenas et al., 2006), although with far weaker slow-inactivated state binding (estimated K_d 30 μM, Cardenas et al., 2006) than for CBD (0.15 μM).

The molecular mechanism of slow inactivation has been studied extensively in Nav1.4 and Nav1.5 channels, where it appears to involve movements in the outer pore region (Townsend and Horn, 1997; Vilin et al., 1999) and immobilization of voltage-sensor regions (Silva and Goldstein, 2013). However, the distinctive properties of slow inactivation in Nav1.8 channels suggest that its structural basis might be different from other sodium channels. So far the only structurally-relevant information on slow inactivation in Nav1.8 channels is that the extent of slow inactivation occurring during strong depolarizations can be regulated by calmodulin (Choi et al. 2006; 2007), which may underlie the variable properties in different types of DRG neurons. Our results suggest that structures of CBD-bound Nav1.8 channels would likely be in the slow inactivated state, which would be stabilized relative to other states by tight CBD binding. A high-resolution X-crystallography study of CBD bound to a bacterial voltage-dependent sodium channel showed a binding site near the pore, located in a hydrophobic "fenestration" that can plausibly account for entry of the hydrophobic CBD molecule from the membrane phase (Sait et al., 2020). Entry of hydrophobic molecules into the pore through such lateral fenestrations in the pore was previously proposed for lidocaine (Gamal El-Din, 2018),

providing a concrete molecular mechanism for the proposal by Hille (1977) for such a pathway for the binding of hydrophobic local anesthetic molecules to mammalian sodium channels. A similar location for CBD binding in mammalian sodium channels seems plausible based on homology modeling (Sait et al., 2020), although CBD inhibition of the bacterial sodium channel is significantly weaker (IC_{50} ~ 17 μM) than for mammalian sodium channels, so it is unclear how good a model the CBD binding to the bacterial channel will be for high-affinity binding to inactivated states of mammalian channels.

Further work will be needed to determine the relative importance of CBD inhibition of TTX-S and TTX-R channels for inhibiting nociceptor firing. With 500 nM CBD, there was little effect on firing of the first few action potentials, and the main effect was reduction of maintained firing during relatively large current injections. While this is consistent with CBD binding to slow inactivated states of TTX-R channels, application of TTX can also reduce maintained firing (unpublished observations), so combined action of CBD on both TTX-R and TTX-S channels is likely important. Studies on cloned Nav1.1-Nav1.7 channels show that CBD binds to inactivated states with higher affinity than resting states (Ghovanloo et al., 2018) but studies on native TTX-S channels in nociceptors have not yet been done. It remains to be seen whether particularly tight binding of CBD to slow inactivated states also occurs in TTX-S channels. In general, inhibition of both TTX-S and TTX-R channels may be a desirable characteristic for an effective analgesic (Goodwin and McMahon, 2021).

Similar to other anti-epileptic drugs like phenytoin and carbamazepine, CBD inhibits not only sodium channels but also voltage-dependent potassium channels and calcium channels (Ross et al., 2008; Hill et al., 2014; Patel et al., 2016; Ghovanloo et al., 2018; Le Marois et al., 2020;

Orvos et al., 2020), as well having effects on a wide variety of other signaling molecules (Gray and Whalley, 2019; Watkins, 2019; Senn et al., 2020), including TRPV1 (Iannotti et al., 2014), TRPV2 (Neumann-Raizel et al., 2019; Qin et al., 2008) and various G-protein-coupled receptors (de Almeida and Devi, 2020). Although CBD affects many channels and receptors, the fact that well-defined binding sites can be seen in structures of CBD-bound proteins (Pumroy et al., 2019; Sait et al., 2020), along with the dramatic state-dependence of binding, suggests that its effects are mediated by specific effects on the operation of particular channels and receptors and not completely non-specific effects on membranes and membrane proteins. It is difficult to know which of these effects, or combination of effects, is most important for CBD's action on either epilepsy and pain. However, given the primary importance of voltage-dependent sodium channels in controlling neuronal excitability, it seems likely that effects on sodium channels are of major importance in pain. As for other anti-epileptic sodium channel inhibitors like carbamazepine, phenytoin, and lamotrigine, and amitriptyline, used to treat neuropathic pain, the clinical effects and tolerability of CBD likely depend critically on relatively small differences in actions on particular channel types together with the importance of each affected channel for excitability of particular neuronal types and other excitable cells. For example, it may be significant that the IC_{50} for CBD inhibition of cardiac Nav1.5 channels is several-fold higher than for neuronal TTX-sensitive channels (Ghovanloo et al., 2018) or Nav1.8 channels (this study). The strong dependence of CBD binding on the gating state of sodium channels and the strong dependence of gating states on membrane voltage are likely to be key factors in determining effects on different types of neurons, as well as on other excitable cells like heart muscle. Recent experiments showed that CBD is much more effective in inhibiting resurgent sodium

current generated by Nav1.2 channels than for inhibiting transient current through these or other channels (Mason and Cummins, 2020), which may help explain potency in epilepsy. Such strong state-dependent actions are impossible to predict *a priori* but once known, can help in designing compounds with improved therapeutic ratios. The particularly strong interaction of CBD with the slow inactivated state of Nav1.8 channels may offer such an opportunity.

The intrinsic potency of CBD for inhibiting nociceptor firing relative to bupivacaine highlights the importance of understanding the complex pharmacokinetics and bioavailability of CBD when applied *in vivo* by various routes (Millar et al., 2019). Because CBD is highly lipid soluble (Ghovanloo et al., 2018), it likely partitions strongly into membranes and lipid-rich environments like the brain and myelinated nerves, and the concentrations actually seen by channels in central neurons or peripheral neurons with *in vivo* application are presently essentially impossible to estimate. Possibly local application (e.g. by dermal application) could be an effective route for producing localized analgesia. However, while our results show effective CBD inhibition of firing in nociceptor cell bodies, excitability of peripheral terminals and axons may well depend on different combinations of ion channels (Goodwin and McMahon, 2021), and CBD inhibition of excitability in these physiologically important cell regions remains to be characterized. Also, while use of dissociated cells allows application of well-defined concentrations of CBD and detailed analysis of effects on ion channels, the process of dissociation and maintenance *in vitro* (including exposure to NGF) almost certainly alters the electrical properties of the neurons, which may have characteristics more like those in damaged or inflamed tissue than normal tissue.

References

Abraham AD, Leung EJY, Wong BA, Rivera ZMG, Kruse LC, Clark JJ, Land BB (2020) Orally consumed cannabinoids provide long-lasting relief of allodynia in a mouse model of chronic neuropathic pain. Neuropsychopharmacology 45:1105–1114.

Argueta DA, Ventura CM, Kiven S, Sagi V, Gupta K (2020) A Balanced Approach for Cannabidiol Use in Chronic Pain. Front Pharmacol 11:561.

Bean BP, Cohen CJ, Tsien RW (1983) Lidocaine block of cardiac sodium channels. J Gen Physiol 81:613–642.

Bennett DL, Clark AJ, Huang J, Waxman SG, Dib-Hajj SD (2019) The Role of Voltage-Gated Sodium Channels in Pain Signaling. Physiol Rev 99:1079–1151.

Binshtok AM, Wang H, Zimmermann K, Amaya F, Vardeh D, Shi L, Brenner GJ, Ji R-R, Bean BP, Woolf CJ, Samad TA (2008) Nociceptors are interleukin-1beta sensors. J Neurosci 28:14062–14073.

Blair NT, Bean BP (2002) Roles of tetrodotoxin (TTX)-sensitive Na+ current, TTX-resistant Na+ current, and Ca2+ current in the action potentials of nociceptive sensory neurons. J Neurosci 22:10277–10290.

Blair NT, Bean BP (2003) Role of tetrodotoxin-resistant Na+ current slow inactivation in adaptation of action potential firing in small-diameter dorsal root ganglion neurons. J Neurosci 23:10338–10350.

Cardenas CA, Cardenas CG, de Armendi AJ, Scroggs RS (2006) Carbamazepine interacts with a slow inactivation state of NaV1.8-like sodium channels. Neurosci Lett 408:129–134.

Carter BC, Bean BP (2009) Sodium entry during action potentials of mammalian neurons:

incomplete inactivation and reduced metabolic efficiency in fast-spiking neurons. Neuron 64:898–909.

Choi J-S, Dib-Hajj SD, Waxman SG (2007) Differential slow inactivation and use-dependent inhibition of Nav1.8 channels contribute to distinct firing properties in IB4+ and IB4- DRG neurons. J Neurophysiol 97:1258–1265.

Choi J-S, Hudmon A, Waxman SG, Dib-Hajj SD (2006) Calmodulin regulates current density and frequency-dependent inhibition of sodium channel Nav1.8 in DRG neurons. J Neurophysiol 96:97–108.

Costa B, Colleoni M, Conti S, Parolaro D, Franke C, Trovato AE, Giagnoni G (2004) Oral anti-inflammatory activity of cannabidiol, a non-psychoactive constituent of cannabis, in acute carrageenan-induced inflammation in the rat paw. Naunyn Schmiedebergs Arch Pharmacol 369:294–299.

Costa B, Trovato AE, Comelli F, Giagnoni G, Colleoni M (2007) The non-psychoactive cannabis constituent cannabidiol is an orally effective therapeutic agent in rat chronic inflammatory and neuropathic pain. Eur J Pharmacol 556:75–83.

Cummins TR, Sheets PL, Waxman SG (2007) The roles of sodium channels in nociception: Implications for mechanisms of pain. Pain 131:243–257.

de Almeida DL, Devi LA (2020) Diversity of molecular targets and signaling pathways for CBD. Pharmacol Res Perspect 8:e00682.

De Col R, Messlinger K, Carr RW (2008) Conduction velocity is regulated by sodium channel inactivation in unmyelinated axons innervating the rat cranial meninges. The Journal of physiology 586:1089–1103.

De Gregorio D, McLaughlin RJ, Posa L, Ochoa-Sanchez R, Enns J, Lopez-Canul M, Aboud M, Maione S, Comai S, Gobbi G (2019) Cannabidiol modulates serotonergic transmission and reverses both allodynia and anxiety-like behavior in a model of neuropathic pain. Pain 160:136–150.

Devinsky O, Cross JH, Laux L, Marsh E, Miller I, Nabbout R, Scheffer IE, Thiele EA, Wright S (2017) Trial of Cannabidiol for Drug-Resistant Seizures in the Dravet Syndrome. N Engl J Med 376:2011–2020.

Devinsky O, Nabbout R, Miller I, Laux L, Zolnowska M, Wright S, Roberts C (2019) Long-term cannabidiol treatment in patients with Dravet syndrome: An open-label extension trial. Epilepsia 60:294–302.

Devinsky O, Patel AD, Cross JH, Villanueva V, Wirrell EC, Privitera M, Greenwood SM, Roberts C, Checketts D, VanLandingham KE, Zuberi SM (2018a) Effect of Cannabidiol on Drop Seizures in the Lennox-Gastaut Syndrome. N Engl J Med 378:1888–1897.

Devinsky O, Patel AD, Thiele EA, Wong MH, Appleton R, Harden CL, Greenwood S, Morrison G, Sommerville K (2018b) Randomized, dose-ranging safety trial of cannabidiol in Dravet syndrome. Neurology 90:e1204–e1211.

Fazan RJ, Whiteis CA, Chapleau MW, Abboud FM, Bielefeldt K (2001) Slow inactivation of sodium currents in the rat nodose neurons. Auton Neurosci 87:209–216.

Franco V, Perucca E (2019) Pharmacological and Therapeutic Properties of Cannabidiol for Epilepsy. Drugs 79:1435–1454.

Gallily R, Yekhtin Z, Hanuš LO (2018) The Anti-Inflammatory Properties of Terpenoids from Cannabis. Cannabis Cannabinoid Res 3:282–290.

Gamal El-Din TM, Lenaeus MJ, Zheng N, Catterall WA (2018) Fenestrations control resting-state block of a voltage-gated sodium channel. Proc Natl Acad Sci U S A 115:13111–13116.

Ghovanloo M-R, Aimar K, Ghadiry-Tavi R, Yu A, Ruben PC (2016) Physiology and Pathophysiology of Sodium Channel Inactivation. Curr Top Membr 78:479–509.

Ghovanloo M-R, Shuart NG, Mezeyova J, Dean RA, Ruben PC, Goodchild SJ (2018) Inhibitory effects of cannabidiol on voltage-dependent sodium currents. J Biol Chem 293:16546–16558.

Goodwin G, McMahon SB. (2021) The physiological function of different voltage-gated sodium channels in pain. Nat Rev Neurosci. 22:263-274.

Gray RA, Whalley BJ (2020) The proposed mechanisms of action of CBD in epilepsy. Epileptic Disord 22:10–15.

Gudes S, Barkai O, Caspi Y, Katz B, Lev S, Binshtok AM (2015) The role of slow and persistent TTX-resistant sodium currents in acute tumor necrosis factor-α-mediated increase in nociceptors excitability. J Neurophysiol 113:601–619.

Hammell DC, Zhang LP, Ma F, Abshire SM, McIlwrath SL, Stinchcomb AL, Westlund KN (2016) Transdermal cannabidiol reduces inflammation and pain-related behaviours in a rat model of arthritis. Eur J Pain 20:936–948.

Hill AJ, Jones NA, Smith I, Hill CL, Williams CM, Stephens GJ, Whalley BJ (2014) Voltage-gated sodium (NaV) channel blockade by plant cannabinoids does not confer anticonvulsant effects per se. Neurosci Lett 566:269–274.

Hille B (1977) Local anesthetics: hydrophilic and hydrophobic pathways for the drug-receptor reaction. J Gen Physiol 69:497–515.

Iannotti FA, Hill CL, Leo A, Alhusaini A, Soubrane C, Mazzarella E, Russo E, Whalley BJ, Di Marzo V, Stephens GJ (2014) Nonpsychotropic plant cannabinoids, cannabidivarin (CBDV) and cannabidiol (CBD), activate and desensitize transient receptor potential vanilloid 1 (TRPV1) channels in vitro: potential for the treatment of neuronal hyperexcitability. ACS Chem Neurosci 5:1131–1141.

Jones NA, Hill AJ, Smith I, Bevan SA, Williams CM, Whalley BJ, Stephens GJ (2010) Cannabidiol displays antiepileptiform and antiseizure properties in vitro and in vivo. J Pharmacol Exp Ther 332:569–577.

Kaplan JS, Stella N, Catterall WA, Westenbroek RE (2017) Cannabidiol attenuates seizures and social deficits in a mouse model of Dravet syndrome. Proc Natl Acad Sci U S A 114:11229–11234.

Karoly R, Lenkey N, Juhasz AO, Vizi ES, Mike A (2010) Fast- or slow-inactivated state preference of Na+ channel inhibitors: a simulation and experimental study. PLoS Comput Biol 6:e1000818.

Khan AA, Shekh-Ahmad T, Khalil A, Walker MC, Ali AB (2018) Cannabidiol exerts antiepileptic effects by restoring hippocampal interneuron functions in a temporal lobe epilepsy model. Br J Pharmacol 175:2097–2115.

Laprairie RB, Bagher AM, Kelly MEM, Denovan-Wright EM (2015) Cannabidiol is a negative allosteric modulator of the cannabinoid CB1 receptor. Br J Pharmacol 172:4790–4805.

Le Marois M, Ballet V, Sanson C, Maizières M-A, Carriot T, Chantoiseau C, Partiseti M, Bohme GA (2020) Cannabidiol inhibits multiple cardiac ion channels and shortens ventricular action potential duration in vitro. Eur J Pharmacol 886:173542.

Liu PW, Blair NT, Bean BP (2017) Action Potential Broadening in Capsaicin-Sensitive DRG Neurons from Frequency-Dependent Reduction of Kv3 Current. J Neurosci 37:9705–9714.

Maione S, Piscitelli F, Gatta L, Vita D, De Petrocellis L, Palazzo E, de Novellis V, Di Marzo V (2011) Non-psychoactive cannabinoids modulate the descending pathway of antinociception in anaesthetized rats through several mechanisms of action. Br J Pharmacol 162:584–596.

Malfait AM, Gallily R, Sumariwalla PF, Malik AS, Andreakos E, Mechoulam R, Feldmann M (2000) The nonpsychoactive cannabis constituent cannabidiol is an oral anti-arthritic therapeutic in murine collagen-induced arthritis. Proc Natl Acad Sci U S A 97:9561–9566.

Mason ER, Cummins TR (2020) Differential Inhibition of Human Nav1.2 Resurgent and Persistent Sodium Currents by Cannabidiol and GS967. Int J Mol Sci 21.

Mechoulam R, Shani A, Edery H, Grunfeld Y (1970) Chemical basis of hashish activity. Science 169:611–612.

Millar SA, Stone NL, Bellman ZD, Yates AS, England TJ, O'Sullivan SE (2019) A systematic review of cannabidiol dosing in clinical populations. Br J Clin Pharmacol 85:1888–1900.

Miller I, Scheffer IE, Gunning B, Sanchez-Carpintero R, Gil-Nagel A, Perry MS, Saneto RP, Checketts D, Dunayevich E, Knappertz V (2020) Dose-Ranging Effect of Adjunctive Oral Cannabidiol vs Placebo on Convulsive Seizure Frequency in Dravet Syndrome: A Randomized Clinical Trial. JAMA Neurol 77:613–621.

Neher E. (1992) Correction for liquid junction potentials in patch clamp experiments. Methods Enzymol. 207:123-231.

Neumann-Raizel H, Shilo A, Lev S, Mogilevsky M, Katz B, Shneor D, Shaul YD, Leffler A, Gabizon

A, Karni R, Honigman A, Binshtok AM (2019) 2-APB and CBD-Mediated Targeting of Charged Cytotoxic Compounds Into Tumor Cells Suggests the Involvement of TRPV2 Channels. Front Pharmacol 10:1198.

Nitecka-Buchta A, Nowak-Wachol A, Wachol K, Walczyńska-Dragon K, Olczyk P, Batoryna O, Kempa W, Baron S (2019) Myorelaxant Effect of Transdermal Cannabidiol Application in Patients with TMD: A Randomized, Double-Blind Trial. J Clin Med 8.

Orvos P, Pászti B, Topal L, Gazdag P, Prorok J, Polyák A, Kiss T, Tóth-Molnár E, Csupor-Löffler B, Bajtel Á, Varró A, Hohmann J, Virág L, Csupor D (2020) The electrophysiological effect of cannabidiol on hERG current and in guinea-pig and rabbit cardiac preparations. Sci Rep 10:16079.

Patel RR, Barbosa C, Brustovetsky T, Brustovetsky N, Cummins TR (2016) Aberrant epilepsy-associated mutant Nav1.6 sodium channel activity can be targeted with cannabidiol. Brain 139:2164–2181.

Pertwee RG (2005) Pharmacological actions of cannabinoids. Handb Exp Pharmacol:1–51.

Philpott HT, O'Brien M, McDougall JJ (2017) Attenuation of early phase inflammation by cannabidiol prevents pain and nerve damage in rat osteoarthritis. Pain 158:2442–2451.

Pumroy RA, Samanta A, Liu Y, Hughes TE, Zhao S, Yudin Y, Rohacs T, Han S, Moiseenkova-Bell VY (2019) Molecular mechanism of TRPV2 channel modulation by cannabidiol. Elife 8.

Qin N, Neeper MP, Liu Y, Hutchinson TL, Lubin M Lou, Flores CM (2008) TRPV2 is activated by cannabidiol and mediates CGRP release in cultured rat dorsal root ganglion neurons. J Neurosci 28:6231–6238.

Renganathan M, Cummins TR, Waxman SG (2001) Contribution of Na(v)1.8 sodium channels to

action potential electrogenesis in DRG neurons. J Neurophysiol 86:629–640.

Rock EM, Limebeer CL, Parker LA (2018) Effect of cannabidiolic acid and Δ(9)-tetrahydrocannabinol on carrageenan-induced hyperalgesia and edema in a rodent model of inflammatory pain. Psychopharmacology (Berl) 235:3259–3271.

Rosenberg EC, Patra PH, Whalley BJ (2017) Therapeutic effects of cannabinoids in animal models of seizures, epilepsy, epileptogenesis, and epilepsy-related neuroprotection. Epilepsy Behav 70:319–327.

Rosenberg EC, Tsien RW, Whalley BJ, Devinsky O (2015) Cannabinoids and Epilepsy. Neurotherapeutics 12:747–768.

Ross HR, Napier I, Connor M (2008) Inhibition of recombinant human T-type calcium channels by Delta9-tetrahydrocannabinol and cannabidiol. J Biol Chem 283:16124–16134.

Roy ML, Narahashi T (1992) Differential properties of tetrodotoxin-sensitive and tetrodotoxin-resistant sodium channels in rat dorsal root ganglion neurons. J Neurosci 12:2104–2111.

Rush AM, Bräu ME, Elliott AA, Elliott JR (1998) Electrophysiological properties of sodium current subtypes in small cells from adult rat dorsal root ganglia. J Physiol 511 (Pt 3):771–789.

Rush AM, Cummins TR, Waxman SG (2007) Multiple sodium channels and their roles in electrogenesis within dorsal root ganglion neurons. The Journal of physiology 579:1–14.

Rush AM, Elliott JR (1997) Phenytoin and carbamazepine: differential inhibition of sodium currents in small cells from adult rat dorsal root ganglia. Neurosci Lett 226:95–98.

Ryberg E, Larsson N, Sjögren S, Hjorth S, Hermansson N-O, Leonova J, Elebring T, Nilsson K, Drmota T, Greasley PJ (2007) The orphan receptor GPR55 is a novel cannabinoid receptor. Br J Pharmacol 152:1092–1101

Sait LG, Sula A, Ghovanloo M-R, Hollingworth D, Ruben PC, Wallace BA (2020) Cannabidiol interactions with voltage-gated sodium channels. Elife 9:e58593

Senn L, Cannazza G, Biagini G (2020) Receptors and Channels Possibly Mediating the Effects of Phytocannabinoids on Seizures and Epilepsy. Pharmaceuticals (Basel) 13.

Silva JR, Goldstein SAN (2013) Voltage-sensor movements describe slow inactivation of voltage-gated sodium channels I: wild-type skeletal muscle Na(V)1.4. J Gen Physiol 141:309–321.

Straiker A, Dvorakova M, Zimmowitch A, Mackie K (2018) Cannabidiol Inhibits Endocannabinoid Signaling in Autaptic Hippocampal Neurons. Mol Pharmacol 94:743–748.

Thiele E, Marsh E, Mazurkiewicz-Beldzinska M, Halford JJ, Gunning B, Devinsky O, Checketts D, Roberts C (2019) Cannabidiol in patients with Lennox-Gastaut syndrome: Interim analysis of an open-label extension study. Epilepsia 60:419–428.

Toib A, Lyakhov V, Marom S. (1998) Interaction between duration of activity and time course of recovery from slow inactivation in mammalian brain Na+ channels. J Neurosci. 18:1893-1903.

Townsend C, Horn R (1997) Effect of alkali metal cations on slow inactivation of cardiac Na+ channels. J Gen Physiol 110:23–33.

Tran T, Kavuluru R (2020) Social media surveillance for perceived therapeutic effects of cannabidiol (CBD) products. Int J Drug Policy 77:102688.

Tripathi PK, Trujillo L, Cardenas CA, Cardenas CG, de Armendi AJ, Scroggs RS (2006) Analysis of the variation in use-dependent inactivation of high-threshold tetrodotoxin-resistant sodium currents recorded from rat sensory neurons. Neuroscience 143:923–938.

Ulbricht W (2005) Sodium channel inactivation: molecular determinants and modulation.

Physiol Rev 85:1271–1301.

Verrico CD, Wesson S, Konduri V, Hofferek CJ, Vazquez-Perez J, Blair E, Dunner KJ, Salimpour P, Decker WK, Halpert MM (2020) A randomized, double-blind, placebo-controlled study of daily cannabidiol for the treatment of canine osteoarthritis pain. Pain.

Vilin YY, Makita N, George ALJ, Ruben PC (1999) Structural determinants of slow inactivation in human cardiac and skeletal muscle sodium channels. Biophys J 77:1384–1393.

Vilin YY, Ruben PC (2001) Slow inactivation in voltage-gated sodium channels: molecular substrates and contributions to channelopathies. Cell Biochem Biophys 35:171–190.

Watkins AR (2019) Cannabinoid interactions with ion channels and receptors. Channels (Austin) 13:162–167.

Xu DH, Cullen BD, Tang M, Fang Y (2020) The Effectiveness of Topical Cannabidiol Oil in Symptomatic Relief of Peripheral Neuropathy of the Lower Extremities. Curr Pharm Biotechnol 21:390–402.

Zheng Y, Liu P, Bai L, Trimmer JS, Bean BP, Ginty DD (2019) Deep Sequencing of Somatosensory Neurons Reveals Molecular Determinants of Intrinsic Physiological Properties. Neuron 103:598-616.e7.

Chapter 2 Cannabidiol inhibits Nav channels through two distinct binding sites

Jian Huang*, Xiao Fan*, Xueqin Jin, Sooyeon Jo, Hanxiong Bear Zhang, Akie Fujita,

Bruce P. Bean and Nieng Yan

*These authors contributed equally

Contributions to the work

I worked together with Akie Fujita to design and carry out the experiments in Figure 2.1C, D, and E. I participated in the initiation of the overall project, in the design of the experiments, and in the organization and writing of the paper. Our collaborators in Nieng Yan's laboratory did the structural experiments, and Xueqin Jin did the electrophysiological experiments using transient transfection to study the effects of mutations on CBD's actions.

Abstract

Cannabidiol (CBD), a major non-psychoactive phytocannabinoid in cannabis, is an effective treatment for some forms of epilepsy and pain. At high concentrations, CBD interacts with a huge variety of proteins, but which targets are most relevant for clinical actions is still unclear. Here we show that CBD interacts with $Na_v1.7$ channels at sub-micromolar concentrations in a state-dependent manner. Electrophysiological experiments show that CBD binds to the inactivated state of $Na_v1.7$ channels with a dissociation constant of about 65 nM. The cryo-EM structure of CBD bound to $Na_v1.7$ channels reveals two distinct binding sites. One is in the IV-I fenestration near the upper pore, suggesting a pathway by which CBD can access the channel protein from the lipid membrane. The other binding site is directly next to the inactivated "wedged" position of the Ile/Phe/Met (IFM) motif on the short linker between repeats III and IV, which mediates fast inactivation. Consistent with producing a direct stabilization of the

inactivated state, mutating residues in this binding site greatly reduced state-dependent binding of CBD. The identification of this novel binding site may enable design of compounds with improved properties compared to CBD itself.

Introduction

Cannabidiol (CBD) is a major phytocannabinoid present in cannabis[1]. Unlike delta-9-tetrahydrocannabinol, the main psychoactive phytocannabinoid, CBD does not activate CB1 or CB2 cannabinoid receptors and does not show intoxicating effects. Nevertheless, CBD has clear effects on neuronal function. Large clinical trials have shown efficacy of CBD for treating several childhood epilepsies[2-6], for which it is now FDA-approved. CBD has also been shown to relieve pain in animal models[7-9], as well as in several small clinical trials[10,11].

CBD has been shown to interact with a huge variety of proteins[12,13], especially membrane proteins[14], and it is still unclear which of these are the most important targets for CBD's action on epilepsy or pain. One of the actions of CBD is to inhibit voltage-gated sodium (Nav) channels[15-19]. As for many drugs that inhibit Nav channels, the interaction of CBD with Nav channels is state-dependent, with higher affinity binding to the closed inactivated state of the channel than the closed resting state[17]. Because Nav channels exist in a steeply voltage-dependent equilibrium between resting and inactivated states at physiological membrane potentials, tight binding to inactivated channels decreases the pool of resting state channels available for activation by a coupled-equilibrium mechanism, even if the drug binding is to a closed state of the channel[20,21].

Classic mutagenesis experiments revealed a key site for state-dependent interactions of local anesthetics like lidocaine and anti-seizure drugs like carbamazepine and phenytoin with Nav

channels, formed by residues in the pore-lining S6 segments in the upper region of the pore[22-24]. Subsequent determinations of the structure of both bacterial and eukaryotic Nav channels revealed the presence of "fenestrations" in the side of the pore near this region[25-29], suggesting a pathway by which hydrophobic molecules can access the binding site from the lipid membrane – providing a concrete structural basis for the "hydrophobic pathway" hypothesized by Hille [20].

Here we have used cryo-EM to determine the structure of CBD-bound Nav1.7 channels. Unexpectedly, structures with and without CBD reveal two distinct binding sites for CBD. One is in a fenestration in the upper pore. The other is a novel site close to where the IFM motif of the intracellular linker between domains III and IV[30] binds to produce the rapid time- and voltage-dependent inactivation characteristic of eukaryotic Nav channels by acting as a "door wedge" to squeeze the intracellular gate of the channel closed[28,29,31,32]. Mutating the residues identified in this binding site for CBD greatly reduced state-dependent CBD inhibition, suggesting a mechanism by which CBD binding stabilizes inactivation quite directly.

Methods and materials

Transient expression of human $Na_v1.7$ in HEK293F cells

Codon-optimized cDNA for full-length human Nav1.7 (Uniprot Q15858), a gift from Tsinghua University, was cloned into the pCAG vector with Twin-Strep-tag and Flag-tag in tandem at the amino terminus while codon-optimized cDNAs for β1 subunit (Uniprot Q07699) and β2 subunit (Uniprot O60939) were cloned separately into the pCAG vector without affinity tag. All the plasmids for transient expression were verified by DNA sequencing. HEK293F suspension cells (Thermo Fisher Scientific, R79007) were cultured in SMM 293T-II medium (Sino Biological Inc.)

at 37 °C, supplied with 5% CO2 under 60% humidity, and transfected with plasmids when the cell density reached 1.5-2.0 × 106 cells per ml. For one liter cell culture, a mixture of expression plasmids including 1.5 mg plasmids for Nav1.7, 0.5 mg plasmids for β1 and 0.5 mg plasmids for β2 was pre-incubated with 4 mg 40-kDa linear polyethylenimines (Polysciences) in 50 ml fresh medium for 15-30 minutes, and then added to the cell culture for transient expression of human Nav1.7 complex.

Protein purification of human Nav1.7-CBD complexes 33 L transfected HEK293F cells were harvested approximately 48 h after transfection by centrifugation at 3,600 g for 10 min and resuspended in the lysis buffer containing 25 mM Tris-HCl (pH 7.5) and 150 mM NaCl. The suspension was supplemented with 10 μM CBD (sigma aldrich) and protease inhibitor cocktail (Selleckchem), and incubated at 4 °C for 30 min. Then n-dodecyl-β-D-maltopyranoside (DDM, Anatrace) was added to a final concentration of 1% (w/v), and cholesteryl hemisuccinate Tris salt (CHS, Anatrace) to 0.1% (w/v). After incubation at 4 °C for another 2 h, the mixture was centrifuged at 16,000 g for 45 min, and the supernatant was applied to anti-Flag M2 affinity gel (Sigma) for affinity purification. The resin was rinsed four times with the wash buffer (buffer W) that contains 25 mM Tris-HCl (pH 7.5), 150 mM NaCl, 0.06% GDN, 10 μM CBD and protease inhibitor cocktail. The target proteins were eluted with buffer W supplemented with 0.2 mg mL−1 Flag peptide (synthesized by GenScript). The eluent was then applied to Strep-Tactin Sepharose (IBA) and flew through by gravity. The resin was rinsed four times with buffer W and the target proteins were eluted with buffer W supplemented with 2.5 mM desthiobiotin (IBA). The eluent was then concentrated using a 100-kDa cut-off Amicon filter unit (Millipore) and further purified through size-exclusion chromatography (Superose 6 10/300 GL, GE Healthcare)

that was pre-equilibrated in the buffer containing 25 mM Tris-HCl (pH 7.5), 150 mM NaCl, 0.02% GDN and 10 µM CBD. The peak fractions were pooled and concentrated to a final concentration of ~ 9 mg mL−1 and incubated with 100 µM CBD at 4 °C for another 30 min before making cryo-girds.

Cryo-EM sample preparation and data acquisition

UltrAuFoil (R1.2/1.3 300 mesh, Quantifoil) grids were glow-discharged with easiGlow (PELCO) using 15 mA for 15s at 0.37 mBar. Vitrobot Mark IV chamber was pre-cooled to 10 °C with 100% humidity. 3 µl concentrated Nav1.7-CBD was applied to freshly treated grid surface, which was then blotted with filter paper for 4 s and plunged into liquid ethane cooled by liquid nitrogen. Grids were loaded to a 300 kV Titan Krios G3i with spherical aberration (Cs) image corrector (Thermo Fisher). SerialEM was used for automated data collection of both no-tilt and tilted micrographs. Micrographs were recorded by a Gif Quantum K2 Summit camera (Gatan) with 20 eV slit in super-resolution mode at a nominal magnification of 105,000×, resulting in a calibrated pixel size of 0.557 Å. Each movie stack was exposed for 5.6 s (0.175 s per frame, 32 frames) with a total electron dose of ~ 50 e−/Å2. The movie stacks were aligned, summed and dose-weighted using Warp and binned to a pixel size of 1.114 Å per pixel.

Data processing

In total 5,862 cryo-EM micrographs were collected from four subsets of micrographs, including two no-tilt subsets (1st: 1,302; 2nd: 2,286), a 30° tilted subset (3rd: 1,271) and a 40° tilted subset (4th: 1,003). Warp52 preprocessed subsets were imported to cryoSPARC53 for patched CTF estimation. 41,155 particles from 130 micrographs were auto-picked by blob picking to generate 2D templates through 2D classification. 21,839 particles in 15 classes were

selected to perform Ab-initio reconstruction and the class averages were used in later template picking for all subsets. Each subset was picked individually with selected templates, yielding 783,670/1,336,960/1,292,889/1,712,983 particles for the 4 subsets. Patch CTF extraction jobs were performed to update local defocus information in both 30° and 40° tilted datasets based on particle coordinates. Obvious junks were excluded from extracted bin4 particles in each subset by 2D classification. Those roughly cleaned subsets were sent to heterogenous refinement with 2 references generated from Ab-initio reconstruction. Bin2 particles were extracted with selected good classes and merged for the 4 subsets. After four rounds of heterogenous refinement and remove duplicates, 590,967 particles in best class left and were extracted into bin1. Those particles were subject to another two rounds of heterogenous refinement using information from higher frequency. After non-uniform (NU) refinement, a good 3D class containing 488,974 particles yielded a reconstruction at an overall resolution of 3.0 Å. These results were exported to Relion54 to perform the Bayesian polishing with the motion parameters estimated by Warp. Polished particles were re-imported to cryoSPARC to perform the NU refinement, which leads to a 2.8-Å final reconstruction.

Model building and refinement

The coordinates of WT apo-Nav1.7 (PDB: 7W9K), was used as the initial model for model building for human Nav1.7-CBD. The published model was docked and saved related to the Nav1.7-CBD EM density in Chimera55. The refitted initial model was adjusted in COOT first56. It was then refined against the corresponding map using the Real-space Refinement option in PHENIX57 with secondary structure and geometry restraints.

Whole cell electrophysiology

Experiments characterizing the state-dependent actions of CBD on wild-type hNav1.7 channels were made using HEK293 cells stably expressing human Nav1.7 channels[58]. Cells were grown in Minimum Essential Medium (ATCC) containing 10% fetal bovine serum (Sigma) and 1% penicillin/streptomycin (Sigma) under 5% CO2 at 37 °C. For electrophysiological recording, cells were grown on coverslips for 12 to 24 h after plating. Whole-cell recordings were obtained using patch pipettes with resistances of 2-3.5 MΩ when filled with the internal solution, consisting of 122 mM CsCl, 9 mM NaCl, 1.8 mM $MgCl_2$, 9 mM EGTA, 14 mM creatine phosphate (tris salt), 4 mM MgATP, and 0.3 mM GTP (tris salt), 9 mM HEPES, pH adjusted to 7.2 with CsOH. The shank of the electrode was wrapped with Parafilm to reduce capacitance and allow optimal series resistance compensation without oscillation. Recordings were made using a Multiclamp 700B amplifier (Molecular Devices) with currents and voltages controlled and sampled using a Digidata 1322A interface using pClamp 9 software (Molecular Devices). Series resistance was compensated by 70-80%. Current and voltage records were filtered at 5-10 kHz and digitized at 100 kHz. Analysis was performed with Igor Pro (Wavemetrics, Lake Oswego, OR) using DataAccess (Bruxton Software) to import pClamp data. Sodium currents were corrected for linear capacitative and leak currents determined using 5 mV hyperpolarizations delivered from the resting potential (-70 or -100 mV) and then appropriately scaled and subtracted.

After establishing whole-cell recording in Tyrode's solution (155 mM NaCl, 3.5 mM KCl, 1.5 mM CaCl2, 1 mM $MgCl_2$, 10 mM HEPES, 10 mM glucose, pH adjusted to 7.4 with NaOH) cells were lifted off the bottom of the recording chamber and placed in front of an array of quartz fiber flow pipes (250 µm internal diameter, 350 µm external diameter, Polymicro Technologies, Catalog # TSG250350) attached with styrene butadiene glue (Amazing Goop, Eclectic Products)

to a rectangular aluminum rod (cross section 1.5 cm × 0.5 cm) whose temperature was controlled by resistive heating elements and a feedback-controlled temperature controller (Warner Instruments, TC-344B). Solutions were changed (in ~ 1 second) by moving the cell from one pipe to another. Recordings were made at either 37 °C or 21 °C.

Sodium currents were recorded in an external solution consisting of : 116 mM NaCl, 39 mM TEACl, 5 mM $BaCl_2$, 10 μM $CdCl_2$, 10 mM HEPES, 10 mM glucose, pH adjusted to 7.4 with NaOH. CBD (Cayman Chemical, Catalog # 90080, CAS 13956-29-1) was prepared as a 10 mM stock solution in DMSO which was diluted in the external solution to the final concentration. DMSO was added to the control solution at the same concentration as in the CBD solution. When using sub-micromolar concentrations of CBD, we used all-glass containers and perfusion tubing to avoid loss of compound by partitioning into plastic59, which is problematic even for ∆9-THC [60,61], which is less lipophilic (logP 5.65) than CBD (logP 6.33).

The effects of CBD on steady-state inactivation were determined using 5-s long prepulses to voltages between -130 mV and -20 mV followed by a 10-ms test pulse to +10 mV. 300 nM CBD was applied for 10 minutes in order to reach steady state. In control experiments, we found that there was a small time-dependent shift in the midpoint of inactivation over this time, and the average shift in control (with DMSO at the concentration present in the 300 nM CBD solutions) over 5 minutes (-3.6 mV, n=8) was subtracted from the average shift with 300 nM CBD (-10.0 mV, n=8) in order to calculate the CBD-induced shift that was used for fitting the state-dependent model in Figure 2.1c. Data are given as mean ± SEM.

Experiments examining the effects of mutations used transient transfections in HEK293T cells. HEK293T cells were cultured in Dulbecco's Modified Eagle Medium (DMEM, BI)

supplemented with 4.5 mg/mL glucose, 10% (v/v) fetal bovine serum (FBS, BI). For patch-clamp recordings, the cells were plated onto glass coverslips and transiently co-transfected with the Nav1.7 variants plasmids and eGFP in the presence of lipofectamine 2000 (Invitrogen). Cells with green fluorescence were selected for patch-clamp recording 18–36 h after transfection. Experiments were performed at room temperature. No authentication was performed for the commercially available cell line. Mycoplasma contamination was not tested.

Whole-cell Na^+ currents were recorded in HEK293T cells using an EPC10-USB amplifier with Patchmaster software v2*90.2 (HEKA Elektronic), filtered at 3 kHz (low-pass Bessel filter) and sampled at 50 kHz. The borosilicate pipettes (Sutter Instrument) used in all experiments had a resistance of 2-4 MΩ and the electrodes were filled with the internal solution composed of 105 mM CsF, 40 mM CsCl, 10 mM NaCl, 10 mM EGTA, 10 mM HEPES, pH adjusted to 7.4 with CsOH. The bath solutions contained: 140 mM NaCl, 4 mM KCl, 10 mM HEPES, 10 mM D-Glucose, 1 mM $MgCl_2$, 1.5 mM $CaCl_2$, pH adjusted to 7.4 with NaOH. Data were analyzed using Origin (OriginLab) and GraphPad Prism (GraphPad Software).

To determine voltage dependence of inactivation, cells were clamped at a holding potential of -100 mV and pre-pulses from -130 mV to 0 mV for either 5 s (for steady-state inactivation) or 50 ms (for fast inactivation) were applied with an increment of 5 mV, followed by a 50-ms test pulse to 0 mV. Fast and steady-state inactivation curves were fitted with a Boltzmann function to obtain V_h and slope values. Leak currents and capacitive transients were subtracted using the P/4 procedure. CBD was dissolved in dimethyl sulfoxide (DMSO, final concentration less than 0.1%, Sigma) to make a stock solution of 30 mM. Solutions with indicated CBD concentrations were freshly prepared and perfused to the recording cell for up to 10 mins to get to the

maximal block using a multichannel perfusion system (VM8, ALA). Prior to CBD perfusion, cells were recorded for 5 min to establish stable peak current. Data is presented as mean ± standard error of the mean (SEM) and n is the number of experimental cells from which recordings were obtained. Statistical significance was assessed using an unpaired t-test with Welch's correction and extra sum-of-squares F test.

Results

CBD stabilizes the inactivated state of $Na_v1.7$

Although CBD is known to interact with a wide variety of proteins, substantial effects at sub-micromolar concentrations have been reported for only a few targets. Among these are Nav1.8 channels[33], which are prominently expressed in primary nociceptors. We tested low concentrations of CBD on Nav1.7 channels, the other major sodium channel driving excitability of primary nociceptors[34,35], using a stable cell line expressing human Nav1.7 channels. Nav1.7 current evoked from a holding potential of -70 mV, near the normal resting potential of nociceptors, was strongly inhibited by 300 nM CBD (Figure 2.1a, b). In collected results, current was reduced to 0.29 ± 0.02 of control by 300 nM CBD applied for two minutes. The inhibition by 300 nM CBD was strongly sensitive to the state of the channels, as assayed by 5-second prepulses to alter the equilibrium between resting states and inactivated states of the channel (Figure 2.1c). The midpoint of channel availability was shifted in the hyperpolarizing direction by an average of 6.4 mV. This shift suggests tighter binding of CBD to inactivated states than resting states, and a simplified model of binding to resting and inactivated states[21] suggests a binding affinity of about 66 nM to inactivated states. One interpretation of the altered availability of Nav channels is that CBD stabilizes the inactivated state of the channel.

Consistent with this, after a depolarizing prepulse to -40 mV to induce high-affinity CBD binding to inactivated states, recovery of availability is much slower than in control (Figure 2.1d).

Figure 2.1 Potent stabilization of $Na_v1.7$ inactivation by CBD. **a** Currents before and after application of 300 nM CBD for two minutes at 37 °C. **b** Time-course of inhibition of $hNa_v1.7$ channels by 300 nM CBD at 37 °C. Mean ± SEM, n=7. **c** Shift in steady-state inactivation (determined by 5-s prepulses followed by a test pulse to +10 mV) by 300 nM CBD. Inset: calculated values for dissociation constants of CBD binding to resting and inactivated states[21]. **d** Slowed recovery from inactivation with CBD, assayed at -100 mV following a 300-ms step to -40 mV to promote binding of CBD to fast inactivated channels. **e** Time-course of entry into slowly-recovering states during steps to -40 mV in the absence and presence of CBD. Dashed line is drawn at 20 ms, showing rapid entry of channels into slowly-recovering states consistent with binding to fast inactivated states.

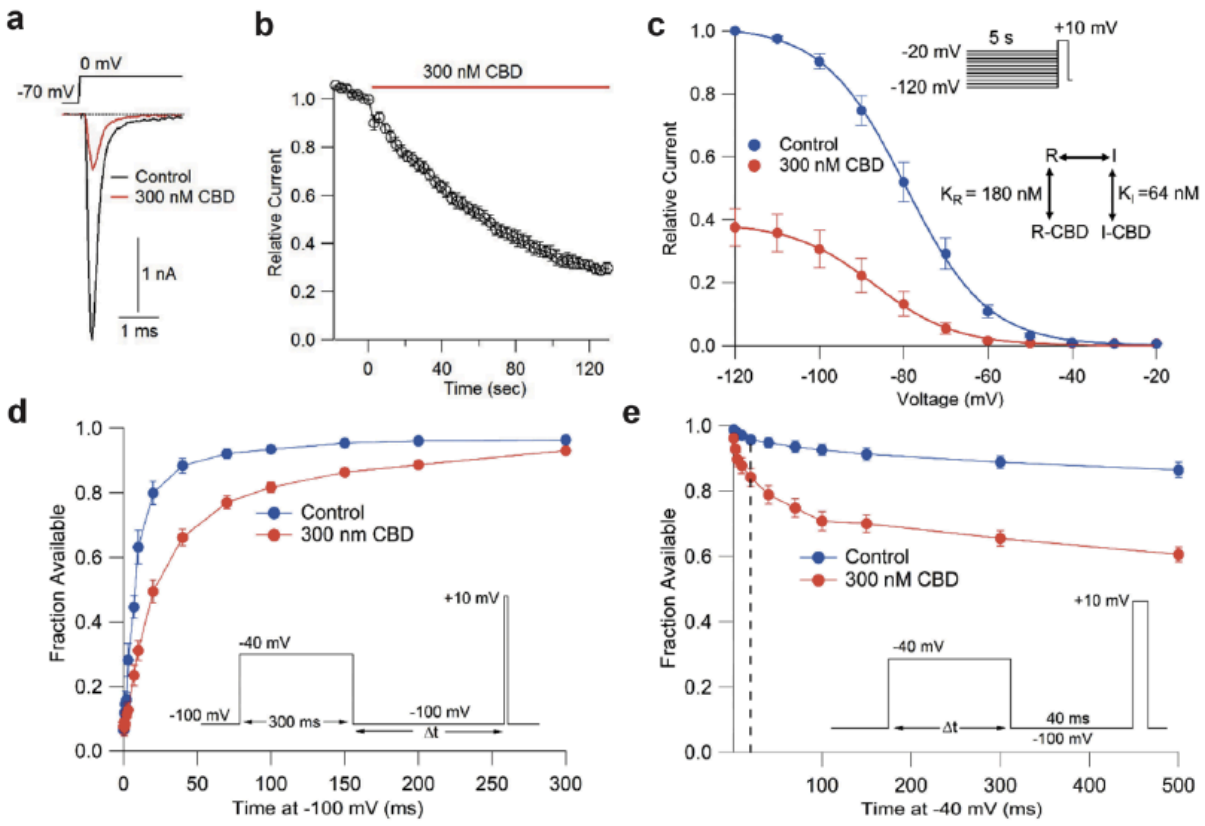

Figure 2.1 (Continued)

Like other Nav channels, Nav1.7 channels can undergo two forms of inactivation, fast inactivation and slow inactivation. With maintained depolarization, especially to strongly depolarized voltages, Nav channels can enter into a distinct slow inactivated state, from which recovery on repolarization is much slower. In principle, the high affinity binding of CBD to inactivated states could involve either fast inactivated or slow inactivated states. Figure 2.1e shows an experiment designed to test whether CBD can bind to fast inactivated channels with high affinity, by examining the time course of entry of channels into slowly recovering states at -40 mV, where there is little slow inactivation. In the presence of CBD, there is substantial entry of channels into slowly recovering states within 20 ms at -40 mV, a time where there is almost no entry into slow inactivated states in control. This implies that CBD binds with high affinity to fast inactivated states. Experiments with long depolarizations to more depolarized voltages (data not shown) show that CBD remains bound with similarly high affinity when channels enter slow inactivated states, suggesting that whatever binding site is formed during fast inactivation remains when channels transition to slow inactivated states.

CBD occupies two distinct sites on the pore domain (PD)

To examine the structural basis of CBD binding, we obtained a cryo-EM structure of CBD bound to human Nav1.7 channels by including CBD throughout purification of the channel protein starting with the first step after cells were harvested. Following our standard protocol for human Nav1.7 purification and cryo-EM analysis, a 3D EM reconstruction of Nav1.7-β1-β2 in the presence of CBD was obtained at 2.8 Å resolution (Figure 2.2a).

Figure 2.2 Cryo-EM structure of the human Nav1.7-CBD complex. a Cryo-EM map of human Nav1.7 bound to CBD. The Nav1.7 complex comprises the transmembrane α1 subunit (domain colored), the auxiliary β1 subunit (light salmon), and β2 subunit (salmon). Sugar moieties and lipids are colored gray and orange, respectively. The same color scheme is applied throughout the manuscript. b Overall structure of the α1 subunit of Nav1.7 bound to CBD. Two CBD molecules, designated as CBD-1 and CBD-2 and shown as light grey spheres, bind to different sites in the pore domain (PD). c Two CBD-binding sites, the inactivation receptor site (the I-site, right) for CBD-1 and the I-IV fenestration site (the F-site, left) for CBD-2, are identified and highlighted with magenta and gray boxes, respectively.

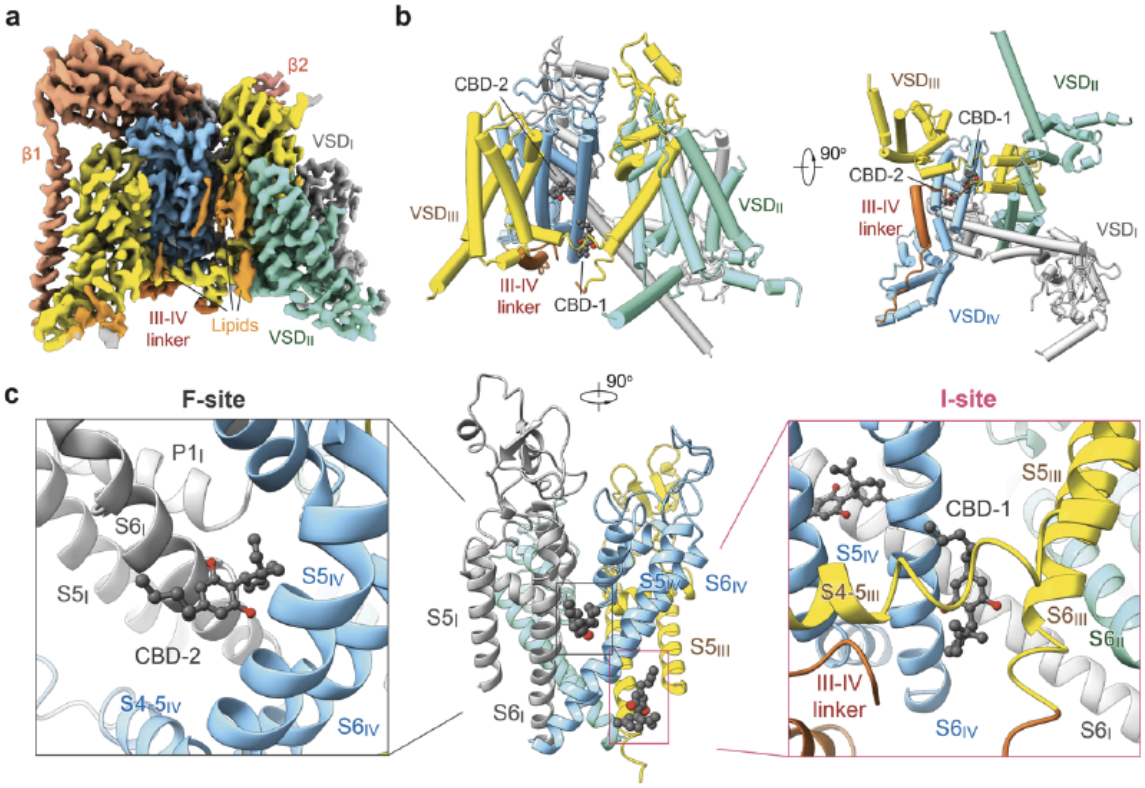

Figure 2.2 (Continued)

Map comparison with the ligand-free Nav1.7 (EMDB: EMD-32368) immediately reveals one extra stretch of density that is right next to the IFM motif. In addition, a linear density that penetrates the IV-I fenestration in apo-Nav1.7 is now replaced by a bulkier one in the presence of CBD. Both densities can be docked well with CBD (Figure 2.2b). This identifies two distinct CBD binding sites from the high-resolution EM map. For description simplicity, we name the site next to the IFM motif as the I-site for CBD-1 and the IV-I fenestration as the F-site for CBD-2 (Figure 2.2c). In the following, we will present detailed analysis of the two binding sites.

CBD reshapes the IFM-binding site

The receptor site for the fast inactivation motif IFM in eukaryotic Nav channels is constituted mainly by hydrophobic residues from S4-S5III, S5III, S6III, S5IV and S6IV. Prominent conformational changes occur to the intracellular half of S6III upon CBD binding. Minor shifts are also observed in the adjacent segments (Figure 2.3a). Although the position of the IFM motif remains unchanged, S6III is pushed away by CBD-1. More dramatically, residues 1461-1465, which fold in two helical turns on the intracellular terminus of S6III in the ligand-free structure, are unwound to a loop in the presence of CBD-1, and the ensuing five residues become invisible (Figure 2.3b). Despite the marked shift of S6III, the intracellular gate remains in a non-conducting state.

.

Figure 2.3 Conformational changes of Nav1.7 upon CBD binding to the I-site. a CBD binding to the I-site induces pronounced conformational shift of the PD. A side view (left) and a bottom view (right) of the superimposed PD of CBD-bound (domain colored) and apo (pale green, PDB: 7W9K) Nav1.7 are shown. CBD molecules are shown as grey spheres. The IFM motifs are shown as sticks, and the conformational changes are indicated with red arrows. b Rearrangement of the IFM binding site and surrounding elements upon CBD binding. Displacement of the corresponding residues upon CBD binding is indicated by red arrows. An enlarged view of the conformational shift of S6III is shown on the bottom. c CBD binds to a hydrophobic pocket in the I-site. Surrounding environment is shown as the electrostatic surface, calculated in ChimeraX[62]. d CBD coordination in the I-site. Surrounding residues are shown as sticks. Potential hydrogen bonds are shown as red dashed lines. e Plane diagram of residues constituting the binding pocket within a 4 Å cutoff distance from the ligand. The binding pocket and potential H-bonds are indicated by gray dashed contour and red dashed lines. f Mutations at I-site residues modify shifts in fast (50-ms prepulses) and steady-state inactivation (5-s prepulses) induced by 1 μM CBD. The ΔV50 values for fast inactivation: -9.26 ± 0.69 mV (WT), -4.46 ± 0.57 mV (S1320A), -2.09 ± 0.69 mV (N1459A) and -3.58 ± 0.61 mV (S1320A+N1459A); for steady-state inactivation: -11.46 ± 0.72 mV (WT), -3.39 ± 0.75 mV (S1320A), -5.02 ± 0.98 mV (N1459A) and -4.76 ± 0.52 mV (S1320A+N1459A).

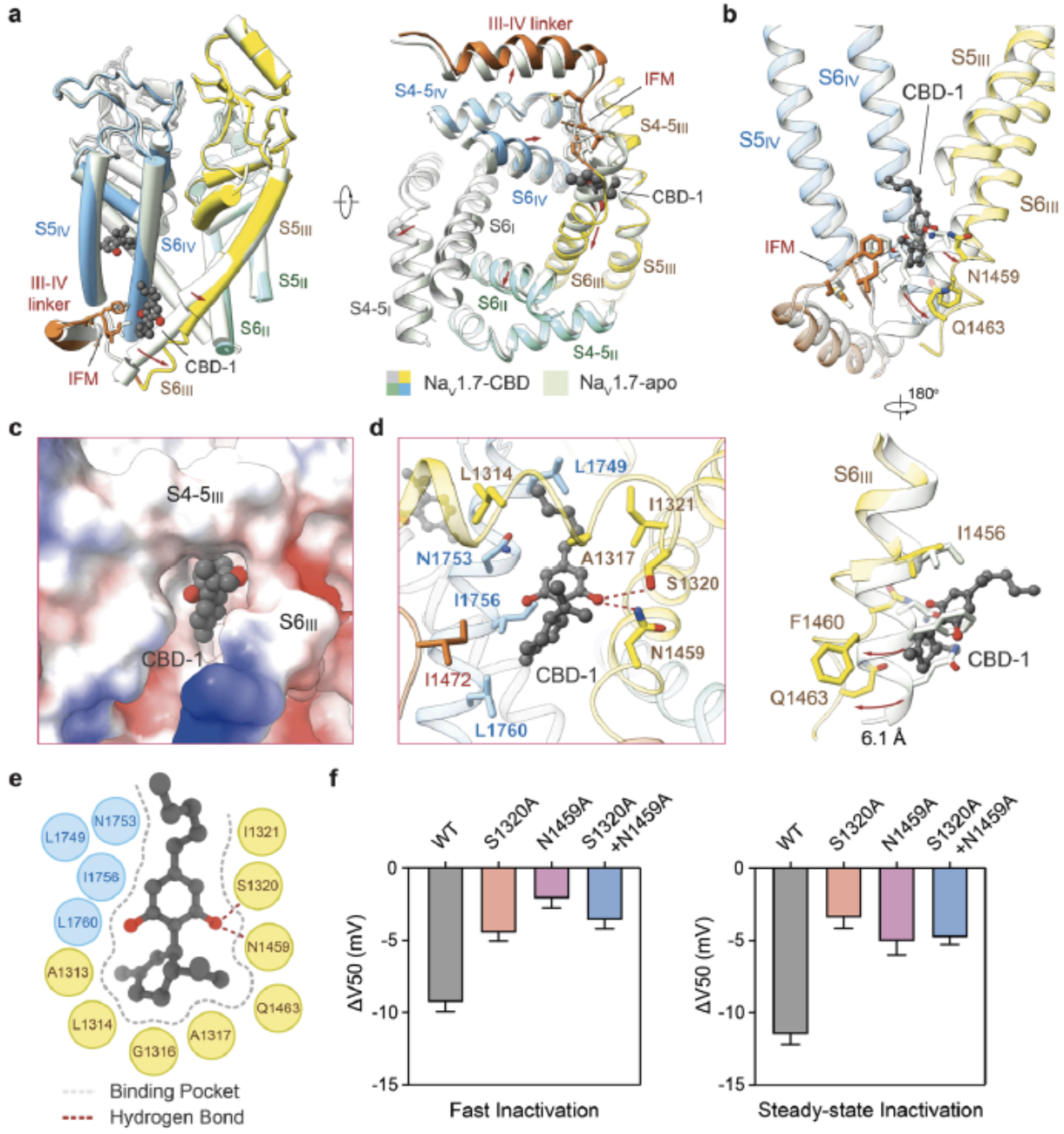

Figure 2.3 (Continued)

CBD-1, with the substituted cyclohexene rings on the intracellular side of the membrane and the n-pentyl tail hooking on the S4-S5III segment, is immersed in a largely hydrophobic environment encompassed by residues on S4-S5III, S5III, S6III, S5IV and S6IV, as well as Ile1472 in the IFM motif (Figure 2.3c). Ser1320 and Asn1459 each form a hydrogen bond with the phenolic hydroxyl group of CBD-1 (Figure 2.3d, e).

To test whether the I-site is involved in CBD stabilization of inactivated states, we examined whether Nav1.7 variants that contain either single point mutations (S1320A, N1459A) or a double mutation combining S1320A and N1459A alter the CBD-induced shift in availability reflecting high-affinity binding to inactivated states. All of the single and double mutations of the identified CBD-1 binding site substantially reduced the shift in availability, and similar reductions were seen using both 5-s prepulses to produce steady-state inactivation or 50-ms prepulses to emphasize fast inactivation (Figure 2.3f). These results suggest that the I-site makes a major contribution to the stabilization of the fast inactivated state by CBD.

CBD binds to the IV-I fenestration site in a conserved pose

The F-site for CBD-2 bound in the IV-I fenestration is mainly composed of hydrophobic residues from S6I, S5IV, S6IV and P1IV (Figure 2.4a). The structure of the F-site remains nearly unchanged with or without CBD (Figure 2.4b). The phenolic hydroxyl group of CBD is hydrogen-bonded by the backbone carbonyl group of Val383, and the phenolic ring is further stabilized by Phe387 through a π-π stacking interaction. The lipophilic tail interacts only with the side chain of Val383 through van der Waals interaction (Figure 2.4a, b).

Figure 2.4 Coordination of CBD at the F-site. a CBD binds to the fenestration enclosed by repeats IV and I of Nav1.7. Surrounding environment, which is highly hydrophobic, is shown as the electrostatic surface, calculated in ChimeraX. Inset: Plane diagram of residues constituting the binding pocket within 5 Å cutoff distance from the ligand. The binding pocket and potential H-bonds are indicated by gray dashed contour and red dashed lines. b The local structures around the F-site (left) remain nearly identical in apo (PDB: 7W9K) and CBD-bound Nav1.7. Surrounding residues are shown as sticks. The only potential hydrogen bond is shown as red dashed lines. c CBD shares similar binding poses in Nav1.7 and TRPV2 at the F-site. Similar fenestration binding site for CBD in Nav1.7 and in TRPV2 is seen in the superimposed structures. A side view (left) and a top view (right) of the comparison between CBD-bound Nav1.7 (domain colored) and TRPV2 (pink, PDB: 6U88) are shown.

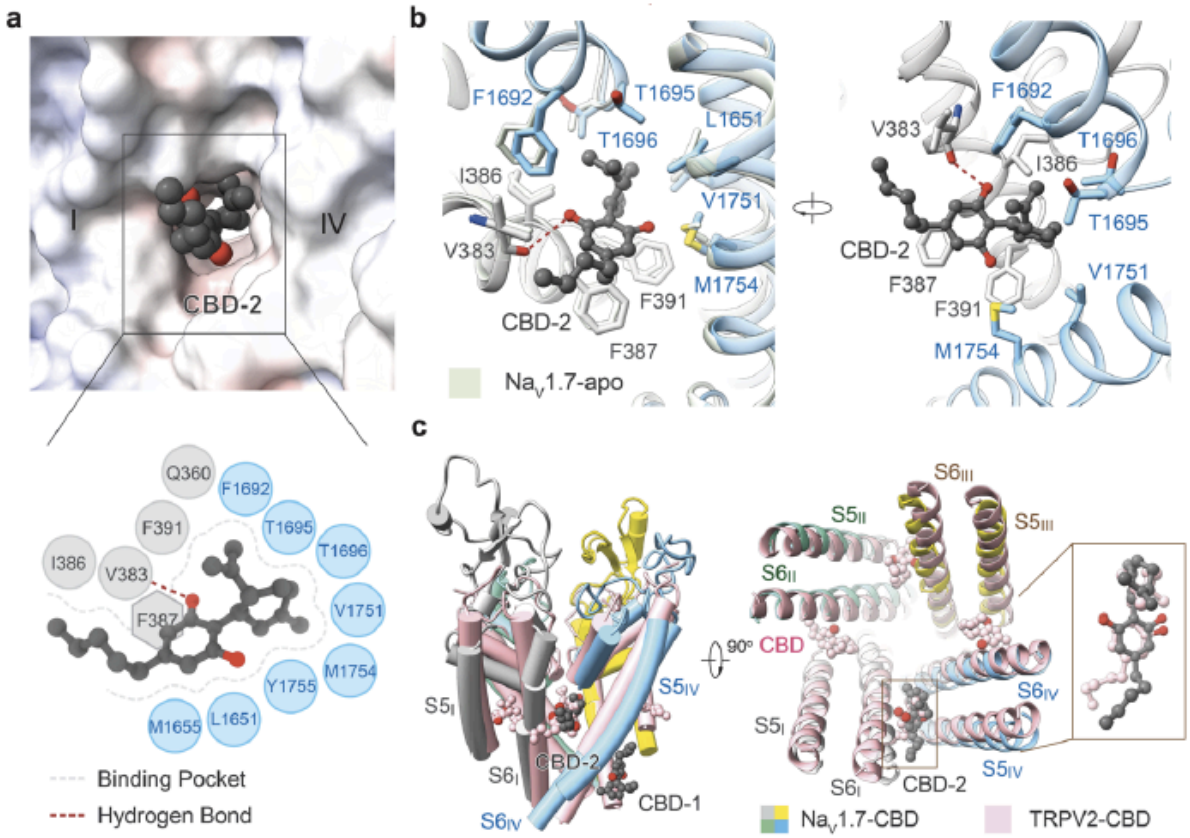

Figure 2.4 (Continued)

Previous work determined a cryo-EM structure of rat TRPV2 treated with CBD36. In the TRPV2 structure, each of the four fenestrations is occupied by a CBD molecule. Unlike in the homotetrameric TRPV2 channel, CBD recognizes only one fenestration enclosed by repeats I and IV in the pseudosymmetric Nav1.7 (Figure 2.4c). Notably, CBD shares a similar binding pose in Nav1.7 and rTRPV2 at the F-site, with the cyclohexene ring pointing towards the central cavity and the n-pentyl tail exposed to the membrane (Figure 2.4c).

A structure of the bacterial channels with bound CBD has also been determined[37]. Interestingly, CBD in NavMS is also present in fenestrations. However, the binding pose in the fenestrations does not overlap with that in Nav1.7, with the molecule extending much deeper into the central cavity in the bacterial channel (Figure 2.5).

Figure 2.5 Comparison of CBD binding in Nav1.7 and NavMs at the Fsite. a Deviation of the CBD binding poses in Nav1.7 and NavMs. A side view (left) and a top view (right) of the superimposed pore domain of CBD-bound Nav1.7 (domain colored) and NavMs (pink, PDB: 6YZ0) are shown. One CBD molecule occupies the fenestration enclosed by repeats I and IV of Nav1.7, whereas four CBD molecules each binds to a fenestration site in NavMs. b Different CBD binding poses at the F-site in Nav1.7 and NavMs. The pore domain of Nav1.7 is shown as a cut-open electrostatic surface.

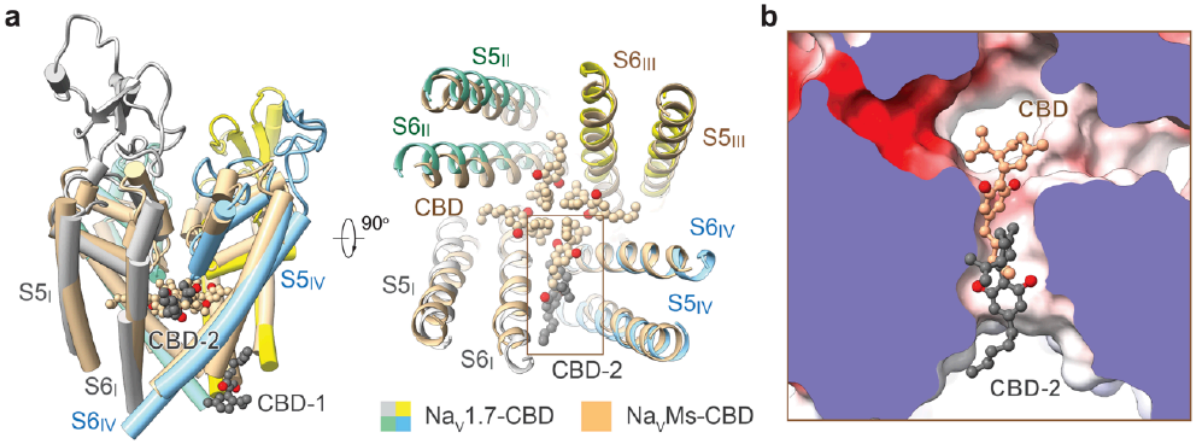

Figure 2.5 (Continued)

Discussion

Unexpectedly, CBD binds to two different sites on Nav1.7 channels, and both sites are different from the binding sites of other small-molecule state-dependent Nav inhibitors previously determined from structural data with mammalian Nav1 channels, including flecainide[38], quinidine[32], propafenone[39], bulleyaconitine A[40], XEN907, TC-N175241 and A-80346742. Neither of the two CBD molecules bound to Nav1.7 channels is in a position to physically occlude the pore. This suggests that CBD acts allosterically to inhibit Nav1.7 channels, and the high-affinity binding to the inactivated state of the channel shown by the electrophysiological experiments suggests that the key allosteric action is a stabilization of the inactivated state. The position of the I-site for CBD-1 binding at the receptor site for the IFM motif, and the dramatic changes in the S6III structure with CBD, suggest that CBD binding at this site may stabilize inactivation very directly, by increasing the binding of the IFM motif, resulting in both a shift of the voltage-dependent equilibrium between resting and inactivated channels and a slowing of recovery from inactivation when the membrane is repolarized.

CBD is an exceptionally lipophilic molecule. With a logP of 6.33, it is expected to be ~ 10^6 times more concentrated in the lipid membrane than in the aqueous extracellular or intracellular solutions. The discovery of fenestrations in Nav channels of both prokaryotes and eukaryotes led to the hypothesis that movement of hydrophobic molecules through the fenestrations could form the basis for the "hydrophobic pathway" hypothesized by Hille[20] to account for the differing kinetics of development and recovery from channels inhibition by charge or uncharged local anesthetics. The idea that the fenestrations can form pathways for effective movement of hydrophobic molecules between the lipid membrane and the channel

pore has been well-supported by both modeling and experiments[43-45]. The presence of a CBD molecule in the IV-I fenestration is consistent with the idea that CBD access to the channel protein from its high concentration in the membrane occurs through this fenestration. Interestingly, in the structure of CBD-bound homotetrameric bacterial Nav channel NavMs, CBD molecules were modeled in each of the four fenestrations to extend into the central cavity of the pore. However, the CBD molecule in the IV-I fenestration of Nav1.7 does not extend into the pore cavity and seems unlikely to directly block the pore. More work will be needed to determine whether binding of this CBD molecule helps stabilize the inactivated state of the channel by an indirect allosteric mechanism.

Many small molecule Nav channel inhibitors, including other antiepileptic drugs and local anesthetics, share the property with CBD of binding more tightly to the inactivated state of the channel than the resting state, even though we now see that the binding sites are quite different. The state-dependent binding to inactivated channels results in inhibition that is more pronounced when the neuronal membrane is more depolarized, typically associated with higher firing rates, and is likely the reason that sodium channel-targeted antiepileptic agents can reduce hyperactivity without debilitating effects on normal activity. Such selectivity is likely also desirable for pain management, since total loss of pain has devastating consequences. Although CBD shares the property of state-dependence with many other clinically useful drugs, the calculated binding affinity of ~ 100 nM for CBD binding to inactivated channels is much higher than for any other anti-epileptic drug with similar state-dependent binding characteristics (e.g. ~ 7 uM for phenytoin[46]; ~9 uM for lamotrigine[47], 25 uM for carbamazepine[48], and ~14 uM for lacosamide[49]) or local anesthetics like lidocaine[50] (~ 20 µM).

Despite its clinical use for epilepsies that cannot be controlled by other agents, cannabidiol has major limitations as a drug, including inducing somnolence, vomiting, diarrhea, and hepatic abnormalities[51]. Many of these adverse effects likely reflect the promiscuity of CBD in affecting so many proteins not likely to be involved in its beneficial actions. The new knowledge of the binding sites for CBD on Nav channels should facilitate structure-based discovery of new drugs deliberately targeted to sodium channels with better specificity.

References

1. Mechoulam, R., Shani, A., Edery, H. & Grunfeld, Y. Chemical basis of hashish activity. Science 169, 611-2 (1970).

2. Devinsky, O. et al. Trial of Cannabidiol for Drug-Resistant Seizures in the Dravet Syndrome. N Engl J Med 376, 2011-2020 (2017).

3. Devinsky, O. et al. Long-term cannabidiol treatment in patients with Dravet syndrome: An open-label extension trial. Epilepsia 60, 294-302 (2019).

4. Devinsky, O. et al. Effect of Cannabidiol on Drop Seizures in the Lennox-Gastaut Syndrome. N Engl J Med 378, 1888-1897 (2018).

5. Devinsky, O. et al. Randomized, dose-ranging safety trial of cannabidiol in Dravet syndrome. Neurology 90, e1204-e1211 (2018).

6. Thiele, E. et al. Cannabidiol in patients with Lennox-Gastaut syndrome: Interim analysis of an open-label extension study. Epilepsia 60, 419-428 (2019).

7. Verrico, C.D. et al. A randomized, double-blind, placebo-controlled study of daily cannabidiol for the treatment of canine osteoarthritis pain. Pain 161, 2191-2202 (2020).

8. Hammell, D.C. et al. Transdermal cannabidiol reduces inflammation and pain-related behaviours in a rat model of arthritis. Eur J Pain 20, 936-48 (2016).

9. Britch, S.C., Babalonis, S. & Walsh, S.L. Cannabidiol: pharmacology and therapeutic targets. Psychopharmacology (Berl) 238, 9-28 (2021).

10. Alaia, M.J. et al. Buccally Absorbed Cannabidiol Shows Significantly Superior Pain Control and Improved Satisfaction Immediately After Arthroscopic Rotator Cuff Repair: A Placebo-Controlled, Double-Blinded, Randomized Trial. Am J Sports Med 50, 3056-3063 (2022).

11. Xu, D.H., Cullen, B.D., Tang, M. & Fang, Y. The Effectiveness of Topical Cannabidiol Oil in Symptomatic Relief of Peripheral Neuropathy of the Lower Extremities. Curr Pharm Biotechnol 21, 390-402 (2020).

12. Ibeas Bih, C. et al. Molecular Targets of Cannabidiol in Neurological Disorders. Neurotherapeutics 12, 699-730 (2015).

13. Franco, V. & Perucca, E. Pharmacological and Therapeutic Properties of Cannabidiol for Epilepsy. Drugs 79, 1435-1454 (2019).

14. Watkins, A.R. Cannabinoid interactions with ion channels and receptors. Channels (Austin) 13, 162-167 (2019).

15. Hill, A.J. et al. Voltage-gated sodium (NaV) channel blockade by plant cannabinoids does not confer anticonvulsant effects per se. Neurosci Lett 566, 269-74 (2014).

16. Patel, R.R., Barbosa, C., Brustovetsky, T., Brustovetsky, N. & Cummins, T.R. Aberrant epilepsy-associated mutant Nav1.6 sodium channel activity can be targeted with cannabidiol. Brain 139, 2164-81 (2016).

17. Ghovanloo, M.R. et al. Inhibitory effects of cannabidiol on voltage-dependent sodium currents. J Biol Chem 293, 16546-16558 (2018).

18. Mason, E.R. & Cummins, T.R. Differential Inhibition of Human Nav1.2 Resurgent and Persistent Sodium Currents by Cannabidiol and GS967. Int J Mol Sci 21(2020).

19. Milligan, C.J. et al. A nutraceutical product, extracted from Cannabis sativa, modulates voltage-gated sodium channel function. J Cannabis Res 4, 30 (2022).

20. Hille, B. Local anesthetics: hydrophilic and hydrophobic pathways for the drug-receptor reaction. J Gen Physiol 69, 497-515 (1977).

21. Bean, B.P. Sodium channel inactivation in the crayfish giant axon. Must channels open before inactivating? Biophys J 35, 595-614 (1981).

22. Ragsdale, D.S., McPhee, J.C., Scheuer, T. & Catterall, W.A. Molecular determinants of state-dependent block of Na+ channels by local anesthetics. Science 265, 1724-8 (1994).

23. Yarov-Yarovoy, V. et al. Role of amino acid residues in transmembrane segments IS6 and IIS6 of the Na+ channel alpha subunit in voltage-dependent gating and drug block. J Biol Chem 277, 35393-401 (2002).

24. Korner, J. et al. Sodium Channels and Local Anesthetics-Old Friends With New Perspectives. Front Pharmacol 13, 837088 (2022).

25. Payandeh, J., Scheuer, T., Zheng, N. & Catterall, W.A. The crystal structure of a voltage-gated sodium channel. Nature 475, 353-8 (2011).

26. Zhang, X. et al. Crystal structure of an orthologue of the NaChBac voltage-gated sodium channel. Nature 486, 130-134 (2012).

27. Payandeh, J., Gamal El-Din, T.M., Scheuer, T., Zheng, N. & Catterall, W.A. Crystal structure of a voltage-gated sodium channel in two potentially inactivated states. Nature 486, 135-9 (2012).

28. Yan, Z. et al. Structure of the Na(v)1.4-beta1 Complex from Electric Eel. Cell 170, 470-482 e11 (2017).

29. Pan, X. et al. Structure of the human voltage-gated sodium channel Na(v)1.4 in complex with beta1. Science 362(2018).

30. McPhee, J.C., Ragsdale, D.S., Scheuer, T. & Catterall, W.A. A mutation in segment IVS6 disrupts fast inactivation of sodium channels. Proc Natl Acad Sci U S A 91, 12346-50 (1994).

31. Li, Z. et al. Structure of human Na(v)1.5 reveals the fast inactivation-related segments as a mutational hotspot for the long QT syndrome. Proc Natl Acad Sci U S A 118(2021).

32. Li, Z. et al. Structural Basis for Pore Blockade of the Human Cardiac Sodium Channel Na(v) 1.5 by the Antiarrhythmic Drug Quinidine*. Angew Chem Int Ed Engl 60, 11474-11480 (2021).

33. Zhang, H.B. & Bean, B.P. Cannabidiol Inhibition of Murine Primary Nociceptors: Tight Binding to Slow Inactivated States of Na(v)1.8 Channels. J Neurosci 41, 6371-6387 (2021).

34. Bennett, D.L., Clark, A.J., Huang, J., Waxman, S.G. & Dib-Hajj, S.D. The Role of Voltage-Gated Sodium Channels in Pain Signaling. Physiol Rev 99, 1079-1151 (2019).

35. Goodwin, G. & McMahon, S.B. The physiological function of different voltage-gated sodium channels in pain. Nat Rev Neurosci 22, 263-274 (2021).

36. Pumroy, R.A. et al. Molecular mechanism of TRPV2 channel modulation by cannabidiol. Elife 8(2019).

37. Sait, L.G. et al. Cannabidiol interactions with voltage-gated sodium channels. Elife 9(2020).

38. Jiang, D. et al. Structure of the Cardiac Sodium Channel. Cell 180, 122-134 e10 (2020).

39. Jiang, D. et al. Open-state structure and pore gating mechanism of the cardiac sodium channel. Cell 184, 5151-5162 e11 (2021).

40. Li, X. et al. Structural basis for modulation of human Na(V)1.3 by clinical drug and selective antagonist. Nat Commun 13, 1286 (2022).

41. Zhang, J. et al. Structural basis for Na(V)1.7 inhibition by pore blockers. Nat Struct Mol Biol 29, 1208-1216 (2022).

42. Huang, X. et al. Structural basis for high-voltage activation and subtype-specific inhibition of human Na(v)1.8. Proc Natl Acad Sci U S A 119, e2208211119 (2022).

43. Boiteux, C. et al. Local anesthetic and antiepileptic drug access and binding to a bacterial voltage-gated sodium channel. Proc Natl Acad Sci U S A 111, 13057-62 (2014).

44. Gamal El-Din, T.M., Lenaeus, M.J., Zheng, N. & Catterall, W.A. Fenestrations control resting-state block of a voltage-gated sodium channel. Proc Natl Acad Sci U S A 115, 13111-13116 (2018).

45. Tao, E. & Corry, B. Characterizing fenestration size in sodium channel subtypes and their accessibility to inhibitors. Biophys J 121, 193-206 (2022).

46. Kuo, C.C. & Bean, B.P. Slow binding of phenytoin to inactivated sodium channels in rat hippocampal neurons. Mol Pharmacol 46, 716-25 (1994).

47. Kuo, C.C. & Lu, L. Characterization of lamotrigine inhibition of Na+ channels in rat hippocampal neurones. Br J Pharmacol 121, 1231-8 (1997).

48. Kuo, C.C., Chen, R.S., Lu, L. & Chen, R.C. Carbamazepine inhibition of neuronal Na+ currents: quantitative distinction from phenytoin and possible therapeutic implications. Mol Pharmacol 51, 1077-83 (1997).

49. Peng, Y.S. et al. Inhibition of neuronal Na(+) currents by lacosamide: Differential binding affinity and kinetics to different inactivated states. Neuropharmacology 179, 108266 (2020).

50. Bean, B.P., Cohen, C.J. & Tsien, R.W. Lidocaine block of cardiac sodium channels. J Gen Physiol 81, 613-42 (1983).

51. Huestis, M.A. et al. Cannabidiol Adverse Effects and Toxicity. Curr Neuropharmacol 17, 974-989 (2019).

52. Tegunov, D. & Cramer, P. Real-time cryo-electron microscopy data preprocessing with Warp. Nat Methods 16, 1146-1152 (2019).

53. Punjani, A., Rubinstein, J.L., Fleet, D.J. & Brubaker, M.A. cryoSPARC: algorithms for rapid unsupervised cryo-EM structure determination. Nat Methods 14, 290-296 (2017).

54. Scheres, S.H. RELION: implementation of a Bayesian approach to cryo-EM structure determination. J Struct Biol 180, 519-30 (2012).

55. Meng, E.C., Pettersen, E.F., Couch, G.S., Huang, C.C. & Ferrin, T.E. Tools for integrated sequence-structure analysis with UCSF Chimera. BMC Bioinformatics 7, 339 (2006).

56. Emsley, P., Lohkamp, B., Scott, W.G. & Cowtan, K. Features and development of Coot. Acta Crystallogr D Biol Crystallogr 66, 486-501 (2010).

57. Afonine, P.V. et al. Towards automated crystallographic structure refinement with phenix.refine. Acta Crystallogr D Biol Crystallogr 68, 352-67 (2012).

58. Liu, P., Jo, S. & Bean, B.P. Modulation of neuronal sodium channels by the sea anemone peptide BDS-I. J Neurophysiol 107, 3155-67 (2012).

59. Zhang, H.B. et al. Cannabidiol activates neuronal Kv7 channels. Elife 11(2022).

60. Christophersen, A.S. Tetrahydrocannabinol stability in whole blood: plastic versus glass containers. J Anal Toxicol 10, 129-31 (1986).

61. Hippalgaonkar, K., Gul, W., ElSohly, M.A., Repka, M.A. & Majumdar, S. Enhanced solubility, stability, and transcorneal permeability of delta-8-tetrahydrocannabinol in the presence of cyclodextrins. AAPS PharmSciTech 12, 723-31 (2011).

62. Pettersen, E.F. et al. UCSF ChimeraX: Structure visualization for researchers, educators, and developers. Protein Sci 30, 70-82 (2021).

Chapter 3 Cannabidiol activation of neuronal Kv7 current

Elife, volume 11, page e73246, 2022

Han-Xiong Bear Zhang*, Laurel Heckman*, Zachary Niday*, Sooyeon Jo*,Akie Fujita, Jaehoon Shim, Roshan Pandey, Hoor Al Jandal, Selwyn Jayakar,Lee B Barrett, Jennifer Smith, Clifford J Woolf, Bruce P Bean

* These authors contributed equally

Contributions to the work

I designed and did most of the experiments in Figure 3.2 on M-current in superior cervical ganglion neurons, with help from Akie Fujita. I participated in the overall design and interpretation of the experiments and in the organization and writing of the paper.

Abstract

Cannabidiol (CBD) is a clinically effective antiepileptic drug whose mechanism of action is unknown. Using a fluorescence-based thallium flux assay, we performed a large-scale screen and found enhancement of flux through heterologously-expressed human Kv7.2/7.3 channels by CBD. Using patch clamp recordings, we found that CBD acts at low concentrations to activate Kv7.2/7.3 channels at subthreshold voltages, with 100 nM CBD producing a doubling of current at -50 mV. CBD shifted the voltage-dependence of channels in the hyperpolarizing direction, producing a shift in the midpoint of activation by ~-14 mV at 300 nM. CBD also effectively enhanced native M-current in both mouse superior cervical ganglion neurons and rat hippocampal neurons. The potent enhancement of Kv2/7.3 channels seems likely to contribute to CBD's effectiveness as an antiepileptic drug.

Introduction

Cannabidiol (CBD), a phytocannabinoid present in marijuana (Mechoulam et al., 1970), is an effective antiepileptic agent for treating Dravet Syndrome (Devinsky et al., 2017, 2018b,2019; Miller et al., 2020) and Lennox-Gastaut syndrome (Devinsky et al., 2018a; Thiele et al., 2018) epilepsies. How CBD ameliorates epileptic activity is unclear (Rosenberg et al., 2015,2017; Franco and Perucca, 2019). Unlike Δ(9)-tetrahydrocannabinol (THC), the other major phytocannabinoid in marijuana, CBD is not psychoactive and does not act as a direct primary ligand at CB1 or CB2 G-protein coupled receptors (Pertwee, 2005). The most potent effect of CBD on electrophysiological function so far reported is an inhibition of the effects of endocannabinoids naturally released by neurons to modulate synaptic transmission (Straiker et al., 2018), where CBD has a negative allosteric effect mediated by cannabidiol binding to CB1

receptors at a site distinct from the primary binding site (Laprairie et al., 2015). Electrophysiologically, this effect is detectable at 100 nM and substantial at 500 nM (Straiker et al., 2018.) At higher concentrations, CBD has inibitory effects on a wide range of proteins, including many receptors and channels (Watkins, 2019). Like many classic antiepileptic agents, CBD inhibits voltage-dependent sodium channels in a state-dependent manner (Hill et al., 2014; Patel et al, 2016; Ghovanloo et al. 2018; Mason and Cummins, 2020), but concentrations of ~2-4 uM are required for half-maximal inhibition of sodium channels and it is unclear whether sodium channel inhibition can account for CBD's anti-convulsant effects (Hill et al., 2014). Other molecular targets that could mediate antiepileptic actions of CBD have been described, notably antagonism of the lipid-activated G protein-coupled receptor GPR55 (Ryberg et al., 2007), but so far electrophysiological effects correlated with GPR55 antagonism have been described only at concentrations of CBD ~10 μM (Kaplan et al., 2017) and their relevance to CBD reduction of overall epileptiform activity, which can be detected in brain slice preparations at concentrations as low as 100 nM (Jones, et al., 2010) remains uncertain.

Here we report that CBD acts at sub-micromolar concentrations to activate neuronal M-current at subthreshold voltages. CBD at concentrations as low as 100 nM shifts the voltage-dependence of activation of the channels in the hyperpolarizing direction, resulting in significant activation of Kv7 current at subthreshold voltages. The results suggest that activation of neuronal M-current is likely one mechanism by which CBD exerts its anti-epileptic action.

Methods and materials

Maintenance of Kv7.2/7.2 cell line

Experiments on cloned 7.2/7.3 channels were done using a cell line in which recombinant human Kv7.2 and 7.3 channels were stably transfected in a Chinese hamster ovary (CHO) cell line (Mayflower Bioscience, BSYS-KV7.2/3-CHO-C). Cells were maintained and passaged in a humidified 37°C incubator in sterile culture flasks containing Ham's F12-Glutamax-l medium (Gibco, Catalog # 31765-035) supplemented with 10% fetal bovine serum (Gibco), 1% penicillin/streptomycin solution (Gibco, Catalog # 15140-122) and 5 μg/mL puromycin (InVivogen, cat #ant-pr-1) and cells were passaged at a confluence of about 50-80%. For electrophysiological recordings, cells were seeded onto 12 mm cover slips (Fisherbrand, Catalog #12-545-80).

Electrophysiology with CHO KV7.2/3 cell line

Whole-cell patch clamp recordings were made using a Multiclamp 700B Amplifier (Molecular Devices). Electrodes were pulled from borosilicate capillaries (VWR International, Catalog # 53432-921) on a Sutter P-97 puller (Sutter Instruments) and shanks were wrapped with Parafilm (American National Can Company) to allow optimal series resistance compensation without oscillation. The resistances of the pipettes were 1.8-3.5 MΩ when filled with the intracellular solution consisting of 140 mm KCl, 10 mM NaCl, 2 mM $MgCl_2$, 1 mm EGTA, 0.2 mm $CaCl_2$, 10 mM HEPES, 14 creatine phosphate (Tris salt), 4 MgATP, and 0.3 GTP (Tris salt), pH adjusted to 7.4 with KOH. Seals were formed in Tyrode's solution consisting of 155 mM NaCl, 3.5 mM KCl, 1.5 mM $CaCl_2$, 1 mM $MgCl_2$, 10 mM HEPES, 10 mM glucose, pH 7.4 adjusted with NaOH. After establishing whole-cell recording, cell capacitance was nulled and series resistance was partially (~70%) compensated. The cell was then lifted and placed in front of an array of quartz fiber flow pipes (250 μm internal diameter, 350 μm external diameter, Polymicro

Technologies, Catalog # TSG250350) attached with styrene butadiene glue (Amazing Goop, Eclectic Products) to a rectangular aluminum rod (cross section 1.5 cm × 0.5 cm) whose temperature was controlled by resistive heating elements and a feedback-controlled temperature controller (Warner Instruments, TC-344B). Solutions were changed (in ~ 1 second) by moving the cell from one pipe to another. Recordings were made at 37 °C.

Voltage commands were delivered and current signals were recorded using a Digidata 1321A data acquisition system (Molecular Devices) controlled by pCLAMP 10.3 software (Molecular Devices). Current and voltage records were filtered at 5 kHz and digitized at 100 kHz. Analysis was performed with Igor Pro 6.12 (Wavemetrics, Lake Oswego, OR), using DataAccess (Bruxton Software) to import pClamp data.

The voltage-dependence of activation was measured from the initial tail current at a step to -50 mV following 1-s depolarizations to voltages between -100 mV and +40 mV from a holding potential of -80 mV. Current records were corrected for linear capacitative and leak current by subtracting scaled responses to signal-averaged 5 mV hyperpolarizations delivered from -80 mV. Tail current was averaged over a 1-msec interval starting at a time when the immediate jump in current had settled, typically 0.8-1.6 ms after the voltage step. Plots of normalized tail current versus test voltage could be fit well by a Boltzmann function raised to the 4^{th} power. The midpoint of activation was measured in a fit-independent manner by calculating the test voltage at which tail current reached half of its maximal value (reached at voltages between 0 to +40 mV), using linear interpolation between the test voltages straddling the midpoint. Calculation of shifts of activation midpoint by CBD was confined to cells in which maximal tail

current at -50 mV remained at least 100 pA in the presence of CBD and in which the activation curve in CBD was fit well by a Boltzmann function raised to the 4^{th} power.

CBD (Cayman Chemical, Catalog # 90080, CAS 13956-29-1) was prepared as a 10 mM stock solution in DMSO which was diluted in the external Tyrodes's solution to the final concentration. DMSO was added to the control solution at the same concentration as in the CBD solution. In early experiments, CBD-containing solutions were prepared in polystyrene test tubes and applied to cells from reservoirs made from 10 mM polypropylene syringe bodies. Realizing that phytocannabinoids have exceptionally high lipophilicity (Thomas et al., 1990) and can apparently partition into plastic (Hippalgaonkar et al., 2011), we then switched to using glass reservoirs from which solutions flowed through hollow quartz fibers to be applied to cells. We found that using glass reservoirs and tubing resulted in larger and more reproducible effects of CBD concentrations of 1 μM and below. Reported data for these concentrations are confined to experiments using glass reservoirs and tubing. Effects of concentrations of 3 μM and above were not less when using plastic reservoirs and collected data for concentrations of 3-20 μM include experiments done with both plastic and glass reservoirs.

Preparation of superior cervical ganglion (SCG) neurons

Superior cervical ganglia were removed from adult Swiss Webster mice of either sex (postnatal day 56), cut in half and treated for 20 minutes at 37°C with 20 U/ml papain (Worthington Biochemical, Catalog # LS003126) in a calcium- and magnesium-free (CMF) Hank's buffer (Gibco, Catalog # 14170-112) containing 137 mM NaCl, 5.36 mM KCl, 0.33 mM Na_2HP_4, 0.44 mM KH_2PO_4, 4.2 mM $NaHCO_3$, 5.55 mM glucose, 0.03 mM phenol red. Ganglia were then treated for 20 minutes at 37°C with 3 mg/ml collagenase (type I; Roche Diagnostics, Catalog #

10103586001) and 4 mg/ml dispase II (Roche Diagnostics, Catalog # 37045800) in CMF Hank's buffer. Cells were dispersed by trituration with a fire-polished glass Pasteur pipette in a solution composed of two media combined in a 1:1 ratio: Leibovitz's L-15 medium (Gibco, Catalog # 11415-064) supplemented with 5 mM HEPES, and DMEM/F12 medium (Gibco, Catalog # 11330-032) and plated onto coverslips. Then cells were incubated at 37°C (5% CO_2) for 2 hours, after which Neurobasal medium (Gibco, Catalog # 10888-022) containing B-27 supplement (Gibco, Catalog # A3582801), and penicillin and streptomycin (Sigma-Aldrich, Catalog # P4333). Cells were stored at room temperature and used within 48 hours.

Electrophysiology with superior cervical ganglion (SCG) neurons

Whole-cell patch clamp recordings were made using a Multiclamp 700B Amplifier (Molecular Devices) interfaced to a Digidata 1321A data acquisition system (Molecular Devices) controlled by pCLAMP 10.3 software (Molecular Devices). Electrodes were 2-4 MΩ when filled with the intracellular solution consisting of 140 mM K aspartate, 13.5 mM NaCl, 1.6 mM $MgCl_2$, 5 mM EGTA, 9 mM HEPES, 14 mM creatine phosphate (Tris salt), 4 mM MgATP, 0.3 mM Tris-GTP, pH 7.2 adjusted with KOH, with shanks wrapped with Parafilm to allow optimal series resistance compensation (70-80%). Seals were formed in Tyrode's solution consisting of 155 mM NaCl, 3.5 mM KCl, 1.5 mM $CaCl_2$, 1 mM $MgCl_2$, 10 mM HEPES, 10 mM glucose, pH 7.4 adjusted with NaOH and cells were lifted in front of quartz fiber flow pipes attached to a temperature-controlled aluminum rod. M-current was recorded with external Tyrode's solution containing 1 µM TTX and 10 µM $CdCl_2$. Recordings were made at 37 °C.

Voltage commands were delivered and current signals were recorded using a Digidata 1321A data acquisition system (Molecular Devices) controlled by pCLAMP 10.3 software (Molecular

Devices). Current and voltage records were filtered at 5 kHz and digitized at 100 kHz. Analysis was performed with Igor Pro 6.12 (Wavemetrics, Lake Oswego, OR), using DataAccess (Bruxton Software) to import pClamp data.

Preparation of rat hippocampal neurons

Primary cultures of hippocampal neurons were prepared from rat embryos (E19 to E20). Pregnant female Sprague-Dawley rats were anesthetized with isoflurane. The skin was washed with 70% ethanol, the peritoneal cavity was opened, and embryos were transferred into ice-cold preparation solution (Ca^{2+}/Mg^{2+}-free HBSS (Gibco, Catalog # 14170-112) with 5 mM HEPES (Gibco, Catalog # 15630-080) and 1 mM sodium pyruvate (Gibco, Catalog # 11360-070) in a 100 mm petri dish on ice. Heads and brains were sequentially dissected from embryos, with the ice-cold preparation solution exchanged during each step. Under a dissecting microscope, the meninges were stripped away from the cerebral hemispheres and dorsal hippocampi were dissected with a fine scissor. The hippocampal pieces were transferred into a pre-warmed preparation solution containing 37 U papain (Worthington, Catalog # LS003126), 5 mM L-cysteine (Sigma, Catalog # C7352), and 1080 U DNase I (Sigma, Catalog # DN-25), incubated at 37 ℃ for 15 minutes, and then washed 3 times with enzyme-free warmed preparation solution. The preparation solution was then exchanged for a titration medium (EMEM, ATCC, Catalog # 30-2003), 5 % FBS (Gibco, Catalog # 16140-071) and 1x penicillin/streptomycin (P/S, Gibco, Catalog # 15140-122), and the hippocampal pieces were titrated using Pasteur pipettes fire-polished to two different tip sizes. After determining cell density using a hematocytometer, a maintenance medium (Neurobasal media (Gibco, Catalog # 21103-049), 2% B27 (Gibco, Catalog # 17504-044), 5 mM Glutamine (Gibco cat # 25030-081), and 1x P/S) was added into cell

suspension to make cell density of 1~1.5 x 10^5/ml. Five poly-D-lysine (Sigma, Catalog # P-7405)-coated coverslips (Fisherbrand, Catalog # 12-545-80) were placed in 35 mm dishes and 2~3 x 10^5 cells were plated in each 35 mm dish (≥ 4~6 x 10^4 cells/coverslip). Neurons were maintained for 13-17 days *in vitro* (DIV). Every 2~3 days, half of the medium was removed from the 35 mm dishes and replaced with the same volume of the fresh maintenance solution.

All experiments using animals were performed according to an institutional IACUC-approved protocol.

Electrophysiology with rat hippocampal neurons

Recordings were made from neurons after 13 to 17 days *in vitro*. Neurons with three processes and a pyramidal shape were selected for recording. To avoid problems arising from absorption of CBD to plasticware, recordings were made in an all-glass chamber made by attaching a glass ring (18 mm outer diameter, 3 mm height, Thomas Scientific 6705R24) to a glass-bottom microwell dish (MatTek # P35G-1.5-20-C). Whole-cell recordings were obtained using patch pipettes with resistances of 2.2 to 2.5 MΩ when filled with the internal solution, consisting of 140 mM K-gluconate, 9 mM NaCl, 1.8 mM $MgCl_2$, 0.09 mM EGTA, 9 mM HEPES, 14 mM creatine phosphate (Tris salt), 4 mM MgATP, and 0.3 mM Tris-GTP, pH adjusted to 7.2 with KOH. The shank of electrode was wrapped with Parafilm to allow optimal series resistance compensation. Seals were obtained and the whole-cell configuration established in Tyrode's solution consisting of 155 NaCl, 3.5 KCl, 1.5 $CaCl_2$, 1 $MgCl_2$, 10 HEPES, 10 Glucose, pH adjusted to 7.4 with NaOH, with added 1 µM TTX. Reported membrane potentials are corrected for a liquid junction potential of -13 mV between the K-gluconate based internal solution and the Tyrode's solution in which current was zeroed at the start of the experiment. The amplifier was

tuned for partial compensation of series resistance (typically 40-70% of a total series resistance of 4-10 MΩ), and tuning was periodically re-adjusted during the experiment. Currents were recorded with a Multiclamp 700B Amplifier (Molecular Devices), filtered at 5 kHz with a low-pass Bessel filter, and digitized using a Digidata 1322A data acquisition interface controlled by pClamp9.2 software (Molecular Devices). Recordings were made at 30 °C.

M-current was evoked by 500-ms steps to -50 mV from a steady holding potential of -30 mV Stock solutions of 10 mM CBD in DMSO and 20 mM XE-991 in DMSO were made in glass vials and diluted into Tyrode's solution (in glass vials) as 20 µM CBD or 60 µM XE-991 on the day of recording. Aliquots of these solutions were applied directly into the glass chamber and mixed with a 100 □L pipettor to make final concentrations of 1 µM CBD or 3 µM XE-991 respectively. To minimize any residual effect of CBD from the previous recording, the glass chamber was rinsed with 70% ethanol for 3 times and distilled water for 3 times before putting a new coverslip into the chamber.

Results

CBD activates heterologously-expressed Kv7.2/7.3 channels

We discovered the ability of CBD to activate Kv7.2/7.3 channels in a high-throughput screen using fluorescence signals from thallium entry evoked by KCl-depolarization of a CHO cell line stably expressing human Kv7.2 and Kv7.3 channels. In a screen of xx compounds chosen from structures with known or possible ion channel modulating activity, CBD was the only compound to produce a substantial enhancement of the fluorescence signal except retigabine and flupirtine, both known activators of Kv7.2/7.3 channels.

We then tested CBD on the Kv7.2/7.3 cell line using whole-cell patch clamp recordings and saw dramatic enhancement of currents activated by depolarization, with particularly large effects for currents activated near -50 mV. Figure 3.1A shows an example, where 100 nM CBD produced a doubling of the current activated at -50 mV, while there was little effect at -20 mV, where channels are near-maximally activated in control. These results were typical. In collected results, 100 nM enhanced the current evoked at -50 mV by an average of 2.0 ± 1.7 (n=13), while 300 nM CBD enhanced the current by 4.7 ± 2.7 (n=13).

Figure 3.1 CBD enhancement of current from cloned human Kv7.2/7.3 channels. (A) Whole-cell recording of hKv7.2/7.3 current evoked by staircase depolarizations before and after application of 100 nM CBD. (B) Collected results (mean ± SEM) for current evoked by a 1-s depolarization from -80 mV to -50 mV after a 6-minute exposure to 100 nM (n=13) or 300 nM CBD (n=11), normalized to current before CBD application. "No CBD" values (n=11) are for 6-minute dummy applications of solution containing only vehicle (DMSO). (C) Voltage-dependent activation of hKv7.2/7.3 channels measured in a cell before and after application of 300 nM CBD. Solid lines: Fits to data points of 4th power Boltzmann function, $[1/(1 + \exp(-(V - V_{hn})/k))]4$, where V is test pulse voltage, V_{hn} is voltage of half-maximal activation for single "n" particle, and k is slope factor for activation of n particles. Control: V_{hn} = -47.8 mV, k = 7.7 mV (midpoint of function= -35.0) ; 300 nM CBD: V_{hn} = -69.0 mV, k = 9.5 mV (midpoint of function -53.1 mV). (D) Collected results for concentration-dependent shift of activation midpoint by CBD. Measurements of midpoint were made before and 10 minutes after exposure to CBD at the various concentrations. Mean ± SEM, n=9 for 30 nM CBD, n=14 for 100 nM CBD, n=14 for 300 nM CBD, n=12 for 500 nM CBD, n=7 for 1 uM CBD, n=15 for 3 uM CBD, n=19 for 10 uM CBD, n=10 for 20 uM CBD. Value for 0 CBD represents measurements of a small shift that occurred with dummy applications of DMSO-containing control solution for 10 minutes (n=11).

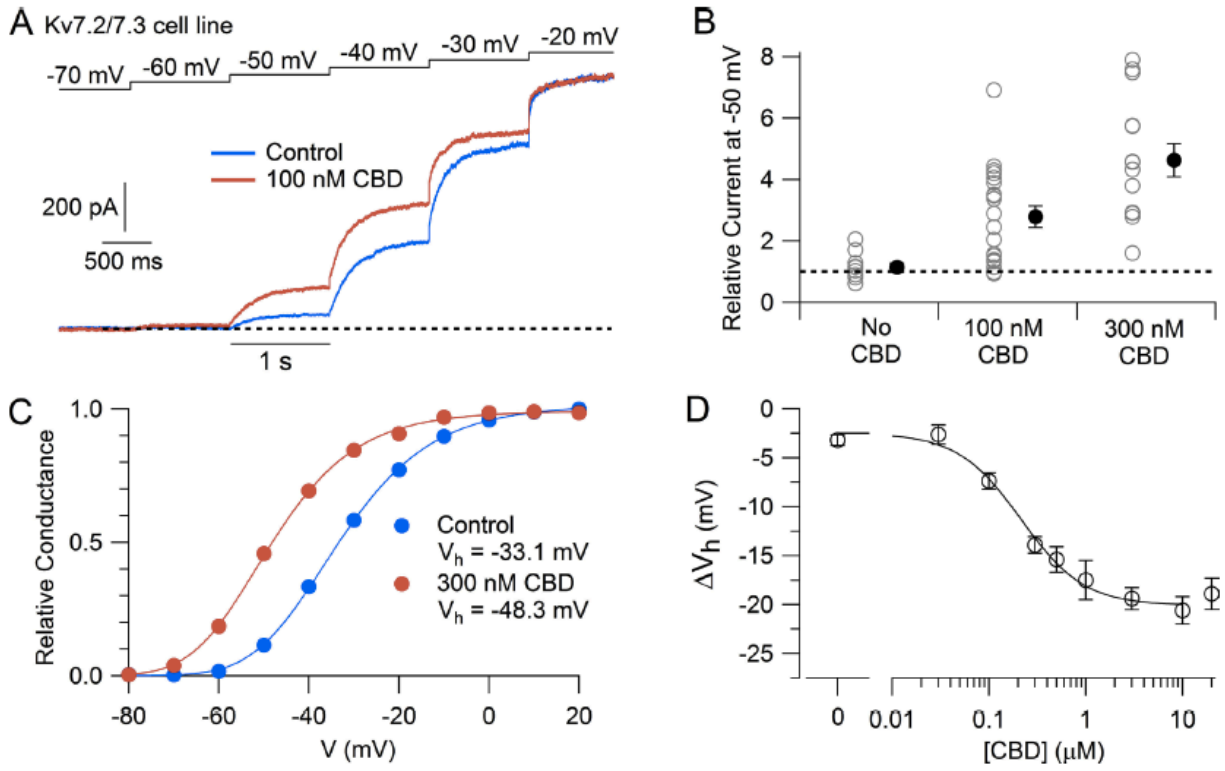

Figure 3.1 (Continued)

The enhancement of Kv7.2/7.3-mediated current was produced by a shift of the voltage-dependent activation of the channels in the hyperpolarizing direction (Figure 3.1C). In collected results, 300 nM CBD shifted the midpoint for channel activation by an average of -13.9 ± 1.0 mV. The effect of CBD to shift the voltage-dependence of activation saturated at a shift of about -20 mV produced by concentrations of 3-10 μM, with CBD acting with a half-maximal concentration of about 200 nM (Figure 3.1D).

We next tested whether CBD can enhance native Kv7 channels in neurons, using measurements of M-current in mouse superior cervical ganglion (SCG) neurons. Using the classic voltage protocol for distinguishing M-current from other kinds of potassium current by virtue of its non-inactivating property and activation at subthreshold voltages (Brown and Adams, 1982), we used a steady holding voltage of -30 mV and used hyperpolarizing voltage steps to quantify M-current from its characteristic slow, voltage-dependent deactivation. Application of 100 nM CBD produced a dramatic enhancement of steady-state outward current at -30 mV and also enhanced the slowly deactivating current seen during a hyperpolarization to -70 mV (Figure 3.2A). It was also clear that CBD shifted the voltage-dependence of M-current activation, resulting in less complete deactivation for a step to -60 mV. In collected results, 100 nM CBD produced an enhancement of steady current at -50 mV by a factor of 2.4 ± 0.3 (n=7).

Figure 3.2 CBD enhancement of M current in mouse sympathetic neurons. (A) Currents evoked by hyperpolarizations to -60 mV and -70 mV from a holding potential of -30 mV before (blue) and after (red) application of 300 nM CBD. (B) Collected results for effect of 300 nM CBD on steady-state current at -50 mV (n=7). (C) Statistics for effects of 300 nM CBD on current at -50 mV, normalized to control current. Gray circles: individual cells. Black circles: mean ± SEM.

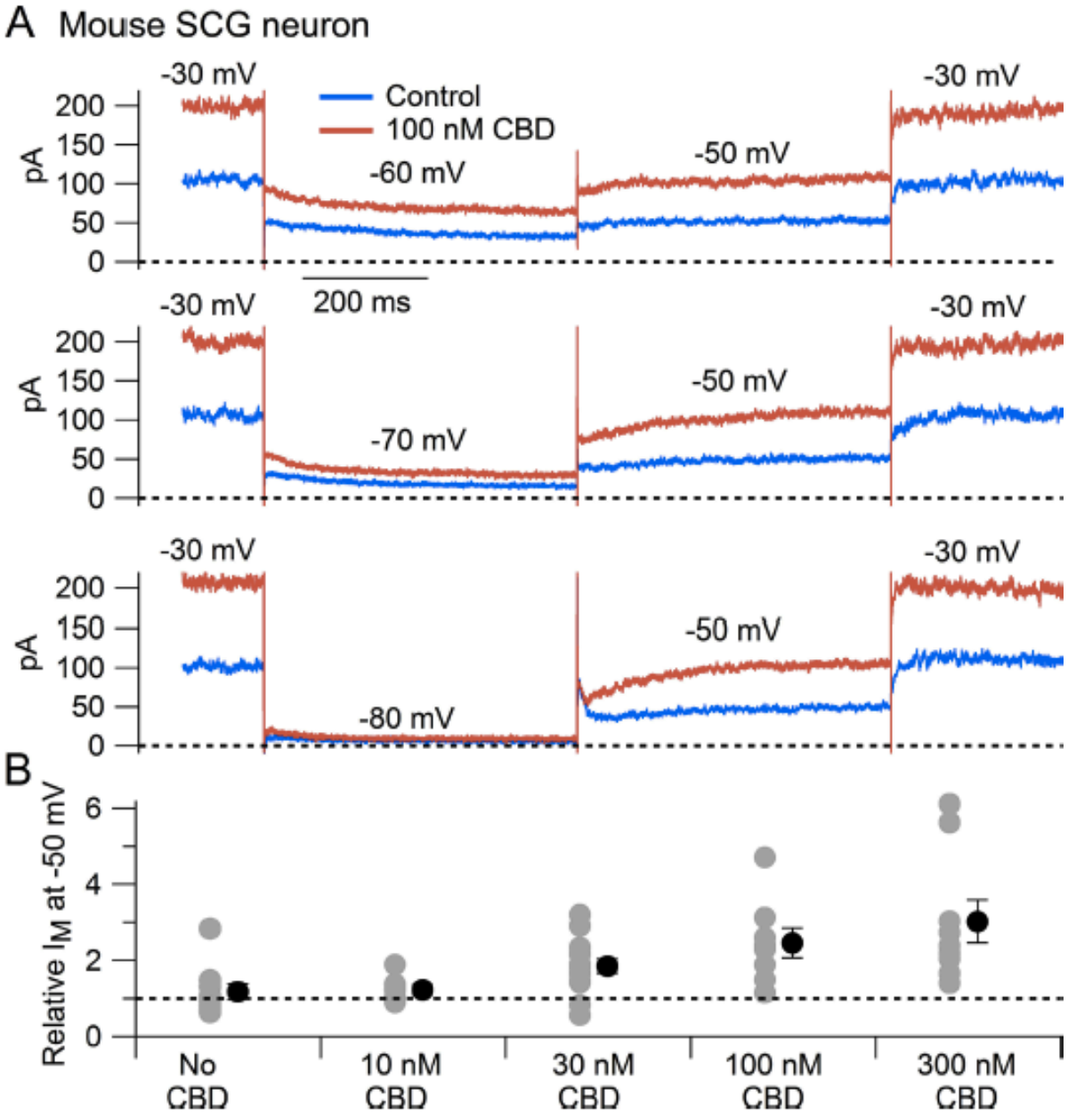

Figure 3.2 (Continued)

To test whether CBD enhancement of M-current also occurs in central neurons likely involved in epilepsy, we tested CBD on potassium currents in hippocampal neurons (Figure 3.3). To facilitate application of well-defined concentrations of CBD without potential problems from absorption into the bulk tissue of brain slices, we used a preparation of cultured rat hippocampal neurons. Using a voltage protocol designed to emphasize M-current (holding the neurons at -30 mV and stepping to -50 mV), CBD enhanced the outward current at both -30 mV and -50 mV in 16 of 20 cells tested. Consistent with being enhancement of Kv7-mediated current, there was no enhancement if CBD was applied in the presence of the Kv7 inhibitor XE-991.

Figure 3.3 CBD enhancement of Kv7 current in rat hippocampal neurons. (A) Currents at a holding voltage of -30 mV and during a 1-s hyperpolarization to -50 mV in control, after application of 1 µM CBD, and after addition of 3 µM XE-991 in the continuing presence of CBD. (B) Collected data with this protocol. Current was measured at the end of the step to -50 mV, normalized to current before application of CBD. Connected open circles indicate data for individual cells (n=20 for application of CBD, n=16 for application of CBD followed by XE-991) and closed circles represent mean ± SEM. (C) Currents in control, after application of 3 µM XE-991, and after addition of 1 µM CBD in the continuing presence of XE-991. (D) Collected data with symbols as in (B); n=15 cells for application of XE-991 followed by CBD.

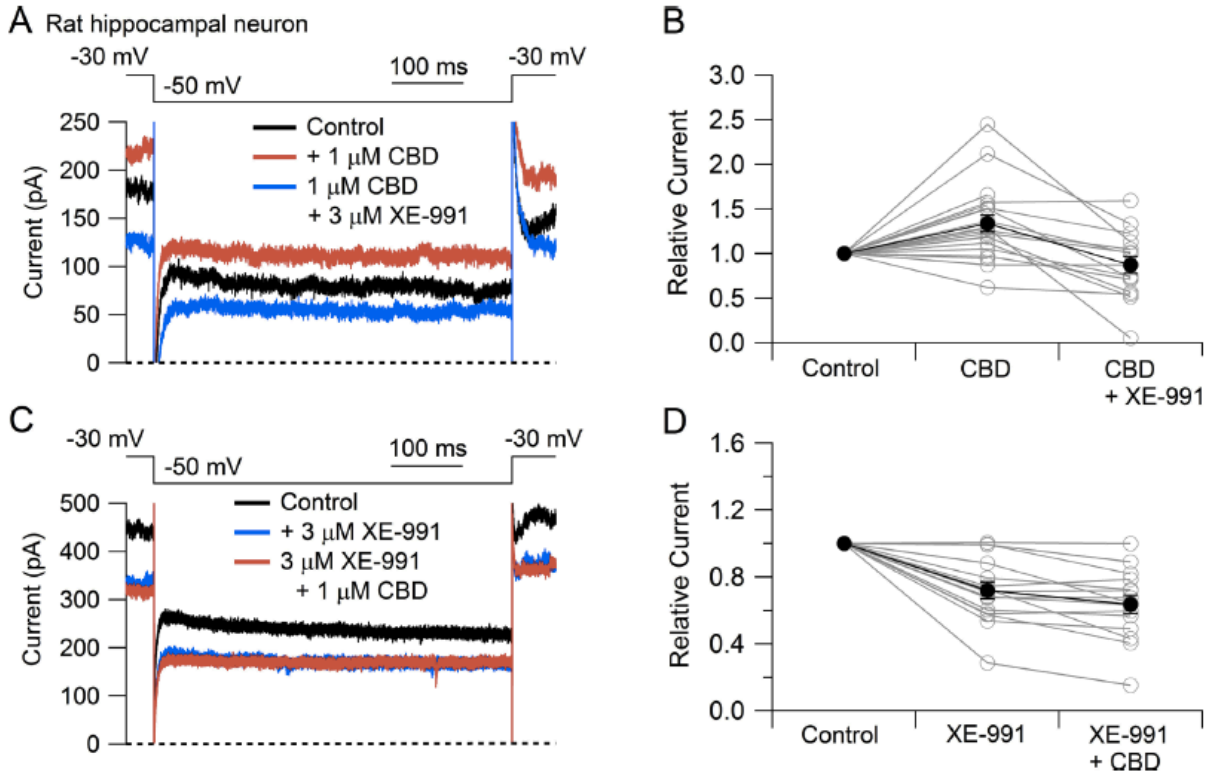

Figure 3.3 (Continued)

Discussion

M-current mediated by Kv7 channels plays a major role in controlling excitability of many types of neurons, including sympathetic neurons and neocortical pyramidal neurons (Barrese et al., 2009; Brown and Passmore, 2009; Gunthorpe et al., 2012; Vigil et al., 2020). Enhancement of M-current is a clinically-proven mechanism of antiepileptic action, as demonstrated by the clinical efficacy of retigabine, an antiepileptic drug that acts by enhancement of current through Kv7 channels (Tatulian et al., 2000; Gunthorpe et al., 2012; Sills and Rogawski, 2020). Our results suggest that the clinical efficacy of CBD could also result largely or in part by enhancement of Kv7-mediated M-current in central neurons. As in the case of retigabine, it remains to be determined exactly which populations of neurons are most sensitive to enhancement of M-current and how these effects alter overall network activity relevant to epileptic activity.

Interestingly, the effect of CBD to enhance neuronal M-current is opposite to the effect of cannabinoids that act as agonists at the CB1 receptor, which inhibit M-current in hippocampal neurons (Schweitzer, 2000). Thus the fact that CBD is not a CB1 agonist –and actually acts as an allosteric antagonist at CB1 receptors (Laprairie et al., 2015; Straiker et al., 2018) – may be an important aspect of its action. The opposite effects on M-current of CBD and CB1 agonists like THC fit well with the history of development of CBD as an anti-epileptic drug, which began with anecdotal evidence that extracts from a particular strain of cannabis with high CBD and low THC ("Charlotte's Web") were an effective adjunctive therapy for a child with Dravet Syndrome (Maa and Figi, 2014; Rosenberg et al., 2015; Williams and Stephens, 2020).

Our results add to other recent experiments demonstrating that Kv7.2/7.3 channels are susceptible to enhancement by a wide variety of agents acting by several different mechanisms (Manville and Abbott, 2018a,b; Wang et al., 2018; Kanyo et al., 2020; Kurata, 2020). Such agents include endogenous compounds like GABA (Manville et al., 2018), the ketone body β-hydroxybutyrate (Manville et al., 2020), and arachidonic acid metabolites and derivatives (Schweitzer et al., 1990, 1993; Larsson et al., 2002a,b), as well as a variety of natural products including cilantro (Manville and Abbott, 2019). Further development of Kv7.2/7.3 enhancers for treating epilepsy and other neuronal disorders seems promising (Barrese et al., 2009; Vigil et al., 2020), especially now that retigabine has now been withdrawn from clinical use because of a number of side effects (Brickel et al. 2020). Of all the classes of other compounds found to enhance Kv7.2/7.3 channels, CBD has the unique distinction of having already been successfully used in multiple clinical trials. However, CBD is far from a perfect drug (Sekar and Pack, 2019), with complex pharmacokinetics that limit effective oral administration and require large dosages (Millar et al., 2019). Improved knowledge of CBD's most important molecular targets should allow design of compounds that retain key molecular actions with improved pharmacokinetics and reduced off-target effects.

References

Barrese V, Stott JB, Greenwood IA (2018) KCNQ-Encoded Potassium Channels as Therapeutic Targets. Annu Rev Pharmacol Toxicol 58:625–648.

Brickel N, Hewett K, Rayner K, McDonald S, De'Ath J, Daniluk J, Joshi K, Boll MC, Tiamkao S, Vorobyeva O, Cooper J. (2020) Safety of retigabine in adults with partial-onset seizures after

long-term exposure: focus on unexpected ophthalmological and dermatological events. Epilepsy Behav. 102: 106580.

Brown, D.A., and Adams, P.R. (1980). Muscarinic suppression of a novel voltage-sensitive K+ current in a vertebrate neurone. Nature *283*, 673–676.

Brown, D.A., and Passmore, G.M. (2009). Neural KCNQ (Kv7) channels. Br J Pharmacol *156*, 1185–1195.

De Silva, A.M., Manville, R.W., and Abbott, G.W. (2018). Deconstruction of an African folk medicine uncovers a novel molecular strategy for therapeutic potassium channel activation. Sci Adv *4*, eaav0824.

Devinsky O, Cross JH, Laux L, Marsh E, Miller I, Nabbout R, Scheffer IE, Thiele EA, Wright S (2017) Trial of Cannabidiol for Drug-Resistant Seizures in the Dravet Syndrome. N Engl J Med 376:2011–2020.

Devinsky O, Nabbout R, Miller I, Laux L, Zolnowska M, Wright S, Roberts C (2019) Long-term cannabidiol treatment in patients with Dravet syndrome: An open-label extension trial. Epilepsia 60:294–302.

Devinsky O, Patel AD, Cross JH, Villanueva V, Wirrell EC, Privitera M, Greenwood SM, Roberts C, Checketts D, VanLandingham KE, Zuberi SM (2018a) Effect of Cannabidiol on Drop Seizures in the Lennox-Gastaut Syndrome. N Engl J Med 378:1888–1897.

Devinsky O, Patel AD, Thiele EA, Wong MH, Appleton R, Harden CL, Greenwood S, Morrison G, Sommerville K (2018b) Randomized, dose-ranging safety trial of cannabidiol in Dravet syndrome. Neurology 90:e1204–e1211.

Franco V, Perucca E (2019) Pharmacological and Therapeutic Properties of Cannabidiol for Epilepsy. Drugs 79:1435–1454.

Ghovanloo M-R, Shuart NG, Mezeyova J, Dean RA, Ruben PC, Goodchild SJ (2018) Inhibitory effects of cannabidiol on voltage-dependent sodium currents. J Biol Chem 293:16546–16558.

Gunthorpe MJ, Large CH, Sankar R (2012) The mechanism of action of retigabine (ezogabine), a first-in-class K+ channel opener for the treatment of epilepsy. Epilepsia 53:412–424.

Hill AJ, Jones NA, Smith I, Hill CL, Williams CM, Stephens GJ, Whalley BJ (2014) Voltage-gated sodium (NaV) channel blockade by plant cannabinoids does not confer anticonvulsant effects per se. Neurosci Lett 566:269–274.

Hippalgaonkar, K., Gul, W., ElSohly, M.A., Repka, M.A., and Majumdar, S. (2011). Enhanced solubility, stability, and transcorneal permeability of δ-8-tetrahydrocannabinol in the presence of cyclodextrins. AAPS PharmSciTech *12*, 723–731.

Jepps TA, Barrese V, Miceli F (2021) Editorial: Kv7 Channels: Structure, Physiology, and Pharmacology. Front Physiol 12:679317.

Jones NA, Hill AJ, Smith I, Bevan SA, Williams CM, Whalley BJ, Stephens GJ (2010) Cannabidiol displays antiepileptiform and antiseizure properties in vitro and in vivo. J Pharmacol Exp Ther 332:569–577.

Kanyo, R., Wang, C.K., Locskai, L.F., Li, J., Allison, W.T., and Kurata, H.T. (2020). Functional and behavioral signatures of Kv7 activator drug subtypes. Epilepsia *61*, 1678–1690.

Kaplan JS, Stella N, Catterall WA, Westenbroek RE (2017) Cannabidiol attenuates seizures and social deficits in a mouse model of Dravet syndrome. Proc Natl Acad Sci U S A 114:11229–11234.

Khan AA, Shekh-Ahmad T, Khalil A, Walker MC, Ali AB (2018) Cannabidiol exerts antiepileptic effects by restoring hippocampal interneuron functions in a temporal lobe epilepsy model. Br J Pharmacol 175:2097–2115.

Kurata HT (2020) Chemical regulation of Kv7 channels: Diverse scaffolds, sites, and mechanisms of action. J Gen Physiol 152.

Laprairie RB, Bagher AM, Kelly MEM, Denovan-Wright EM (2015) Cannabidiol is a negative allosteric modulator of the cannabinoid CB1 receptor. Br J Pharmacol 172:4790–4805.

Larsson JE, Frampton DJA, Liin SI (2020a) Polyunsaturated Fatty Acids as Modulators of K(V)7 Channels. Front Physiol 11:641.

Larsson, J.E., Karlsson, U., Wu, X., and Liin, S.I. (2020b). Combining endocannabinoids with retigabine for enhanced M-channel effect and improved KV7 subtype selectivity. J Gen Physiol *152*.

Li, X., Zhang, Q., Guo, P., Fu, J., Mei, L., Lv, D., Wang, J., Lai, D., Ye, S., Yang, H., et al. (2021). Molecular basis for ligand activation of the human KCNQ2 channel. Cell Res *31*, 52–61.

Maa, E., and Figi, P. (2014). The case for medical marijuana in epilepsy. Epilepsia 55, 783–786.

Madamba, S.G., Schweitzer, P., and Siggins, G.R. (1999). Dynorphin selectively augments the M-current in hippocampal CA1 neurons by an opiate receptor mechanism. J Neurophysiol *82*, 1768–1775.

Maljevic S, Lerche H (2014) Potassium channel genes and benign familial neonatal epilepsy. Prog Brain Res 213:17–53.

Manville, R.W., and Abbott, G.W. (2018a). Ancient and modern anticonvulsants act synergistically in a KCNQ potassium channel binding pocket. Nat Commun *9*, 3845.

Manville, R.W., and Abbott, G.W. (2018b). Gabapentin Is a Potent Activator of KCNQ3 and KCNQ5 Potassium Channels. Mol Pharmacol *94*, 1155–1163.

Manville, R.W., and Abbott, G.W. (2019). Cilantro leaf harbors a potent potassium channel-activating anticonvulsant. FASEB J *33*, 11349–11363.

Manville, R.W., Papanikolaou, M., and Abbott, G.W. (2018). Direct neurotransmitter activation of voltage-gated potassium channels. Nat Commun *9*, 1847.

Manville, R.W., Papanikolaou, M., and Abbott, G.W. (2020). M-Channel Activation Contributes to the Anticonvulsant Action of the Ketone Body β-Hydroxybutyrate. J Pharmacol Exp Ther *372*, 148–156.

Mason ER, Cummins TR (2020) Differential Inhibition of Human Nav1.2 Resurgent and Persistent Sodium Currents by Cannabidiol and GS967. Int J Mol Sci 21.

Mechoulam R, Shani A, Edery H, Grunfeld Y (1970) Chemical basis of hashish activity. Science 169:611–612.

Miceli F, Soldovieri MV, Ambrosino P, Manocchio L, Mosca I, Taglialatela M (2018) Pharmacological Targeting of Neuronal Kv7.2/3 Channels: A Focus on Chemotypes and Receptor Sites. Curr Med Chem 25:2637–2660.

Millar SA, Stone NL, Bellman ZD, Yates AS, England TJ, O'Sullivan SE (2019) A systematic review of cannabidiol dosing in clinical populations. Br J Clin Pharmacol 85:1888–1900.

Miller I, Scheffer IE, Gunning B, Sanchez-Carpintero R, Gil-Nagel A, Perry MS, Saneto RP, Checketts D, Dunayevich E, Knappertz V (2020) Dose-Ranging Effect of Adjunctive Oral Cannabidiol vs Placebo on Convulsive Seizure Frequency in Dravet Syndrome: A Randomized Clinical Trial. JAMA Neurol 77:613–621.

Patel RR, Barbosa C, Brustovetsky T, Brustovetsky N, Cummins TR (2016) Aberrant epilepsy-associated mutant Nav1.6 sodium channel activity can be targeted with cannabidiol. Brain 139:2164–2181.

Pertwee RG (2005) Pharmacological actions of cannabinoids. Handb Exp Pharmacol:1–51.

Raucci, U., Pietrafusa, N., Paolino, M.C., Di Nardo, G., Villa, M.P., Pavone, P., Terrin, G., Specchio, N., Striano, P., and Parisi, P. (2020). Cannabidiol Treatment for Refractory Epilepsies in Pediatrics. Front Pharmacol 11, 586110.

Rosenberg EC, Patra PH, Whalley BJ (2017) Therapeutic effects of cannabinoids in animal models of seizures, epilepsy, epileptogenesis, and epilepsy-related neuroprotection. Epilepsy Behav 70:319–327.

Rosenberg EC, Tsien RW, Whalley BJ, Devinsky O (2015) Cannabinoids and Epilepsy. Neurotherapeutics 12:747–768.

Ryberg E, Larsson N, Sjögren S, Hjorth S, Hermansson N-O, Leonova J, Elebring T, Nilsson K, Drmota T, Greasley PJ (2007) The orphan receptor GPR55 is a novel cannabinoid receptor. Br J Pharmacol 152:1092–1101

Schweitzer, P., Madamba, S., and Siggins, G.R. (1990). Arachidonic acid metabolites as mediators of somatostatin-induced increase of neuronal M-current. Nature *346*, 464–467.

Schweitzer, P., Madamba, S., Champagnat, J., and Siggins, G.R. (1993). Somatostatin inhibition of hippocampal CA1 pyramidal neurons: mediation by arachidonic acid and its metabolites. J Neurosci *13*, 2033–2049.

Sekar, K., and Pack, A. (2019). Epidiolex as adjunct therapy for treatment of refractory epilepsy: a comprehensive review with a focus on adverse effects. F1000Res 8.

Shah, M.M., Mistry, M., Marsh, S.J., Brown, D.A., and Delmas, P. (2002). Molecular correlates of the M-current in cultured rat hippocampal neurons. J Physiol *544*, 29–37.

Sills GJ, Rogawski MA (2020) Mechanisms of action of currently used antiseizure drugs. Neuropharmacology 168:107966.

Silva, G.D., Del Guerra, F.B., de Oliveira Lelis, M., and Pinto, L.F. (2020). Cannabidiol in the Treatment of Epilepsy: A Focused Review of Evidence and Gaps. Front Neurol 11, 531939.

Straiker A, Dvorakova M, Zimmowitch A, Mackie K (2018) Cannabidiol Inhibits Endocannabinoid Signaling in Autaptic Hippocampal Neurons. Mol Pharmacol 94:743–748.

Tatulian, L., Delmas, P., Abogadie, F.C., and Brown, D.A. (2001). Activation of expressed KCNQ potassium currents and native neuronal M-type potassium currents by the anti-convulsant drug retigabine. J Neurosci *21*, 5535–5545.

Thiele E, Marsh E, Mazurkiewicz-Beldzinska M, Halford JJ, Gunning B, Devinsky O, Checketts D, Roberts C (2019) Cannabidiol in patients with Lennox-Gastaut syndrome: Interim analysis of an open-label extension study. Epilepsia 60:419–428.

Thomas, B.F., Compton, D.R., and Martin, B.R. (1990). Characterization of the lipophilicity of natural and synthetic analogs of delta 9-tetrahydrocannabinol and its relationship to pharmacological potency. J Pharmacol Exp Ther *255*, 624–630.

Vigil, F.A., Carver, C.M., and Shapiro, M.S. (2020). Pharmacological Manipulation of K (v) 7 Channels as a New Therapeutic Tool for Multiple Brain Disorders. Front Physiol *11*, 688.

Wang CK, Lamothe SM, Wang AW, Yang RY, Kurata HT (2018) Pore- and voltage sensor-targeted KCNQ openers have distinct state-dependent actions. J Gen Physiol 150:1722–1734.

Watkins AR (2019) Cannabinoid interactions with ion channels and receptors. Channels (Austin) 13:162–167.

Wickenden, A.D., Yu, W., Zou, A., Jegla, T., and Wagoner, P.K. (2000). Retigabine, a novel anti-convulsant, enhances activation of KCNQ2/Q3 potassium channels. Mol Pharmacol *58*, 591–600.

Williams, C.M., and Stephens, G.J. (2020). Development of cannabidiol as a treatment for severe childhood epilepsies. Br J Pharmacol 177, 5509–5517.

Conclusions and discussion

This thesis work aimed to study the effect of CBD on excitability of primary nociceptive neurons and three types of voltage-gated ion channels: Nav1.8, Nav1.7 and Kv7. Using current clamp, I found that CBD inhibits firing of primary nociceptive neurons with greater potency than the local anesthetic bupivacaine. The reduced excitability can be explained by inhibition of Nav1.8 and Nav1.7 channels by CBD. The molecular mechanism of action of CBD involves tight binding to the slow inactivated states of Nav1.8. CBD also binds tightly to the inactivated states of hNav1.7. Structure of CBD-bound hNav1.7 from our collaborators reveals two binding sites: an "F-site" sitting in the fenestration between domain IV and I and an "I-site" located next to the Ile/Phe/Met (IFM) motif important for allosteric inactivation. Lastly, CBD enhances Kv7 currents in a cell line, in SCG neurons, and in hippocampal CA1 neurons by shifting the activation to the hyperpolarizing direction. Together, my results help provide some potential molecular effects by which CBD exerts its anti-epileptic and analgesic efficacy *in vivo*. It also suggests a strategy for future drug discovery for pain and epilepsy, by searching for compounds that inhibit neuronal excitability by a similar combination of effects of inhibiting sodium channels in a state-dependent manner and activating Kv7 channels.

CBD inhibition of voltage-gated potassium channels

I characterized the effects of CBD on three kinds of ion channels, but CBD may also have important effects on other channels. In the experiment in Figure 1.3 C, I saw that CBD inhibits outward currents evoked by a voltage step from -80 mV to 20 mV. Some of the questions following from the inhibition of outward currents are the following: 1. What is the consequence of CBD inhibition of outward currents on nociceptor firing? 2. What is the molecular identity of

the ion channels that give rise to the outward currents inhibited by CBD?. To start to answer these questions, I did some preliminary experiments using current clamp and action potential clamp. Interestingly, when 1μM CBD was applied, I observed a transient enhancement in firing of nociceptors within 1 minute of CBD application, before the inhibition described after 4 minutes of application in Chapter 1. In addition, CBD reduced the amplitude of the afterhyperpolarization following action potentials. These observations are consistent with CBD inhibition of potassium currents. Previously Pin Liu in our lab performed action potential clamp with waveforms recorded from nonpeptidergic nociceptors during repetitive firing and isolated different potassium currents with sequential application of potassium channel blockers (unpublished data, see method in (Zheng et al., 2019)). I analyzed her data and found that three major types of voltage-gated potassium channels contribute to the outward currents that flow between the 1st and the 2nd action potential during nociceptor repetitive firing: Kv1 channels, Kv2 channels and Kv4 channels. On average Kv1 channels contribute 19% to the outward currents between spikes; Kv2 channels contribute 54% and Kv4 channels contribute 22%. To explore CBD inhibition of potassium channels using more physiological stimuli than the voltage steps in Figure 1.3, I used an action potential clamp protocol made with previously-recorded repetitive firing waveforms and discovered that CBD reduced the outward currents that flow between spikes. After 1 minute of CBD wash-on, net outward current was inhibited by an average of about 60%. It is known that CBD inhibits Kv2.1 with an IC_{50} of 3.7 μM measured by automated patch clamp (Ghovanloo et al., 2018). Further experiments are needed to determine the potency of CBD on Kv1 channels, Kv2 channels and Kv4 channels. One option is to use a combination of blockers to isolate one potassium channel then test the effect CBD on that

potassium channel in nociceptors. A complementary way would be to test CBD on the three channels expressed separately in a heterologous system.

Structure of CBD-bound hNav1.7

One complication of correlating the structural results with the functional results in chapter 2 is the difference in CBD concentrations used: in cryo-EM experiments our collaborators used 10 μM CBD while in electrophysiological experiments we used sub-micromolar CBD to reveal potent binding to inactivated states of the channel. At 10 μM CBD was found to bind to both the F-site and the I-site, but it remains uncertain which one of these sites is responsible for the high-affinity binding to inactivated channels. To test the relevance of those two binding sites in the context of sub-micromolar inhibition of hNav1.7 channels, one experiment to do could be to solve the structure of hNav1.7 with CBD at sub-micromolar concentrations. If any binding site is more frequently occupied at sub-micromolar concentration, then it suggests a stronger functional correlation between that binding site and CBD inhibition of hNav1.7.

The exact function of the F-site remains unclear. To study the functional significance of the F site, two single point mutations in hNav1.7 (V383A and F387A) were made by our collaborators. They found that both point mutations moderately reduced the sensitivity of hNav1.7 to CBD with the IC_{50} right-shifted from 1.82 ± 0.10 μM to 3.56 ± 0.58 μM by V383A and to 3.65 ± 0.78 μM by F387A. However, a puzzling aspect of the F-site is that the binding of CBD does not seem to change the position of the residues in the bound versus unbound states. Thus, it is not clear how binding of CBD alters the function of the channel, especially since the binding site is not in the pore of the channel. One possibility is that the F-site is necessary for forming a pathway for hydrophobic molecules such as CBD to access the I-site (Hille, 1977). However, access to the I-

site might not require entry from the F-site because the I-site is located outside of the pore domain and seems accessible directly from cell membrane. In the future, molecular dynamics might be applied to study the movement of CBD from extracellular solution to the F-site and the I-site.

Although mutations at the I site reduced the effect of CBD on shifts of V_h (Figure 2.3 f), the effects of CBD were not eliminated by the mutations. This suggests that CBD may interact with hNav1.7 channels at other sites which are somehow not captured by cryo-EM due to its limitations. One potentially important site for CBD inhibition of hNav1.7 channels is a key phenyalanine residue hNav1.7-F1748 in the upper region of the pore. Mutating the equivalent residue F1586 in Nav1.4 channels resulted in reduced CBD inhibition of Nav1.4 (Ghovanloo et al., 2021). To test this hypothesis, our collaborators discovered that mutating hNav1.7-F1748 had a modest effect on CBD inhibition of hNav1.7 channels, even though the structure does not show CBD bound near this residue. The shift induced by CBD in hNav1.7 channels with F1748A mutation was decreased to -6 mV compared to -9 mV in WT channels. One possibility is that CBD does interact with this phenylalanine, but in a manner without the well-defined localization that is required for detection of a bound compound with cryo-EM. Also there is a general caveat about interpreting the effects of mutations, which can produce allosteric changes in binding sites distant from the residue being mutated. To validate the binding sites in a more deterministic way, it would be interesting to solve the structure of CBD with hNav1.7 mutants. If CBD becomes absent in the structure of certain hNav1.7 mutants, then one can draw a more deterministic conclusion about the role of that mutation site being the major binding site of CBD in hNav1.7.

Hydrophobicity of CBD

CBD is a highly hydrophobic compound with an estimated logD of 6 (Ghovanloo et al., 2022). The logD suggests CBD is $10^{\wedge 6}$ times more concentrated in lipid than in aqueous solution. Previous studies showed that Δ8-THC, which has very similar physicochemical properties and is similarly hydrophobic, is lost from aqueous solution by 80% during storage in plastic containers (but not glass containers) after 30 min, probably from adsorption into the plastic (Hippalgaonkar et al., 2011). This raises the question about the accuracy of measurements done with CBD when using conventional plastic containers and tubing. For experiments in hNav1.7 and Kv7 in chapter 2 and 3, which were done later in my thesis work, I used an all-glass drug delivery system but for the earlier experiments in nociceptors in Chapter 1, CBD solutions were prepared in plastic test tubes and the solution reservoirs were plastic syringe barrels. Partial loss of CBD from the solutions in reservoirs could result in an underestimation of CBD potency in the measurements on nociceptor firing and on Nav1.8 channels. Further experiments will be needed to establish the potency of CBD for these actions. The experiments done with sub-micromolar concentrations of CBD are likely most susceptible to partial loss of CBD. Previous experiments in the literature were very likely conducted with conventional plastic-tubing based drug delivery systems, and the potency of CBD may very well have been underestimated in these experiments because of adsorption by plastic. In automated patch clamp systems, drug samples are typically pipetted from plastic compound plates with reservoirs that have a small volume and high surface area, which may exacerbate loss by adsorption into plastic. For future experiments, researchers should avoid using plastics for storing or delivering CBD and other hydrophobic cannabinoids to improve accuracy of measurements.

Because CBD has been reported to affect so many different proteins, knowing which of these effects are most important for CBD's clinical actions depends on knowing the dose-dependence for each effect along with the *in vivo* concentrations of CBD when used clinically. The dose-dependence for *in vitro* experiments reported in the literature are difficult to interpret because of the likely loss of low concentrations of CBD when using plastic labware and tubing to prepare and study the CBD solutions. Most of the effects reported in the literature were seen with concentrations of CBD in the micromolar range. Previous to my work, the most potent effect of CBD reported was its action as a negative allosteric modulator of CB1 receptor, with significant effects at levels as low as 100 nM (Straiker et al., 2018). This thesis reports similar potency on the slow inactivated states of Nav1.8 (K_d of 150 nM) and on the inactivated states of hNav1.7 (K_d of 65 nM) and the experiments on Kv7.2/7.3 channels showed significant effects at concentrations as low as 30 nM. Whether the difference in the potency for sodium channel inhibition between my results and previous experiments characterizing dose-response curves using automated patch clamp (Ghovanloo et al., 2018) are biologically real or due to loss of CBD in plastic drug delivery system is to be determined.

Pharmacokinetics of CBD

The high lipophilicity of CBD also results in poor bioavailability in humans (Millar et al., 2018). With a high dose of oral ingestion of 800 mg CBD, peak plasma concentration reaches 700 nM (Millar et al., 2018), a concentration many times the EC_{50} for its effects on sodium channels or Kv7.2/7.3 channels. However, this seemingly high concentration represents total concentration, including both plasma protein bound-CBD and unbound-CBD. A preliminary experiment attempted to separate plasma protein-bound CBD from unbound-CBD (Tayo et al., 2020). Only

10% of CBD was found to be free and unbound to plasma protein. This suggests that the free concentration of CBD available for binding to therapeutic targets might fall into the range of tens of nanomolar. My thesis reports CBD acting on Nav1.8, hNav1.7 and Kv7 at concentrations from tens nanomolar to hundreds of nanomolar. This suggests that the actions of CBD to inhibit voltage-dependent sodium channels and to activate Kv7 channels may be important at therapeutically relevant concentrations and may contribute to the efficacy of CBD in pain and epilepsy. However, the results leave open the possibility that effects on other targets may also be important at clinical concentrations.

References:

Abraham AD, Leung EJY, Wong BA, Rivera ZMG, Kruse LC, Clark JJ, Land BB (2019) Orally consumed cannabinoids provide long-lasting relief of allodynia in a mouse model of chronic neuropathic pain. Neuropsychopharmacology:1–10 Available at: http://dx.doi.org/10.1038/s41386-019-0585-3.

Alaia MJ, Hurley ET, Vasavada K, Markus DH, Britton B, Gonzalez-Lomas G, Rokito AS, Jazrawi LM, Kaplan K (2022) Buccally Absorbed Cannabidiol Shows Significantly Superior Pain Control and Improved Satisfaction Immediately After Arthroscopic Rotator Cuff Repair: A Placebo-Controlled, Double-Blinded, Randomized Trial. Am J Sports Med 50:3056–3063.

Ali RM, Al Kury LT, Yang KHS, Qureshi A, Rajesh M, Galadari S, Shuba YM, Howarth FC, Oz M (2015) Effects of cannabidiol on contractions and calcium signaling in rat ventricular myocytes. Cell Calcium 57:290–299 Available at: http://dx.doi.org/10.1016/j.ceca.2015.02.001.

Alsaloum M, Higerd GP, Effraim PR, Waxman SG (2020) Status of peripheral sodium channel blockers for non-addictive pain treatment. Nat Rev Neurol 2020 1612 16:689–705 Available at: https://www.nature.com/articles/s41582-020-00415-2 [Accessed February 28, 2023].

Anand U, Jones B, Korchev Y, Bloom SR, Pacchetti B, Anand P, Sodergren MH (2020) CBD effects on TRPV1 signaling pathways in cultured drg neurons. J Pain Res 13:2269–2278.

Bean BP (2007) The action potential in mammalian central neurons. Nat Rev Neurosci 8:451–465 Available at: http://www.nature.com/articles/nrn2148 [Accessed April 16, 2018].

Bean BP, Cohen CJ, Tsien RW (1983) Lidocaine block of cardiac sodium channels. J Gen Physiol

81:613–642.

Bennett DL, Clark XAJ, Huang J, Waxman SG, Dib-Hajj SD (2019) The role of voltage-gated sodium channels in pain signaling. Physiol Rev 99:1079–1151.

Blair NT, Bean BP (2002) Roles of Tetrodotoxin (TTX)-Sensitive Na Current, TTX-Resistant Na Current, and Ca 2 Current in the Action Potentials of Nociceptive Sensory Neurons. Available at: https://www.jneurosci.org/content/jneuro/22/23/10277.full.pdf [Accessed July 2, 2019].

Blair NT, Bean BP (2003) Cellular/Molecular Role of Tetrodotoxin-Resistant Na Current Slow Inactivation in Adaptation of Action Potential Firing in Small-Diameter Dorsal Root Ganglion Neurons. Available at: https://www.jneurosci.org/content/jneuro/23/32/10338.full.pdf [Accessed September 13, 2019].

Bosmans F, Puopolo M, Martin-Eauclaire M-F, Bean BP, Swartz KJ (2011) Functional properties and toxin pharmacology of a dorsal root ganglion sodium channel viewed through its voltage sensors. J Gen Physiol 138:59–72.

Brodie MJ (2017) Sodium Channel Blockers in the Treatment of Epilepsy. CNS Drugs 31.

Brown DA, Passmore GM (2009) Neural KCNQ (Kv7) channels. Br J Pharmacol.

Cox JJ, Reimann F, Nicholas AK, Thornton G, Roberts E, Springell K, Karbani G, Jafri H, Mannan J, Raashid Y, Al-Gazali L, Hamamy H, Valente EM, Gorman S, Williams R, McHale DP, Wood JN, Gribble FM, Woods CG (2006) An SCN9A channelopathy causes congenital inability to experience pain. Nature 444:894–898.

Cummins TR, Dib-Hajj SD, Black JA, Akopian AN, Wood JN, Waxman SG (1999) A novel

persistent tetrodotoxin-resistant sodium current in SNS-null and wild-type small primary sensory neurons. J Neurosci Off J Soc Neurosci 19:RC43.

de Petrocellis L, Orlando P, Moriello AS, Aviello G, Stott C, Izzo AA, di Marzo V (2012) Cannabinoid actions at TRPV channels: Effects on TRPV3 and TRPV4 and their potential relevance to gastrointestinal inflammation. Acta Physiol 204:255–266.

Devinsky O, Cross JH, Laux L, Marsh E, Miller I, Nabbout R, Scheffer IE, Thiele EA, Wright S (2017) Trial of Cannabidiol for Drug-Resistant Seizures in the Dravet Syndrome. N Engl J Med 376:2011–2020.

Devinsky O, Roberta Cilio M, Cross H, Fernandez-Ruiz J, French J, Hill C, Katz R, Consultant I, Di Marzo V, Jutras-Aswad D, George Notcutt W, Martinez-Orgado J, Robson PJ, Rohrback BG, Thiele E, Whalley B, Friedman D (2014) Cannabidiol: Pharmacology and potential therapeutic role in epilepsy and other neuropsychiatric disorders CRITICAL REVIEW AND INVITED COMMENTARY. Epilepsia 55:791–802 Available at: https://onlinelibrary-wiley-com.ezp-prod1.hul.harvard.edu/doi/pdf/10.1111/epi.12631 [Accessed June 27, 2019].

Eagles DA, Chow CY, King GF (2022) Fifteen years of NaV1.7 channels as an analgesic target: Why has excellent in vitro pharmacology not translated into in vivo analgesic efficacy? Br J Pharmacol 179:3592–3611.

Ghovanloo M-R, Shuart NG, Mezeyova J, Dean RA, Ruben PC, Goodchild SJ (2018) Inhibitory effects of cannabidiol on voltage-dependent sodium currents. J Biol Chem 293:16546–16558 Available at: http://www.ncbi.nlm.nih.gov/pubmed/30219789 [Accessed May 23, 2019].

Ghovanloo MR, Choudhury K, Bandaru TS, Fouda MA, Rayani K, Rusinova R, Phaterpekar T,

Nelkenbrecher K, Watkins AR, Poburko D, Thewalt J, Andersen OS, Delemotte L, Goodchild SJ, Ruben PC (2021) Cannabidiol inhibits the skeletal muscle nav1.4 by blocking its pore and by altering membrane elasticity. J Gen Physiol 153.

Ghovanloo MR, Dib-Hajj SD, Goodchild SJ, Ruben PC, Waxman SG (2022) Non-psychotropic phytocannabinoid interactions with voltage-gated sodium channels: An update on cannabidiol and cannabigerol. Front Physiol 13:1–8.

Hammell DC, Zhang LP, Ma F, Abshire SM, Mcilwrath SL, Stinchcomb AL, Westlund KN (2015) Transdermal cannabidiol reduces inflammation and pain-related behaviours in a rat model of arthritis. Available at: https://onlinelibrary-wiley-com.ezp-prod1.hul.harvard.edu/doi/pdf/10.1002/ejp.818 [Accessed June 27, 2019].

Han C, Yang Y, Te Morsche RH, Drenth JPH, Politei JM, Waxman SG, Dib-Hajj SD (2017) Familial gain-of-function Na(v)1.9 mutation in a painful channelopathy. J Neurol Neurosurg Psychiatry 88:233–240.

Harding EK, Souza IA, Gandini MA, Gadotti VM, Ali MY, Huang S, Antunes FTT, Trang T, Zamponi GW (2023) Differential regulation of Cav3.2 and Cav2.2 calcium channels by CB1 receptors and cannabidiol. Br J Pharmacol.

Hill AJ, Jones NA, Smith I, Hill CL, Williams CM, Stephens GJ, Whalley BJ (2014) Voltage-gated sodium (Na V) channel blockade by plant cannabinoids does not confer anticonvulsant effects per se. Neurosci Lett 566:269–274 Available at: http://dx.doi.org/10.1016/j.neulet.2014.03.013 [Accessed June 27, 2019].

Hille B (1977) Local anesthetics: Hydrophilic and hydrophobic pathways for the drug-receptor reaction. J Gen Physiol 69:497–515.

Hippalgaonkar K, Gul W, ElSohly MA, Repka MA, Majumdar S (2011) Enhanced solubility, stability, and transcorneal permeability of δ-8-tetrahydrocannabinol in the presence of cyclodextrins. AAPS PharmSciTech 12:723–731.

HODGKIN AL, HUXLEY AF (1952) A quantitative description of membrane current and its application to conduction and excitation in nerve. J Physiol 117:500–544.

Isaev D, Shabbir W, Dinc EY, Lorke DE, Petroianu G, Oz M (2022) Cannabidiol Inhibits Multiple Ion Channels in Rabbit Ventricular Cardiomyocytes. Front Pharmacol 13:1–11.

Jo S, Bean BP (2017) Lacosamide inhibition of Nav1.7 voltage-gated sodium channels: Slow binding to fast-inactivated states. Mol Pharmacol 91:331–338.

Kaplan JS, Stella N, Catterall WA, Westenbroek RE (2017) Cannabidiol attenuates seizures and social deficits in a mouse model of Dravet syndrome. Proc Natl Acad Sci 114:11229–11234.

Khan AA, Shekh-Ahmad T, Khalil A, Walker MC, Ali AB (2018) Cannabidiol exerts antiepileptic effects by restoring hippocampal interneuron functions in a temporal lobe epilepsy model. Br J Pharmacol 175:2097–2115.

Köhling R (2002) Voltage-gated Sodium Channels in Epilepsy. Epilepsia 43:1278–1295 Available at: https://onlinelibrary.wiley.com/doi/full/10.1046/j.1528-1157.2002.40501.x [Accessed February 28, 2023].

Kreitzer AC, Regehr WG (2001) Retrograde inhibition of presynaptic calcium influx by endogenous cannabinoids at excitatory synapses onto Purkinje cells. Neuron 29:717–727.

Kuo CC, Bean BP (1994) Slow binding of phenytoin to inactivated sodium channels in rat hippocampal neurons. Mol Pharmacol 46:716–725.

Kuo CC, Chen RS, Lu L, Chen RC (1997) Carbamazepine inhibition of neuronal Na+ currents:

Quantitative distinction from phenytoin and possible therapeutic implications. Mol Pharmacol 51:1077–1083.

Kuo CC, Lu L (1997) Characterization of lamotrigine inhibition of Na+ channels in rat hippocampal neurones. Br J Pharmacol 121:1231–1238.

Laprairie RB, Bagher AM, Kelly MEM, Denovan-Wright EM (2015) Cannabidiol is a negative allosteric modulator of the cannabinoid CB1 receptor. Br J Pharmacol 172:4790–4805.

Lee S (2013) Pharmacological inhibition of voltage-gated Ca2+ channels for chronic pain relief. Curr Neuropharmacol 11:606–620.

Malfait AM, Gallily R, Sumariwalla PF, Malik AS, Andreakos E, Mechoulam R, Feldmann M (2000) The nonpsychoactive cannabis constituent cannabidiol is an oral anti-arthritic therapeutic in murine collagen-induced arthritis. Proc Natl Acad Sci U S A 97:9561–9566.

Mason ER, Cummins TR (2020) Differential inhibition of human Nav1.2 resurgent and persistent sodium currents by cannabidiol and GS967. Int J Mol Sci 21:1–21.

Mechoulam R, Shani A, Edery H, Grunfeld Y (1970) Chemical Basis of Hashish Activity. Science (80-) 169:611–612 Available at: http://www.jstor.org.ezp-prod1.hul.harvard.edu/stable/1730378.

Millar SA, Stone NL, Yates AS, O'Sullivan SE (2018) A systematic review on the pharmacokinetics of cannabidiol in humans. Front Pharmacol 9.

Minett MS, Nassar MA, Clark AK, Passmore G, Dickenson AH, Wang F, Malcangio M, Wood JN (2012) Distinct Nav1.7-dependent pain sensations require different sets of sensory and sympathetic neurons. Nat Commun 3.

Orvos P, Pászti B, Topal L, Gazdag P, Prorok J, Polyák A, Kiss T, Tóth-Molnár E, Csupor-Löffler B,

Bajtel Á, Varró A, Hohmann J, Virág L, Csupor D (2020) The electrophysiological effect of cannabidiol on hERG current and in guinea-pig and rabbit cardiac preparations. Sci Reports 2020 101 10:1–9 Available at: https://www.nature.com/articles/s41598-020-73165-2 [Accessed February 28, 2023].

Patel RR, Barbosa C, Brustovetsky T, Brustovetsky N, Cummins TR (2016) Aberrant epilepsy-associated mutant Nav1.6 sodium channel activity can be targeted with cannabidiol. Brain 139:2164–2181.

Peng YS, Wu HT, Lai YC, Chen JL, Yang YC, Kuo CC (2020) Inhibition of neuronal Na+ currents by lacosamide: Differential binding affinity and kinetics to different inactivated states. Neuropharmacology 179:108266 Available at: https://doi.org/10.1016/j.neuropharm.2020.108266.

Pertwee RG (2008) The diverse CB 1 and CB 2 receptor pharmacology of three plant cannabinoids: Δ 9-tetrahydrocannabinol, cannabidiol and Δ 9-tetrahydrocannabivarin. Br J Pharmacol 153:199–215.

Pozo A, Barker-haliski M (2023) Cannabidiol reveals a disruptive strategy for 21st century epilepsy drug discovery. Exp Neurol 360:114288 Available at: https://doi.org/10.1016/j.expneurol.2022.114288.

Pumroy RA, Samanta A, Liu Y, Hughes TET, Zhao S, Yudin Y, Rohacs T, Han S, Moiseenkova-Bell VY (2019) Molecular mechanism of TRPV2 channel modulation by cannabidiol. Elife 8:1–17.

Qin N, Neeper MP, Liu Y, Hutchinson TL, Lubin M Lou, Flores CM (2008) TRPV2 is activated by cannabidiol and mediates CGRP release in cultured rat dorsal root ganglion neurons. J

Neurosci 28:6231–6238.

Rosenberg EC, Chamberland S, Bazelot M, Scharfman HE, Whalley BJ, Tsien RW, Rosenberg EC, Chamberland S, Bazelot M, Nebet ER, Wang X, Mckenzie S, Woodhall G, Scharfman HE, Whalley BJ, Tsien RW (2023) Article Cannabidiol modulates excitatory-inhibitory ratio to counter hippocampal hyperactivity Cannabidiol modulates excitatory-inhibitory ratio to counter hippocampal hyperactivity. :1–19.

Ross HR, Napier I, Connor M (2008) Inhibition of recombinant human T-type calcium channels by Δ9-tetrahydrocannabinol and cannabidiol. J Biol Chem 283:16124–16134.

Rush AM, Bräu ME, Elliott AA, Elliott JR (1998) Electrophysiological properties of sodium current subtypes in small cells from adult rat dorsal root ganglia. J Physiol 511:771–789.

Ryberg E, Larsson N, Sjögren S, Hjorth S, Hermansson N-O, Leonova J, Elebring T, Nilsson K, Drmota T, Greasley PJ (2007) The orphan receptor GPR55 is a novel cannabinoid receptor. Br J Pharmacol 152:1092–1101 Available at: http://www.ncbi.nlm.nih.gov/pubmed/17876302 [Accessed May 20, 2019].

Simms BA, Zamponi GW (2014) Neuronal voltage-gated calcium channels: Structure, function, and dysfunction. Neuron 82:24–45 Available at: http://dx.doi.org/10.1016/j.neuron.2014.03.016.

Straiker A, Dvorakova M, Zimmowitch A, MacKie K (2018) Cannabidiol inhibits endocannabinoid signaling in autaptic hippocampal neurons. Mol Pharmacol 94:743–748.

Tayo B, Taylor L, Sahebkar F, Morrison G (2020) A Phase I, Open-Label, Parallel-Group, Single-Dose Trial of the Pharmacokinetics, Safety, and Tolerability of Cannabidiol in Subjects with Mild to Severe Renal Impairment. Clin Pharmacokinet 59:747–755.

Thiele E, Marsh E, Mazurkiewicz-Beldzinska M, Halford JJ, Gunning B, Devinsky O, Checketts D, Roberts C (2019) Cannabidiol in patients with Lennox-Gastaut syndrome: Interim analysis of an open-label extension study. Epilepsia 60:419–428.

Topal L, Naveed M, Orvos P, Pászti B, Prorok J, Bajtel Á, Kiss T, Csupor-Löffler B, Csupor D, Baczkó I, Varró A, Virág L, Jost N (2021) The electrophysiological effects of cannabidiol on action potentials and transmembrane potassium currents in rabbit and dog cardiac ventricular preparations. Arch Toxicol 95:2497–2505 Available at: https://doi.org/10.1007/s00204-021-03086-0.

Vilin YY, Ruben PC (2001) Slow inactivation in voltage-gated sodium channels: Molecular substrates and contributions to channelopathies. Cell Biochem Biophys 35:171–190.

Wilson RI, Nicoll RA (2001) Endogenous cannabinoids mediate retrograde signalling at hippocampal synapses. Nature 410:588–592.

Xu DH, Cullen BD, Tang M, Fang Y (2020) The Effectiveness of Topical Cannabidiol Oil in Symptomatic Relief of Peripheral Neuropathy of the Lower Extremities. Curr Pharm Biotechnol 21:390–402.

Yang Y, Wang Y, Li S, Xu Z, Li H, Ma L, Fan J, Bu D, Liu B, Fan Z, Wu G, Jin J, Ding B, Zhu X, Shen Y (2004) Mutations in SCN9A, encoding a sodium channel alpha subunit, in patients with primary erythermalgia. J Med Genet 41:171–174.

Zheng Y, Liu P, Bai L, Trimmer JS, Bean BP, Ginty DD (2019) Deep Sequencing of Somatosensory Neurons Reveals Molecular Determinants of Intrinsic Physiological Properties. Neuron 103:598-616.e7.